Gamow-Teller transitions in the light $N = Z$ odd-odd nuclei: Proton-neutron correlation and SU(4) symmetry with clusters

Hiroyuki Morita

Abstruct

$N = Z$ odd-odd nuclei are singular subjects in nuclear physics. There are competing isovector ($T = 1$) and isoscalar ($T = 0$) states in the low-lying spectra. In mean field theories and shell models, it is pointed out that isovector and isoscalar proton-neutron correlations are important to understand these low-lying states. The isoscalar proton-neutron correlations show different natures from the isovector correlations which are analogous to like-particle correlations such as two-neutron correlations in $J^\pi = 0^+$ states of even-even nuclei. Spin degree of freedom is alive in the isoscalar states and thus the proton-neutron correlations have different two components; aligned type $[jj]_{J=2j;T=0}$ and deuteron type $[jj]_{J=1;T=0}$. Traditionally, the former case was discussed in the relation to high-spin nuclear physics. Recently, it has been found that the latter $J = 1; T = 0$ proton-neutron correlations showed characters of the LS-coupling proton-neutron pairs.

The degeneracy of isovector and isoscalar states was defined as SU(4) symmetry. Searches for SU(4) symmetry in the neutron-rich nuclei have been known as giant Gamow-Teller resonance near the isobaric analog state. However, recent theoretical and experimental investigations give new features on SU(4) symmetry. The mean-field calculations for ^{42}Ca $\to$ ^{42}Sc using isoscalar proton-neutron pairings as well as isovector ones find the strong Gamow-Teller (GT) strengths near the isobaric analog state in the low-lying regions. The similar features have been found in experimental spectra and these are called low-energy super Gamow-Teller (LeSGT) transitions which correspond to SU(4) symmetric phases in the nuclei.

In the real nuclei, deformation effects are not negligible if the core nuclei are off the doubly magic numbers. The relations between proton-neutron correlations and deformations were investigated before the suggestion of LeSGT. In the most cases, deformations disturb proton-neutron parings and make the Gamow-Teller strengths into many fragments. These effects shall cause SU(4) symmetry breaking.

The theoretical frameworks for treating proton-neutron pairing using mean field theories were developed. However, these methods are not stable for describing quantum correlations such as formation of di-nucleons and clusters, which are broadly found in the light nuclei. These are characteristic phenomena that some nucleons form units like nn (di-neutron), ^{4}He, and ^{12}C inside the nuclei. Therefore, it is hesitated to investigate the the light $N = Z$ odd-odd nuclei using the mean-field theories. Reflecting this fact, there are no works discussing the light $N = Z$ odd-odd nuclei in the context of SU(4) symmetry by proton-neutron correlations and SU(4) symmetry breaking because of deformation.

The purpose of this thesis is to extend the idea of proton-neutron pairing and SU(4) symmetry in the Gamow-Teller transitions in the light nuclei. To this end, we have to develop a new framework which can deal with proton-neutron correlations and clustering in the same footing. Firstly, I have extended antisymmtrized molecular dynamics (AMD)

with constraints on quadrupole deformation to that with isospin projection before energy variation. The problems of isospin competitions between isoscalar and isovector states in the low-lying spectra of $N = Z$ odd-odd nuclei have been solved with this method called $T\beta\gamma$-AMD. I have succeeded in reproducing low-lying spectra and nuclear properties of ^{10}B, which is the light deformed $N = Z$ odd-odd nuclei.

I have investigated Gamow-Teller transitions from the $N = Z + 2$ nuclei to the $N = Z$ odd-odd nuclei in the p-shell regions using the $T\beta\gamma$-AMD. I have found the strong Gamow-Teller transitions exhausting 50% of the sum-rule in $^6\mathrm{He}(0^+_1 1) \to {}^6\mathrm{Li}(1^+_1 0)$, $^{10}\mathrm{Be}(0^+_1 1) \to {}^{10}\mathrm{B}(1^+_1 0)$, and $^{14}\mathrm{C}(0^+_1 1) \to {}^{14}\mathrm{N}(1^+_2 0)$. These are signatures of the LeSGT related to SU(4) symmetry because of the $T = 0, S = 1$ proton-neutron pairs in the final states $^6\mathrm{Li}(1^+_1 0)$, $^{10}\mathrm{B}(1^+_1 0)$, and $^{14}\mathrm{N}(1^+_2 0)$. The LS-coupling proton-neutron pairs and cluster formations play important role to support SU(4) symmetry in these systems.

I have applied the $T\beta\gamma$-AMD to ^{22}Na comparing with ^{10}B and comprehensively investigated SU(4) symmetry in the light deformed $N = Z$ odd-odd nuclei. The proton-neutron pairs are formed at surfaces of the prolately deformed cores ($^{20}\mathrm{Ne} = {}^{16}\mathrm{O} + \alpha$, $^8\mathrm{Be} = 2\alpha$) in both nuclei. I have obtained the Gamow-Teller strengths $^{22}\mathrm{Ne}(0^+_1 1) \to {}^{22}\mathrm{Na}(1^+_{1,2} 0)$ whose summation exhausts 50% of the sum-rule value, but the strengths are fragmented into the half. This is consistent with the results of the mirror Gamow-Teller transitions $^{22}\mathrm{Mg}(0^+_1 1) \to {}^{22}\mathrm{Na}(1^+_{1,2} 0)$ which show fragmentation into two final states. The $^{22}\mathrm{Na}(1^+_{1,2} 0)$ have different K-quanta, which are defined in the deformed state, with $K = 0$ and $K = 1$. Each state contains a proton-neutron pair with anti-aligned spin ($S_z = 0$) and with aligned spin ($S_z = 1$), respectively. This indicates that the fragmentation is a result of spin-orbit interactions on quadrupole deformations, that is, SU(4) symmetry breaking.

Publication List

This thesis is mainly based on the following three papers that I was involved in.

- Chapters 2 and 3 are based on the paper [1]:
  H. Morita, Y. Kanada-En'yo, "Isospin-projected antisymmetrized molecular dynamics and its application to ^{10}B", Prog. Theor. Exp. Phys., 2016:103D02, 2016.

- Chapters 4 and 5 are based on the papers [2, 3]:
  H. Morita, Y. Kanada-En'yo, "Gamow-Teller transitions and proton-neutron pair correlation in $N = Z =$ odd p-shell nuclei", Phys. Rev. C, 96:044318, 2017.
  H. Morita, Y. Kanada-En'yo, "Low-Energy Gamow-Teller Transitions in deformed $N = Z$ odd-odd Nuclei" Phys. Rev. C, 98:034307, 2018.

Contents

Chapter 1

Background

1.1 $N = Z$ nuclei

Most of the nuclei, even stable ones, have more numbers of neutrons than those of protons. To investigate the quantum many-body correlations, enormous sophisticated methods have been developed and applied to many systems. These methods established the typical concepts of parings and deformations for each fermionic ingredient. However, the nuclei are constructed by two components; protons and neutrons. The interaction between a proton and a neutron is well known as the origin of the isoscalar bound state of a deuteron. This interaction also causes the proton-neutron correlation not only in a deuteron but also in the $N = Z$ nuclei.

The singularity of the $N = Z$ nuclei was recognized at the first stage of nuclear physics as "odd-even staggering" and "Wigner energy" [4]. "odd-even staggering" is the phenomenon on the binding energies of nuclei with $|N = Z| \approx 0$ that the values of odd-odd nuclei do not equal to the average of the two neighbor even-even nuclei. The reason is considered as the proton-neutron (pn) pairing and their blocking effect [5,6]. The pn pairs are separated into two channels, that is, the isoscalar ($T = 0$) and the isovector ($T = 1$). If the $T = 1$ pn pairs are formed but the $T = 0$ ones are not formed, this unpaired channel blocks the formation of the $T = 1$ pn pair and reduces the pairing energy. After the nuclear structure theories were developed, the problem has been discussed from the microscopic view point. In the mean field theory, it is recognized both pairing and deformation effects are important to understand this problem [7, 8].

"Wigner energy" is the extra-binding energy proportional to $|N = Z|$ in $N = Z$ nuclei suggested by Wigner's super multiplet theory [9]. Initially, it was considered that the $T = 0$ pn pairing majorly contributed to this anomalous feature [10], but the recent study of Bentley and Frauendorf suggests that "Wigner Energy" is apparent behavior of binding energy [11]. They argued that "Wigner energy" is originated from a consequence of restoring isospin symmetry which adds the $T(T + 1)$ term into the Hamiltonian not from the $T = 0$ pn correlations.

These concepts were invented in the phenomenology of $N = Z$ nuclei. In order to reach the comprehensive understanding of $N = Z$ nuclei, modern nuclear structure theories, which contain collective motions such as pairing and deformations, need to be developed.

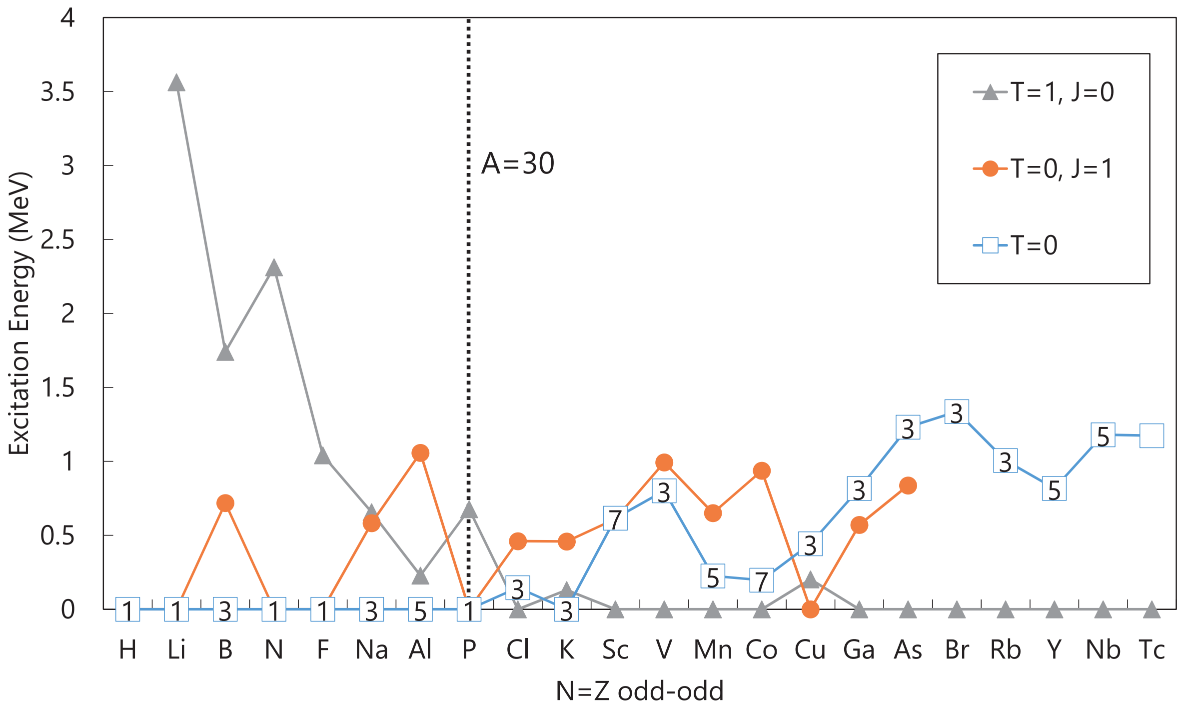

Figure 1.1: Low-Lying spectra of N=Z odd-odd nuclei. The triangles, circles, and squares refer to $T = 1, J = 0$ states, $T = 0, J = 1$ states, and $T = 0$ states, respectively. The numbers in the squares represent total angular momenta J.

1.1.1 $N = Z$ odd-odd nuclei

Few attentions have been paid to the theoretical studies of the odd-odd nuclei though the even-even nuclei usually have $J^\pi = 0^+$ ground states and it is easily explained by introducing like-particle pair correlation in the mean field theories. In 1970's, high-spin states in the nuclei were focused to find the new phases of nuclei. These states were investigated by the shell models based on the strong coupling scheme of deformation. For example, on the $N > Z$ odd-odd nuclei (^{190,192,194}Au [12], ^{198}Tl [13], ^{120}Cs [14], ^{72}As [15]), the alignments of the unpaired proton and neutron were discussed. The high-spin state search reached out to the $N = Z$ line and the $N = Z$ odd-odd nucleus ^{58}Cu was discussed in the experiment [16]. After that, a number of studies on proton-neutron correlations have been produced along the $N = Z$ line.

The spectra of $N = Z$ odd-odd nuclei are specified as competing isospin states in the low-lying regions (see Fig. 1.1). We can find three types of spectra with $J^\pi T = 0^+1$, 1^+0, and J^+0 $(J \geq 1)$. The 0^+1 state are analogous states to the 0^+ ground stats of even-even nuclei. In fact, the ground states of $N = Z$ odd-odd $A > 30$ nuclei are 0^+1. This indicates that the like-particle and the isovector $(T = 1)$ proton-neutron pairings are important even in $N = Z$ odd-odd nuclei. On the other hand, the isoscalar states $(T = 0)$ exists in the low-lying spectra. This refers to significance of the isoscalar proton-neutron pairings as well as isovector pn pairings. In the lighter nuclei $(A < 30)$, indeed, all the $N = Z$ odd-odd nuclei have the isoscalar ground states. This is a singular feature for $N = Z$ odd-odd nuclei.

1.1.1.1 Proton-neutron correlation in $N = Z$ odd-odd nuclei

The importance of the proton-neutron correlations in nuclear structure was recognized in 1970's and the Hartree-Fock-Bogoliubov method with the $T = 0, 1$ pn pairings were applied to even-even nuclei in pf-shell (^{44}Ti, ^{48}Cr, ^{52}Fe, ^{56}Ni, ^{60}Zn [17–20] and ^{76}Sr, ^{80}Zr, ^{84}Mo, ^{88}Ru, ^{92}Pd, ^{96}Cd [21, 22]).

Simple shell model calculations were performed on $N = Z$ odd-odd nuclei including the $T = 0$ pn pair correlations and the quadrupole correlations in the $g_{9/2}$-shell [23] and in the fpg-shell [24, 25]. These studies presented that the high-J spectra in low-lying states of $N = Z$ odd-odd nuclei were reproduced by introducing $T = 0$ pn correlations in the shell model orbits. In short, the $T = 0$ high-J states contain a so-called aligned pair with a proton and a neutron in the same ℓ_j-orbit and they are coupled to the $[jj]_{J=2j;T=0}$ states. These are not surprising results, but it suggested that it is not necessary to use the sophisticated method to understand the low-lying spectra in $N = Z$ odd-odd nuclei. This type of proton-neutron pair was also found in ^{70}Br as a $J^\pi = 9^+$ isomer in the low-lying states [26]. In this study, however, the authors also argued that there were only weak $T = 0$ proton-neutron pairings because the other $T = 0$ pairings $[jj]_{J=1;T=0}$ were not found in the low-lying states though many $J^\pi = 1^+$ states had been found in the lighter $N = Z$ odd-odd nuclei; ^{46}V, ^{50}Mn, and ^{54}Co.

Another side of the proton-neutron pairing was found in the rotational alignment. This is a phenomenon that the $T = 1$ pn pairs are broken into the $T = 0$ pn pairs as the angular momenta increase because only the $J = 0$ two-body correlations are allowed in the $T = 1$ states, but there are high-J channels gaining energies in the $T = 0$ states. To discuss this breaking of the pn pair, some theoretical frameworks were applied to $N = Z$ even-even nuclei such as cranked HFB in ^{48}Cr [27], isospin cranked mean-field in ^{48}Cr [28], cranked pf-shell model [29], cranked HFB in ^{80}Zr [30], and projected shell model in ^{72}Kr, ^{76}Sr, ^{80}Zr [31].

The recent studies on proton-neutron pairing are based on the re-coupling scheme. In this picture, there are more than one $[jj]_{J=2j;T=0}$ pn pairs are formed in the ground states and the low-lying excitations arise from re-coupling of these pairs. Friedman and Bertsch pointed out their importance in DFT on $N = Z$ odd-odd nuclei [32] and the concept is taken into the fpg-shell model in ^{92,94,96}Pd [33]. The validity of this scheme is examined in some experiments about ^{92,94,96}Pd [34] and ^{40}K [35].

However, $T = 0, J = 1$ pn pairing, which corresponds to deuteron formation, had not been paid attention though aligned pn pairs $[jj]_{J=2j;T=0}$ were investigated as seen above. Recently, this type of proton-neutron correlation has been discussed as a LS-coupling pn pair. Sagawa, Tanimura, and Hagino performed the systematical studies of the $N = Z$ odd-odd nuclei focusing on the changes of the jj coupling scheme into the LS coupling scheme in the valence proton and neutron. In the first study [36], the three body model of core+p+n in the $1f2p$-shell was applied to fp-shell nuclei seeking for the $T = 0$ spin-triplet pairing correlations. They concluded that such types of pairing were weakened in the $1f$-shell and, on the other hand, $T = 0$ spin-triplet pairing in the $2p$-shell overcame the $T = 1$ spin-singlet pairing because the spin-orbit splitting was smaller in the $2p$-shell than in the $1f$-shell. This $2p$-shell nucleus was realized as ^{58}Cu and they managed to obtain the magnetic dipole moment (μ) value of its ground state ($J^\pi T = 1^+0$) consistent with the experimental one by changing the ratio of pairing interaction between $T = 0$ and $T = 1$.

In the next study [37], the model was applied to the lighter nuclei; ^{14}N, ^{18}F, ^{30}P, ^{34}Cl, ^{42}Sc, ^{58}Cu. They obtained the lowest $J^\pi T = 0^+1$ and $J^\pi T = 1^+0$ spectra with the consistent level-ordering with the experimental spectra. The spin-orbit splitting disturbed the $T = 0$ spin-triplet pairing and the ground states of ^{34}Cl and ^{42}Sc have $J^\pi T = 0^+1$. In contrast, the lowest 1^+0 states of ^{18}F and ^{42}Sc have well-developed $T = 0$ spin-triplet pairing. As a result, $M1$ transitions from the lowest 0^+1 states and Gamow-Teller (GT) transitions from the 0^+1 ground states of the neighbor $N = Z + 2$ nuclei; ^{18}O and ^{42}Ca, are sufficiently strong to exhaust the major parts of the sum-rule values. After that, the model was extended to relativistic one and it was applied to ^{102}Sb which is the unobsurved $N = Z$ odd-odd nucleus with the heaviest doubly-magic ^{100}Sn core [38]. Unfortunately, the valence proton and neutron in the relativistic model favored occupation of the $g_{7/2}$-shell rather than formation of the LS-coupling $T = 0$ pn pair. Moreover, there are problems that these three-body models are based on the spherical cores and lack effects of deformation.

Recently, proton-neutron pairings on the deformed $N = Z$ even-even nuclei have been discussed by using shell-model like diagonalization [39] and BCS on the deformed orbits obtained from the self-consistent mean-field calculation [40, 41]. These calculations did not focus on the relation between deformation and proton-neutron correlations since the shell-model orbits were determined before introducing paring correlations, but enable us to discuss the competition of $T = 0$ and $T = 1$ proton-neutron parings on the deformed nuclei. They found the consistent results in ^{44}Ti, ^{48}Cr, ^{52}Fe, ^{56}Ni, ^{60}Zn, ^{64}Ge [39] and in $^{64-76}$Ge [40] that deformation reduces the pairing correlations especially for the $T = 1$ channel in ^{56}Ni [39] and it does for all shapes and species of $^{64-76}$Ge [39]. The latter method was applied to lighter nuclei, ^{24}Mg(prolate), ^{28}Si(oblate), and ^{32}S(prolate) [41]. In these cases, there can be a coexistence of the $T = 0$ and $T = 1$ pairings in largely deformed states and more importantly the pairing energies change the positions of energy minimums for the quadrupole deformation parameters. Despite many efforts have been made for these $N = Z$ even-even nuclei, there are few studies for $N = Z$ odd-odd nuclei focusing on deformation.

1.1.2 Light $N = Z$ nuclei

The idea of proton-neutron pairings in $N = Z$ nuclei have been succeeded, but it is hesitated to apply the concept immediately to the the lighter nuclei ($A < 30$) because the pn pairing was invented in HFB theory which were applied to heavier nuclei ($A > 30$) where mean field approximation were valid. In the light nuclei, the quantum many-body correlation such as paring and deformation might be realized as the formation of di-nucleons and clusters as seen in Sec. 1.3.

1.2 Gamow-Teller transitions

Gamow-Teller (GT) transition is one of the allowed β transitions derived from the weak interaction. I write about the role of GT transitions for the nuclear structures. Firstly, the GT transitions were investigated by Wigner using the SU(4) supermultiplet model [9]. The model assumes SU(4) symmetry on the two-body interaction in the $S = 1, T = 0$ and $S = 0, T = 1$ channel that the six components in these channel have the same energies.

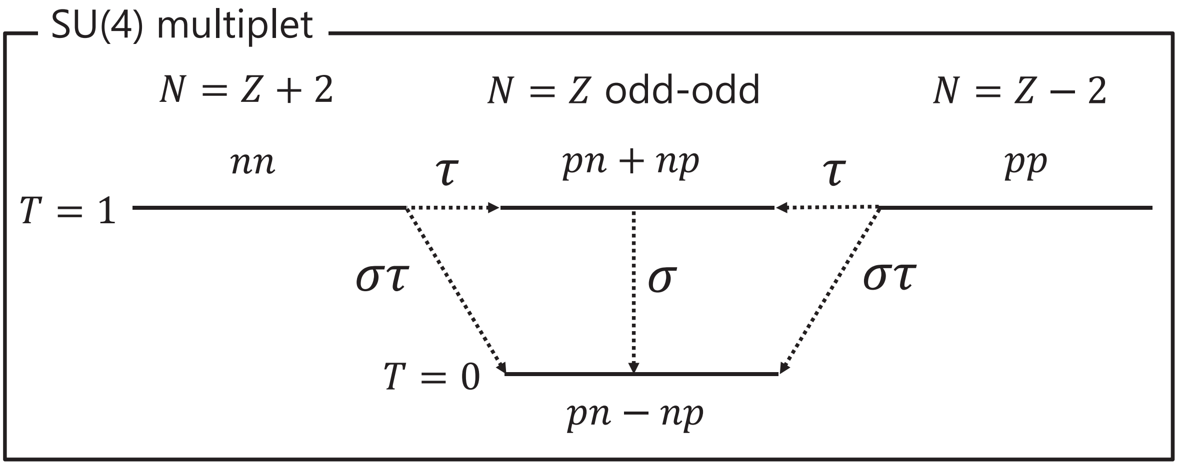

Figure 1.2: SU(4) multiplets in $N = Z$ odd-odd nuclei and $N = Z \pm 2$ neighbors.

Since the GT operator is written as

$$\boldsymbol{Y}^{\pm} = \sum_i \boldsymbol{\sigma}_i \tau_i^{\pm}, \tag{1.1}$$

which does not contain the spatial parts, the overlap between the initial state $|\Phi\rangle$ and the final state $\sum_i \boldsymbol{\sigma}_i \tau_i^{\pm} |\Phi\rangle$ is exactly unit. This extremely simplified model succeeded in reproducing the strong GT transition such as $^6\mathrm{He}(0_1^+1) \to {}^6\mathrm{Li}(1_1^+0)$ qualitatively, but it did not quantitatively as the model did not consider the nuclear structure such as paring and deformation.

Schematically, the SU(4) multiplets are described as the spectra in the $N = Z$ odd-odd nuclei and the $N = Z \pm 2$ neighbors (see Fig. 1.2). Each state corresponds to isovector ($T = 1$) states nn, $pn+np$, pp and an isoscalar ($T = 0$) state $pn-np$ in the two-body NN systems. These states are connected with allowed beta decays such as Fermi transitions (τ) and Gamow-Teller transitions ($\sigma\tau$).

This ideal SU(4)-symmetry is explicitly broken because the nuclear force depends on the intrinsic spin such as a tensor force and a spin-orbit force. However, Ikeda and J.I. Fujita suggested that such strong GT transitions between Wigner's supermultiplets can be realized in heavier $N > Z$ nuclei not as state-to-state transitions but as giant resonances [42]. If the neutron numbers exceed to the proton numbers, there are some single particle orbits ℓ_j which are occupied for neutrons and opened for protons. The GT transitions can be considered as the excitation that the operator $\boldsymbol{\sigma}\tau^{\pm}$ changes the neutrons in some single particle orbits into the protons with the difference of $\Delta T = 1$ and $\Delta S = 1$. These one neutron-hole and one proton-particle states are convoluted coherently and make resonant states. This phenomenon is called Gamow-Teller Giant Resonance (GTGR) and it was direcly observed in the charge-exchange experiments (^{48}Ca, ^{90}Zr, ^{120}Sn, ^{208}Pb) [43]. Afterwards, theoretical works have been made pursuing the precise description for the peak position of the energy and the lacks of the sum-rule values [44–49].

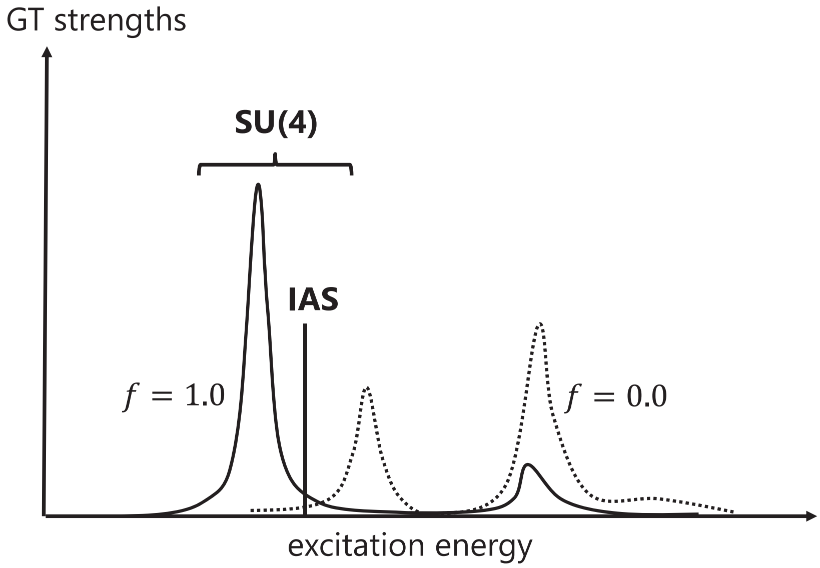

Figure 1.3: SU(4) symmetry in GT transition strengths.

1.2.1 Gamow-Teller transitions in $N = Z$ nuclei

Apparently, the GTGR cannot be found in $N = Z$ nuclei because the Fermi surfaces for protons and neutrons are almost equivalent. Nevertheless, GTGR is not forbidden even in $N = Z$ nuclei (^{56}Ni, ^{64}Ge, ^{76}Sr, ^{100}Sn [50],^{52}Fe, ^{94}Ag [51]) because the GT operators can change the intrinsic spin with $\Delta S = 1$ unlike Fermi transitions ($\sum_i \tau_i^{\pm}$).

1.2.1.1 Proton-neutron pairing and Gamow-Teller transitions

The relation between GT transitions and proton-neutron pairing has been investigated in the $N = Z$ nuclei. Bai et al. investigated the role of isoscalar spin-triplet ($T = 0, S = 1$) pairing interaction in the $N = Z$ even-even nuclei ^{48}Cr, ^{52}Fe, ^{56}Ni, ^{60}Zn, and ^{64}Ge by using the HFB+QRPA [52]. They found that some strengths in the GTGR were isolated into the lower energy region by changing $T = 0, S = 1$ interaction to $T = 1, S = 0$ one with the ratio f. Such double peak structure had been observed in ^{56}Ni and the ratio should be $f \approx 1.5$ in order to reproduce this experimental $B(\mathrm{GT})$ spectra. By using this ratio, the strength of the lower peak and that of the higher peak had comparable values especially for ^{48}Cr and ^{52}Fe. In these nuclei, the pf-shell configurations coherently contributed to forming the lower peak, and they concluded that the low-energy GT transitions $^{48}\mathrm{Cr} \to {}^{48}\mathrm{Mn}$ and $^{52}\mathrm{Fe} \to {}^{52}\mathrm{Co}$ could be considered as the super-allowed transitions in SU(4) supermultiplet.

This model was applied to the $N = Z$ odd-odd sd-shell nuclei ^{42}Sc, ^{46}V, ^{50}Mn, and ^{54}Co [53]. These nuclei also had double peaks at the low- and high-energy regions and the lower peaks grew up to the comparable values to the the higher peaks as the f increased (see Fig. 1.3). However, the ratio was not necessary to excessively larger than $f = 1.0$ and the lower peak height in $^{42}\mathrm{Ca} \to {}^{42}\mathrm{Sc}$ was reproduced with $f = 1.05$. Because one side of the proton orbits $j_{\gtrless} \equiv \ell_{j=\ell\pm1/2}$ is opened in the $N = Z$ odd-odd nuclei, Fermi β transitions from the $N = Z+2$ nuclei to $N = Z$ odd-odd ones are also allowed, where the final states are generally called isobaric analog states (IAS). In their calculation, each lower peak of

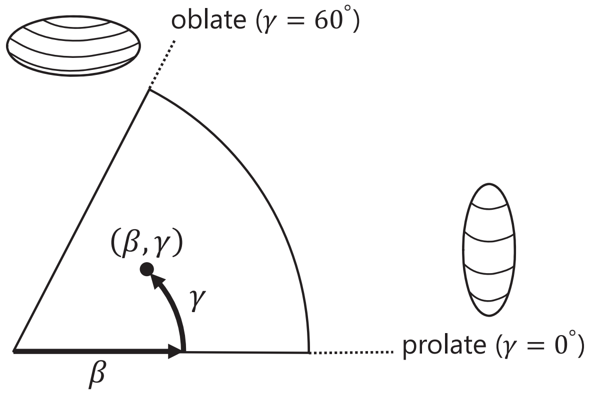

Figure 1.4: Deformation in nuclei.

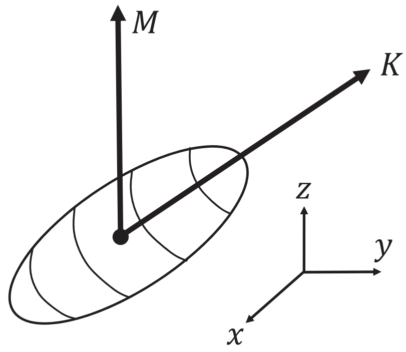

Figure 1.5: Angular momenta in the deformed nuclei.

GT transition was found near the IAS and this indicated that the SU(4) supermultiplet was exactly formed because of $T = 0$ paring force comparable with $T = 1$ one ($f \approx 1.0$). Though the strong GT transition strengths to the lower peaks were reproduced, there are some problems that the experimental GT strengths are fragmented into the second and the above states except for ^{42}Ca $\to$ ^{42}Sc. They pointed out that deformation in ^{50}Cr, ^{54}Fe, and ^{58}Ni might cause the fragmentation in ^{50}Cr $\to$ ^{50}Mn, ^{54}Fe $\to$ ^{54}Co, and ^{58}Ni $\to$ ^{58}Cu, respectively.

1.2.1.2 Deformation and Gamow-Teller transitions

Deformation in the nuclei is defined as fluctuations on the spherical nuclear surfaces with the radius $R_0 > 0$

$$R(\theta, \phi) = R_0 \left[1 + \sum_{\mu=-2}^{2} \alpha_\mu^* Y_{2\mu}(\theta, \phi) \right], \tag{1.2}$$

where θ, ϕ and $Y_{2\mu}(\theta, \phi)$ denote spherical coordinates and spherical harmonic functions, and the coefficients $\{\alpha_\mu\}_{\mu=-2}^{2}$ are the parameters for deformations. If we use the body-fixed frame, the surface is symmetric for z-axis, $x = 0$ plane, and $y = 0$ plane. Therefore, the parameters have the conditions

$$\alpha_{-1} = \alpha_1 = 0, \tag{1.3}$$

$$\alpha_{-2} = \alpha_2. \tag{1.4}$$

The residual two parameters $\alpha_{0,2}$ determine the shapes of nuclei in the body-fixed frame. For convenience, we usually use β and γ parameters defined as

$$\alpha_0 = \beta \cos\gamma, \tag{1.5}$$

$$\alpha_2 = \frac{1}{\sqrt{2}} \beta \sin\gamma. \tag{1.6}$$

Because of cyclic symmetry about x-, y-, and z-axis, γ parameter is restricted to $\gamma \in [0^\circ, 60^\circ]$. I call this parameter space a $\beta\gamma$-plane in this thesis. The ideal shapes in the nuclei are called prolate ($\gamma = 0^\circ$) and oblate ($\gamma = 60^\circ$) (see Fig. 1.4). In the nuclear systems, z

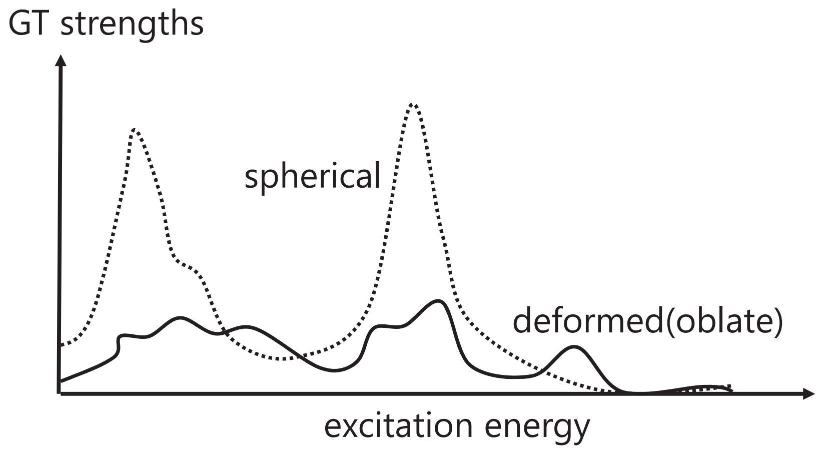

Figure 1.6: Fragmentations of GT transition strengths by deformation.

components of the angular momenta J are good quantum numbers and denoted as M in the space-fixed frame (see Fig. 1.5). K-quanta are the z components of J defined in the body-fixed frame. The wavefunctions of the deformed nuclei in the body-fixed frame are usually called intrinsic states.

The deformation in $N \approx Z \approx 40$ nuclei is complicated because of prolate-oblate shape coexistence for ^{68}Se and ^{72}Kr. In order to clarify the existence of such strange phenomena, the experimental GT accumulated strengths

$$f(E) = \sum_{E_f < E} B(\mathrm{GT}; i \to f) \tag{1.7}$$

have been compared with those from the deformed (oblate or prolate) bases calculations. This method was applied to $N = Z$ even-even nuclei and revealed the shape for ^{72}Kr (oblate [54]), ^{76}Sr(prolate [55]) , ^{78}Sr (prolate [56]). Recent comprehensive theoretical studies for neutron-rich nuclei are seen in [57](Zr, Mo) and [58](Ge, Se, Kr, Sr, Ru, Pd). Sarriguren et al. applied the deformed HF+RPA to the GT transition ^{74}Kr $\to$ ^{74}Br and found that the accumulated GT strength in Eq. (1.7) strongly depends on quadrupole deformation [59]. If the initial state is oblately deformed, the accumulated GT strength becomes the half of prolately deformed one for each E. They found that the deformation caused the decouple of the K-quanta. In the prolately deformed case, the $K = 1$ state constructed the peak and $K = 0$ component was hindered, which also made a small peak at higher energy. On the other hand, in the oblately deformed case, $K = 0, 1$ components were also decoupled, but the strengths were fragmented into many single particle states and the peaks were not formed in any energy region (see Fig. 1.6). The experimental accumulated GT strength [60] showed clearly intermediate features of oblate and prolate. This can be one of the evidences for the prolate-oblate shape coexistence in ^{74}Kr.

The accumulated GT strength was also discussed by Bai et al. [53] and their values for ^{46}Ti $\to$ ^{46}V, ^{50}Cr $\to$ ^{50}Mn, and ^{54}Fe $\to$ ^{54}Co insufficiently match to experimental ones though that for ^{42}Ca $\to$ ^{42}Sc is good agreement with the data. Recently, the answer to this problem has been given by another group [61] from the view point of SU(4)-symmetry breaking caused by a spin-orbit force on the quadrupole deformed states. They performed the pf-shell model calculation and reproduced the $B(\mathrm{GT}; 0^+_1 1 \to 1^+_1 0)$ of nuclei listed above by introducing the spin-orbit force, $T = 1, J = 2$ pairing interaction, and QQ interaction combined with $T = 0, J = 1$ and $T = 1, J = 0$ paring interactions. The important point was that without QQ interaction, $B(\mathrm{GT}; 0_1^+1 \to 1_1^+0)$ of ^{46}Ti $\to$ ^{46}V and ^{50}Cr $\to$ ^{50}Mn were estimated twice larger. This indicates that deformation plays a decisive role to define the low-lying states of $N = Z$ odd-odd nuclei. Moreover, the accumulated GT strengths of their model agree with the experimental ones for ^{46}Ti $\to$ ^{46}V and ^{50}Cr $\to$ ^{50}Mn, but that of ^{54}Fe $\to$ ^{54}Co does not. The effect of deformation on $B(\mathrm{GT})$ fragmentation is limited in ^{54}Fe $\to$ ^{54}Co where many particle-hole excitations or particle-vibration coupling also contribute to $B(\mathrm{GT})$ fragmentation [53].

Ha and Cheoun investigated GT transitions in the lighter deformed nuclei ^{30,32,34}Mg by using the deformed QRPA method without proton-neutron pairing interaction [62]. In their results, prolate deformations pushed the $B(\mathrm{GT})$ spectra, which were already fragment into many states near the spherical case, up to the higher energy. They also studied $N \approx Z$ nuclei ^{24,26}Mg [63] with proton-neutron pairing interaction. The conclusion is that the proton-neutron pairing enhanced the low-lying GT strengths, but the effect of deformation was much stronger than *pn* pairing because the energy minimums on the deformation parameter β was not determined by *pn* pairing and the accumulated GT strengths were not changed between with and without the *pn* pairing. They also applied the same model including *pn* pairing and deformation to ^{24}Mg, ^{28}Si, and ^{32}S [64]. The results were consistent with the above cases. Deformation was more important than *pn* pairings in order to understand the broadly distributed GT strengths.

1.2.1.3 Low-Energy Super Gamow-Teller transitions

Recently, the low-lying states near the $N = Z$ line have been systematically discussed in the experiments and clear SU(4) symmetry was found in the real spectra. The low-lying states of the $N = Z$ odd-odd $f_{7/2}$-shell nuclei were measured at Research Center of Nuclear Physics (RCNP), Osaka by using Grand Raiden spectrometer; ^{42}Ca $\to$ ^{42}Sc [65], ^{46}Ti $\to$ ^{46}V [66], ^{50}Cr $\to$ ^{50}Mn [67], ^{54}Fe $\to$ ^{54}Co [68], ^{58}Ni $\to$ ^{58}Cu [69–71]. The high-energy resolution with $\Delta E = 45$ keV for GT transition has been achieved for charge-exchange (^{3}He$, t$) reaction (see [72]) by detecting the forward scattering near the 0°, which corresponds to $\Delta L = 0$ derived from the GT transition operator Eq. (1.1). These improvements of detecting technology give us the detailed information about Gamow-Teller transitions $0_1^+1(\mathrm{g.s.}) \to 1_n^+0$.

The authors argued that the lowest 1^+0 state at 0.611 MeV of ^{42}Sc corresponded to the Wigner's SU(4)-supermultiplet state because there were negligible GT strengths above this state [73]. This GT strengths distribution is especially characteristic compared with the $B(\mathrm{GT})$ spectra of ^{46}Ti $\to$ ^{46}V and ^{50}Cr $\to$ ^{50}Mn because these strengths are fragmented into the Gamow-Teller resonances around 6–11 MeV. They also compared the accumulated GT strengths with the shell-model calculations and obtained good agreements. The lowest ^{42}Sc(1_1^+0) is named "low-energy super GT" (LeSGT) state in this paper as a SU(4)-multiplet state assisted by $T = 0$ proton-neutron effective residual interactions. The systematicity of LeSGT is observed in ^{6}He $\to$ ^{6}Li and ^{18}O $\to$ ^{18}F. Consequently, LeSGT is unique phenomena when the $N = Z + 2$ nuclei have $N = Z$ even-even closed core such as ^{4}He, ^{16}O, and ^{40}Ca. These closed core nuclei are inert on GT transitions since both orbits $j_{\gtrless}$ are occupied and the transitions between these sates are clearly forbidden.

However, little attention has been paid to transitional nuclei ^{46}V and ^{50}Mn even though there are a few strong GT strengths in the low-lying region of $^{46}\mathrm{Ti} \to {}^{46}\mathrm{V}$ and $^{50}\mathrm{Cr} \to {}^{50}\mathrm{Mn}$ which are not found in $^{54}\mathrm{Fe} \to {}^{54}\mathrm{Co}$, which is near the closed shell ($N = Z = 28$). Recently, it is pointed out that deformation and spin-orbit interactions play an essential role to reproduce the low-lying GT strengths in these transitional nuclei [61]. Moreover, such fragmentation has already been measured in $^{26}\mathrm{Mg} \to {}^{26}\mathrm{Al}$ [72] and compared with the spectra obtained by the spherical HFB+QRPA method [74]. The theoretical GT spectra were succeeded in forming the low-lying peak but it did not predict the fragmentation of them into the two states; $^{26}\mathrm{Al}(1^+_{1,2}0)$. For another example, in the measument of GT; $^{34}\mathrm{S} \to {}^{34}\mathrm{Cl}$ [75], the strengths toward lowest states $(1^+_{1,2}0)$ were hindered as $B(\mathrm{GT}) \approx 0.019, 0.064$ though those to the next states $(1^+_{3,4}0)$ were sufficiently strong with $B(\mathrm{GT}) \approx 0.299, 1.369$. These facts support that LeSGTs are not always found in the lowest $1^+_1 0$ states but in the higher $1^+_{n>1}0$ states. Therefore, it is necessary to refine nuclear structure theory for the low-lying but not the lowest 1^+0 states of $N = Z$ odd-odd nuclei.

The enhancement of an energy resolution on charge-exchange reactions gives us opportunities to see the details of the $J = 1$ state in the low-lying and high-lying states in $N = Z$ odd-odd nuclei. However, the theoretical treatment of these nuclei is limited as QRPA phonon excitations from the neighbor $N = Z + 2$ nuclei in mean field theories [52–59, 62–64, 74]. In order to reveal the identity of these 1^+0 states, it is necessary to perform the direct calculations obtaining 1^+0 states not as phonons on $N = Z+2$ nuclei. This challenge has been done by Konieczka et al. but the model lacks proton-neutron pairing and there are rooms for futher development [76]. Shell models are succeeded in reproducing low-lying and high-lying 1^+0 states in $N = Z$ odd-odd nuclei [77], but physical descriptions are ambiguous because these shell models include all the effects on the interaction and the collective motions at the same time. There are rooms to do complementary studies that reveals the essential correlations in these 1^+0 states [61].

1.2.2 Gamow-Teller transitions in light nuclei

There are theoretical limitations for the lower *sd*-shell nuclei (^{18}F, ^{22}Na, ^{26}Al) and *p*-shell nuclei (^{6}Li, ^{10}B, ^{14}N) in mean field theories and shell-model calculations because degree of freedom of the α clusters plays a crucial role and the like-particle and proton-neutron parings are questionable as shown in the next section. The heaviest $N = Z$ odd-odd and $A < 30$ nucleus ^{26}Al was treated as the final states of QRPA calculations for $^{26}\mathrm{Mg} \to {}^{26}\mathrm{Al}$ transitions in Ref. [63]. However, for these extremely light nuclei, the mean field approximations may be not suitable to describe deformation as well as *pn* pairing because deformation in these region might be caused by cluster correlations.

The GT transition $^{14}\mathrm{C}(0^+_1 1) \to {}^{14}\mathrm{N}(1^+_1 0)$ shows interesting feature that the strength is extremely hindered $B(\mathrm{GT}) = 1.90 \times 10^{-6}$ which is in the same magnitude of the first forbidden transition. After the development of radiocarbon dating using this long life time of 5730 year in 1947, Jancovici and Talmi discussed this problem in 1954 by using the LS-coupling shell model [78] and obtained the anomalous hindrance by tuning spin-orbit and tensor force to cancel out the matrix element. From this first attempt, many theoretical and experimental have been performed pursuing the real wavefunction of $^{14}\mathrm{C}(0^+_1 1)$ and $^{14}\mathrm{N}(1^+_1 0)$. In the most recent, the GT spectra of $^{14}\mathrm{N}(1^+_1 0) \to {}^{14}\mathrm{C}(2^+_n 1)$ have been systematically measured [79] and they have obtained the fragmented spectra for ^{14}C($2^+_{1,2,3}1$). This is not consistent with the theoretical result by a no-core shell model (NCSM) that predicts the GT strengths is concentrated into the lowest ^{14}C($2^+_1 1$) state with B(GT) = 2.609 [80]. The same feature is obtained in the calculation where the cluster correlations are taken into account, but the concentration ^{14}N($1^+_1 0$) $\to$ ^{14}C($2^+_1 1$) is found with B(GT) = 2.4 [81]. The NCSM with a three-nucleon force of chiral perturbation theory achieved the vanishment of the GT strength of ^{14}C($0^+_1 1$) $\to$ ^{14}N($1^+_1 0$) [82], but this problem remains a state-of-art challenge for the low-lying GT transitions in the $N = Z$ odd-odd light nuclei because it has not been revealed what nuclear correlations are important to understand the ground state of the heaviest stable $N = Z$ odd-odd nucleus ^{14}N($1^+_1 0$).

1.3 Clustering of light nuclei

For the light nuclei ($A < 30$), the $N = Z$ even-even nuclei (^{8}Be, ^{12}C, ^{16}O, ^{20}Ne, ^{24}Mg, ^{28}Si) have been enthusiastically investigated after the suggestion of the α cluster correlation which is the four-particle correlations of $p\uparrow$, $p\downarrow$, $n\uparrow$, $n\downarrow$ forming ^{4}He units inside the nuclei. The original purpose of this idea is to find theoretical description for the low-lying $J^\pi = 0^\pm$ excitations and the rotational $K = 0$ bands in $^{12}\mathrm{C} = 3\alpha$, $^{16}\mathrm{O} = {}^{12}\mathrm{C} + \alpha$, and $^{20}\mathrm{Ne} = {}^{16}\mathrm{O} + \alpha$ [83–91]. The α clustering was called "molecular-like structure" at first [93] and the rough conjecture that such states would be found near the thresholds was given for the light $N = Z$ even-even nuclei by Ikeda et al. [92] (see Fig. 1.7). After that, much higher excited $0^+_{n\geq 2}$ states and strongly deformed 0^+ states have been discussed. The former states are called "α condensation" [94–105] which are the states described by the picture that many α particles are trapped in the harmonic oscillator potential. The latter states are named "linear chain" [106–118], where strings of beads made by α are formed in their intrinsic states.

1.3.1 Theoretical approaches for clustering

Many models have been developed in order to solve the relative motions between the clusters, which correspond to the molecular-like structures. In the simplest method, the α particles are theoretically treated as point particles without internal structures under the assumption that the relative motions are determined by orthogonality conditions to the lower states (^{12}C [119], ^{20}Ne [120–122]).

However, the modern studies of clustering have been mostly based on the antisymmetrized molecular dynamics (AMD). This is a microscopic method without assumption of the clusters, where the nuclear dynamics are solved in the scale of nucleons by using Gaussian wavepackets (see Sec. 2.1). These Gaussians are suitable to describe α clusters in S-wave. The definition of the AMD was given by Ono et al. for description of low-energy heavy-ion reactions [123]. After that, this model was applied to nuclear structure calculations in the light nuclei (Li, Be [124], B [125], ^{12}C [126], ^{20}Ne [127]). This method has been developed into various extensions in order to incorporate the quantum many-body correlations. For example, multi-Slater determinants are used in [128], constraint on the distances between clusters are introduced in [129], and Brueckner theory is applied in [130]. Cluster structure in the odd-A nuclei was also investigated with AMD because

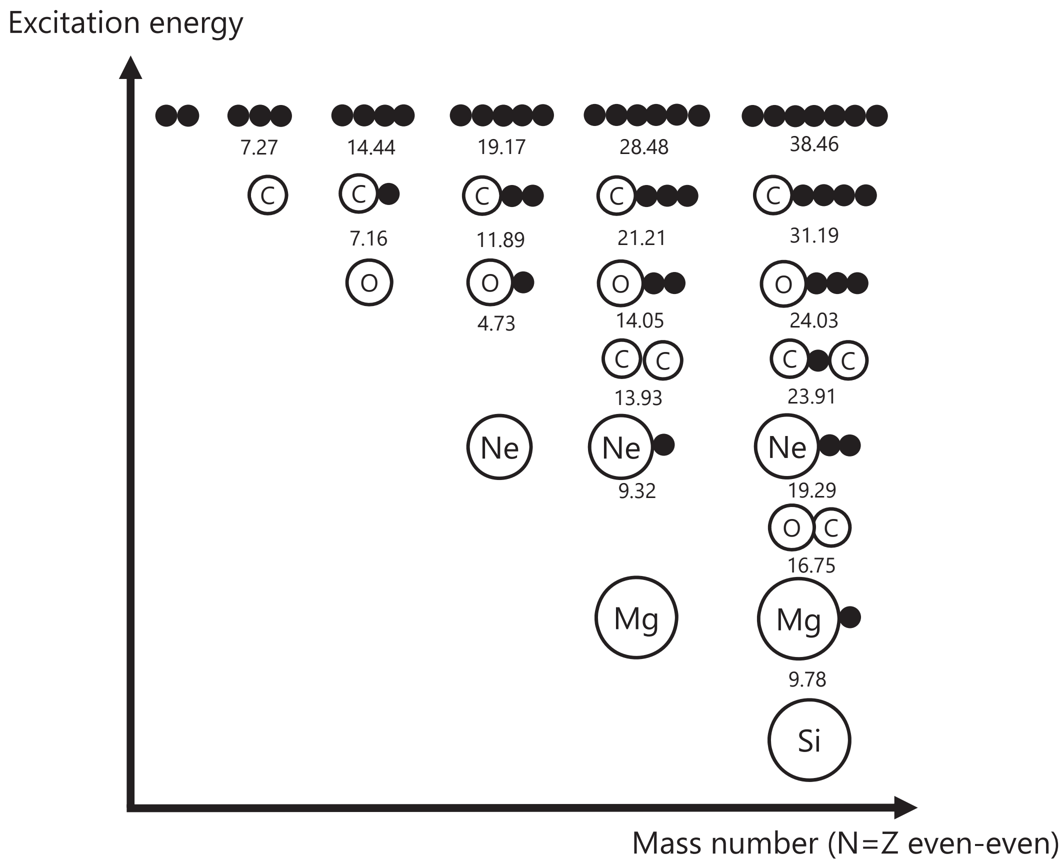

Figure 1.7: Clustering structures near the thresholds in the $N = Z$ even-even nuclei predicted by Ikeda et al [92]. The black dots show α particles. The numbers near the pictures represent the threshold energies for each channel.

the method can deal with nucleon's spins and it is not limited to $J = 0$ states of even-even nuclei (^{11}B, ^{11}C [131], ^{9,11}Li, ^{9,11}Be [132], ^{9}Li [133]).

These light nuclei have been investigated also with *ab initio* frameworks. No-core shell model (NCSM) is notable one where harmonic oscillator bases up to large principal quantum numbers are diagonalized with effective or realistic interactions including those derived from the chiral effective theories. However, some states in the light nuclei are insufficiently described because of clustering. The first excited 0^+ state of ^{12}C and ^{16}O are typical examples showing the limitations for these *ab initio* calculations, in which enormous shell orbits are needed in order to reproduce cluster structures. In fact, it was pointed out that $^{12}\mathrm{C}(0_2^+) = 3\alpha$ was not obtained [134–138] and $^{16}\mathrm{O}(0_2^+) = {}^{12}\mathrm{C} + \alpha$ was also difficult [139].

1.3.2 Deformation on cluster structures

Quadruple deformation and clustering are closely related to each other. For instance, ^{28}Si has prolately deformed $K^\pi = 0^+$ bands corresponding to the cluster $^{16}\mathrm{O} + {}^{12}\mathrm{C}$ [140, 141] and $^{24}\mathrm{Mg} + \alpha$ [140]. Similarly, ^{32}S has prolately deformed bands of $^{16}\mathrm{O} + {}^{16}\mathrm{O}$ cluster structure [141]. Oblate deformations are also found as clustering. $K^\pi = 5^-$ and 3^- bands of ^{28}Si and ^{12}C are described by 7α and 3α clusters placed to make pentagon and triangle shapes in their intrinsic states, respectively [142].

The AMD can describe deformation and clustering in the same footing. The deformed bases AMD is a method using deformed Gaussian wavepackets for the single-particle orbits [143]. The merit is that this method can deal with both deformed mean-field structures found in the low-lying states and cluster structures in the highly excited states. In the results of application to ^{20}Ne, it is found that $J^\pi = 1^-$ ($K^\pi = 0^-$) and $J^\pi = 2^-$ ($K^\pi = 2^-$) energy surfaces correspond to $^{16}\mathrm{O}+\alpha$ and a deformed mean-field-like character, respectively.

In principle, the AMD without deformed bases can also describe the mean-field structures because the AMD is one of the Hartree Fock methods that uses Gaussian wavepackets as single-particle orbits instead of the solutions of the self-consistent one-body potential problem. Another extension called $\beta\gamma$-AMD is based on this fact [144]. This is a method performing energy variation under the constraint on quadrupole deformation parameters β and γ, but the basis wavefunctions are spherical Gaussian wavepackets. It is succeeded in finding mean-field-like structures and cluster structures of $N = 6$ isotones (^{9}Li, ^{10}Be, ^{11}B, ^{12}C) in the small and large β regions, respectively. Because the method puts constraint on γ as well as β, the prolately deformed structures ($\gamma = 0°$) in ^{10}Be and oblately deformed structures ($\gamma = 60°$) in ^{11}B and ^{12}C are obtained in the same framework.

1.3.3 Di-neutron correlation

The light neutron-rich nuclei have been investigated to search a new physics near the neutron-drip line [145] and the neutron magic numbers [146].

Neutron halo is one of the most characteristic phenomena in the light neutron-rich nuclei. This phenomenon was firstly observed in ^{11}Li as a ground state with an extremely large radius. ^{11}Li was enthusiastically studied by experimental and theoretical methods pursuing the origin of such a strange ground state [147,148]. The essential reason why such a large radius is realized in ^{11}Li is that the nucleus is well described as $^{11}\mathrm{Li} = {}^{9}\mathrm{Li} + n + n$ and these two excessed neutrons are loosely bound near the neutron threshold energy. Halo structures are also found in proton orbits in ^{8}B [149]. Recently, the halo structures have been extended into a deformed state in ^{37,38}Mg [150].

Neutron skin is another interesting phenomenon for neutron rich nuclei. This is also defined as a ground state with a large radius. The examples are ^{6,8}He [151] and neutron-rich Na isotopes [152]. The different point from the neutron halo is that not only valence neutrons but also neutrons in the core nuclei should be considered. Namely, the neutron skin is caused by the deviation between the proton and neutron Fermi surfaces because of excessed neutrons.

The theoretical interests for neutron halo and skin have been paid into the correlations of these excessed neutrons. The di-neutron correlations in these excessed neutrons have been investigated in some theoretical methods. Usually, two nucleon correlations are described as residual interactions forming two nucleons pairs in the same shell orbits: $(\ell_j)^2_{J=0}$. This types of two-neutron correlations are investigated in ^{11}Li [153, 154]. The authors performed shell model calculations with the assumption of the ^{9}Li core and found that many neutron shell orbits $(p_{1/2})^2_{J=0}$, $(s_{1/2})^2_{J=0}$, $(d_{5/2})^2_{J=0}$, $(d_{3/2})^2_{J=0}$, $(p_{3/2})^2_{J=0}$, $(f_{7/2})^2_{J=0}$, $(f_{5/2})^2_{J=0}$, $(g_{9/2})^2_{J=0}$, and $(g_{7/2})^2_{J=0}$ are necessary to produce the reasonable binding energy of ^{11}Li. However, they also pointed out that this model space was insufficient to reproduce the binding energy and di-neutron cluster moving around the ^{9}Li core might be needed.

These insufficiency of the model spaces were also pointed out in the mean-field theories [155, 156]. These calculations suggested that the two-neutron pairings in the continuum states of the single-particle orbits were important to understand the neutron halo. This phenomenon is called continuum coupling.

The three body model calculation including the continuum states, where the relative motion among $^{9}\mathrm{Li} + n + n$ clusters were solved, established a comprehensive description of two valence neutrons in the halo and skin structures [157, 158]. In the model, the two-neutron density distributions were shown for $^{11}\mathrm{Li} = {}^{9}\mathrm{Li} + n + n$ and $^{6}\mathrm{He} = {}^{4}\mathrm{He} + n + n$. The authors found two types of two-neutron configurations are enable in these systems. One is the BCS-type configuration, which have been already investigated in the mean field theories, and the other is the di-neutron configuration, where the two neutrons are located close to each other. Such di-neutron configurations dominate in both ^{11}Li and ^{6}He. In these systems, the di-neutron configuration is specified as a dominant $S = 0$ component in the LS-coupling scheme and a long-tail amplitude about a distance between the core nucleus (^{9}Li, ^{4}He) and the residual two neutrons.

The di-neutron can be considered as one of the cluster structures of two neutrons around the core nuclei. From such a point of view, ^{6,8}He were investigated using AMD and its extensions [159–161]. In these studies, $^{8}\mathrm{He}(0^+_1)$ showed both the $p_{3/2}$ sub-shell closed feature and the LS coupling feature because of the di-neutron correlation. $^{8}\mathrm{He}(0^+_2)$ was also investigated and this state corresponded to the $^{4}\mathrm{He} + 2n + 2n$ state analogous to the 3α structure in $^{12}\mathrm{C}(0^+_2)$. In this state, the two di-neutrons are moving around the ^{4}He core in S-wave with dilute density. Di-neutron correlation, which is $S = 0$ spatial two-neutron correlation, is rather stronger in $^{6}\mathrm{He}(0^+_1)$ than $^{8}\mathrm{He}(0^+_1)$ by seeing two-neutron densities [162].

Kobayashi et al. developed the framework directly treating the di-neutron configurations in the light neutron-rich nuclei [163,164]. In the application to ^{10}Be, the deformation effects of the core nuclei on di-neutron formation were investigated in detail. In this system, the core nucleus is ^{8}Be which is deformable by forming 2α structure. They found that the two neutrons were in the $p_{3/2}$ orbit with the undeformed ^{8}Be core and they favored the di-neutron configuration with the deformed 2α core.

Despite possibility for finding the counterpart of the di-neutron correlation, there are few theories treating proton-neutron correlations in the light nuclei ($A < 30$). Proton-neutron correlations are limitedly discussed in the $A > 30$ region for the $N = Z$ odd-odd nuclei (see Sec. 1.1.1.1). It might be worthwhile to construct the theoretical methods focusing on proton-neutron correlations in the light nuclei considering di-neutron correlations are different from two-neutron correlations.

1.3.4 Light $N = Z$ odd-odd nuclei

The $N = Z$ odd-odd nuclei (^{6}Li, ^{10}B, ^{14}N, ^{18}F, ^{22}Na, ^{26}Al) have not been paid attention. However, as we have seen above, the counterpart of di-neutron correlation in proton-neutron correlations may be found in these nuclei. Moreover, the relation between the deformation and the Gamow-Teller transition can be discussed as is done in heavier nuclei (see Sec. 1.2.1.2). In the light nuclei, the deformation accompanied by clusters and the GT transition will relate to each other.

Chapter 2

Theoretical methods in the light $N = Z$ odd-odd nuclei

In this chapter, I introduce the methods used in this thesis. An extension of the antisymmtrized molecular dynamics (AMD) is constructed in the first section. In the preceding sections, I formulate Gamow-Teller transitions and their sum-rule in the extended method. The analysis techniques to investigate proton-neutron correlations in the light nuclei are also given.

2.1 Isospin-projected AMD+GCM

The isospin symmetry is explicitly broken in nuclei because of charge-dependent interaction such as Coulomb force. However, isospin has been approximated as $T \approx |N - Z|/2$, $T_z \approx (N - Z)/2$ in the most of theoretical frameworks considering the low-lying excitations off the $N = Z$ line. On the $N = Z$ line, actually, we can find the competing isoscalar and isovector spectra in the low-lying regions (see Fig. 1.1).

Recently, the density functional theory (DFT) has been extended to study the unique phenomena on the $N = Z$ line including odd-even staggering, pn pairing correlations, and superallowed Fermi β decays. For the first attempt, the density functionals were made by rediagonalization of the Hamiltonian including isospin-breaking terms such as Coulomb force [165]. After that, the method was sophisticated into using isospin projection before the rediagonalizations [166]. This framework was succeeded in evaluatting the Cabibbo-Kobayashi-Maskawa matrix element $|V_{ud}|$ from the ft values of the superallowed Fermi β decays with a precision of better than 0.1% [167, 168]. Nevertheless, there are rooms for further improvements because pn-pairing correlations and particle-hole interactions were not taken into account and the configuration mixing and time-odd current densities in odd-odd nuclei were not considered. The latter problems were solved [169] and the method was applied to calculate the GT transition strengths near the $N = Z$ line [76], where pn correlations had been still ignored.

In the light nuclei, the pn correlations shall be realized as formation of di-nucleon cluster though competitions of $T = 0$ and $T = 1$ states in the low-lying spectra and isospin symmetry-breaking by Coulomb interaction also occur as well as in the heavier nuclei. In order to discuss these types of pn correlations in the $N = Z$ odd-odd nuclei, I extended the AMD combined with the Generator Coordinate Method (GCM) on the quadrupole deformation parameters ($\beta\gamma$-AMD+GCM) [144] to the isospin-projected one before energy variation.

The AMD wavefunction is a Slater determinant of single-particle orbits as in the HF method

$$|\Phi\rangle = \mathcal{A}\,|\phi_1\rangle\,|\phi_2\rangle \cdots |\phi_A\rangle\,, \tag{2.1}$$

where a Gaussian wavepacket is used as the ansatz of a cluster state which contains spatially localized nucleons

$$|\phi_i\rangle = |\boldsymbol{Z}_i\rangle\,|\boldsymbol{\xi}_i\rangle\,|n_i\rangle\,, \tag{2.2}$$

with

$$\langle \boldsymbol{r} \mid \boldsymbol{Z}_i\rangle = \left(\frac{2\nu}{\pi}\right)^{\frac{3}{4}} \exp\left[-\nu\left(\boldsymbol{r} - \frac{\boldsymbol{Z}_i}{\sqrt{\nu}}\right)^2 + \frac{1}{2}\boldsymbol{Z}_i^2\right], \tag{2.3}$$

$$|\boldsymbol{\xi}_i\rangle = \xi_{i\uparrow}\,|\uparrow\rangle + \xi_{i\downarrow}\,|\downarrow\rangle\,, \tag{2.4}$$

$$|n_i\rangle \in \{|p\rangle\,, |n\rangle\}\,. \tag{2.5}$$

Here, $\boldsymbol{Z}_i$ is the centroid in $\mathbb{C}^3$ and real number ν is introduced as the width of the harmonic oscillator potential, in which the $\langle \boldsymbol{r} \mid \boldsymbol{Z}_i = \boldsymbol{0}\rangle$ becomes the ground state. $\xi_{i\uparrow}$ and $\xi_{i\downarrow}$ denote the arbitrary spin parameters in the SU(2) space, but the isospin is fixed into a proton or a neutron in order to conserve the particle numbers Z and N.

The parameters $\{\boldsymbol{Z}_i, \boldsymbol{\xi}_i\}_{i=1,2,\ldots,A}$ are determined by energy variations. The variations should be performed after some projections on the good quantum numbers because the nuclear forces allow to conserve parity π, angular momentum J, and approximately isospin T. In usual cases, the variation after parity projection P^π is applied so as to reproduce the parity-broken intrinsic states. More precisely, the variation after parity and angular momentum projection P^{J^π} is necessary and this is uesd to study the light nuclei comprehensively [170]. However, the competing isoscalar ($T = 0$) and isovector ($T = 1$) spectra in $N = Z$ odd-odd nuclei request to separate isospin T by projection. Hence, I use the variation after parity and isospin projections $P^{\pi T}$ in my framework:

$$\delta\left[\frac{\langle \Phi \mid P^{\pi T\dagger} H P^{\pi T} \mid \Phi\rangle}{\langle \Phi \mid P^{\pi T\dagger} P^{\pi T} \mid \Phi\rangle}\right] = 0. \tag{2.6}$$

The isospin projection is numerically performed in my framework as in DFT [166–168]. However, because no $T > 1$ states have been found in the low-lying stats of $N = Z$ odd-odd nuclei satisfying $A < 30$, I approximate the isospin projection operator as

$$P^T \equiv \frac{1}{2}(1 + \pi^T P_{pn}), \tag{2.7}$$

where π^T is the parameter for separating $T = 0$ and $T = 1$ states with $(-1)^Z$ $(T = 0)$ and $-(-1)^Z$ $(T = 1)$ and P_{pn} is an operator exchanging a proton and a neutron for all nucleons in the $|\Phi\rangle$.

The AMD wavefunction is limited to a single Slater determinant. However, configuration mixing is also necessary to describe collective motions such as deformations and pair formations. The treatment of quadrupole deformation on the AMD was initiated by Suhara et al. [144]. They introduced the constraint on the quadrupole deformation parameter β and γ besides physical Hamiltonian H_0 to obtain the optimum wavefunction for $(\beta, \gamma) = (\beta_a, \gamma_a)$ as

$$\langle H \rangle = \langle H_0 \rangle + \eta \left[(\beta \cos\gamma - \beta_a \cos\gamma_a)^2 + (\beta \sin\gamma - \beta_a \sin\gamma_a)^2 \right], \tag{2.8}$$

where η denotes the sufficiently large positive real number corresponding to the penalty on violating the rule $(\beta, \gamma) = (\beta_a, \gamma_a)$. The definition of β and γ is given as

$$\beta \cos\gamma = \frac{\sqrt{5\pi}}{3} \frac{2\langle z^2 \rangle - \langle x^2 \rangle - \langle y^2 \rangle}{R^2}, \tag{2.9}$$

$$\beta \sin\gamma = \sqrt{\frac{5\pi}{3}} \frac{\langle x^2 \rangle - \langle y^2 \rangle}{R^2}, \tag{2.10}$$

$$R^2 = \frac{5}{3} \left[\langle x^2 \rangle + \langle y^2 \rangle + \langle z^2 \rangle \right]. \tag{2.11}$$

This method is called $\beta\gamma$-AMD, but I use an expectation value on the parity and isospin projected state;

$$\langle \bullet \rangle \equiv \frac{\langle \Phi \,|\, P^{\pi T \dagger} \bullet P^{\pi T} \,|\, \Phi \rangle}{\langle \Phi \,|\, P^{\pi T \dagger} P^{\pi T} \,|\, \Phi \rangle}. \tag{2.12}$$

Hence, I define this method as isospin-projected $\beta\gamma$-AMD ($T\beta\gamma$-AMD).

By superposing the wavefunctions on the $\beta\gamma$-plane, quantum fluctuations of quadrupole deformations are incorporated into the model. To this end, the GCM is performed as a subsequent procedure in the $\beta\gamma$-AMD and the $T\beta\gamma$-AMD. The complete wavefunction for the $(T)\beta\gamma$-AMD combined with GCM ($(T)\beta\gamma$-AMD+GCM) is

$$|\Psi(J^\pi T; M)\rangle = \sum_a \sum_{K=-J}^{J} g_{aK}^{J^\pi T} P_{MK}^J P^\pi P^T \, |\Phi(\beta_a, \gamma_a)\rangle, \tag{2.13}$$

where $g_{aK}^{J^\pi T}$ is the coefficient on the superposition determined by solving the discretized Hill-Wheeler equation [171]:

$$\sum_a \sum_{K=-J}^{J} g_{aK}^{J^\pi T} \left[\mathcal{H}_{bK';aK}^{J^\pi T} - E(J^\pi T) \mathcal{N}_{bK';aK}^{J^\pi T} \right] = 0 \tag{2.14}$$

with the Hamiltonian and norm kernels:

$$\mathcal{H}_{bK';aK}^{J^\pi T} = \left\langle \Phi(\beta_b, \gamma_b) \middle| P_{MK'}^{J\dagger} P^{\pi\dagger} P^{T\dagger} H P_{MK}^J P^\pi P^T \middle| \Phi(\beta_a, \gamma_a) \right\rangle, \tag{2.15}$$

$$\mathcal{N}_{bK';aK}^{J^\pi T} = \left\langle \Phi(\beta_b, \gamma_b) \middle| P_{MK'}^{J\dagger} P^{\pi\dagger} P^{T\dagger} P_{MK}^J P^\pi P^T \middle| \Phi(\beta_a, \gamma_a) \right\rangle. \tag{2.16}$$

2.2 Gamow-Teller transitions

Gamow-Teller transition operator is defined in Eq. (1.1). The expectation value between the initial $|J_i\rangle$ state and the final $|J_f\rangle$ state has the form

$$B(\mathrm{GT}^\pm; J_i \to J_f) = \frac{1}{2J_i + 1} \left| \langle J_f || \sum_i \boldsymbol{\sigma}_i \tau_i^\pm || J_i \rangle \right|^2, \tag{2.17}$$

where the initial and final states correspond to the GCM wavefunctions defined in Eq. (2.13) in the preceding chapters.

Gamow-Teller transition strengths satisfy the Ikeda sum-rule [172]

$$\sum_n B(\mathrm{GT}^-; 0_1^+ 1 \to 1_n^+ 0) = 3(N-Z) \tag{2.18}$$

for the given nuclei having the neutron and proton numbers of N and Z. The proof of this theorem is given as follows. The summation of the GT strengths is transformed as

$$\begin{aligned} \sum_n B(\mathrm{GT}^\pm; 0_1^+ 1 \to 1_n^+ 0) &= \sum_n \langle 0_1^+ 1 | \boldsymbol{Y}^\mp | 1_n^+ 0 \rangle \langle 1_n^+ 0 | \boldsymbol{Y}^\pm | 0_1^+ 1 \rangle \\ &= \langle 0_1^+ 1 | \boldsymbol{Y}^\mp \boldsymbol{Y}^\pm | 0_1^+ 1 \rangle . \end{aligned}$$

Therefore, the left side of the sum-rule has the form

$$\begin{aligned} & \sum_n B(\mathrm{GT}^-; 0_1^+ 1 \to 1_n^+ 0) \\ = \; & \langle 0_1^+ 1 | \boldsymbol{Y}^+ \boldsymbol{Y}^- | 0_1^+ 1 \rangle - \langle 0_1^+ 1 | \boldsymbol{Y}^- \boldsymbol{Y}^+ | 0_1^+ 1 \rangle + \sum_n B(\mathrm{GT}^+; 0_1^+ 1 \to 1_n^+ 0) \\ = \; & 3(N-Z) + \sum_n B(\mathrm{GT}^+; 0_1^+ 1 \to 1_n^+ 0). \end{aligned}$$

If the initial nuclei have the condition $N > Z$, the GT^+ strengths are sufficiently small because the final states of the protons are already occupied by the neutrons. Thus, the second term of the equation can be ignored and we obtain Eq. (2.18).

2.3 Proton-neutron pair densities

Proton-neutron correlations in the light nuclei might be realized as cluster formations of the proton-neutron pairs. These types of two-body correlations can be seen in the two-body densities corresponding proton-neutron channels. In this thesis, I use the two-body density for the given intrinsic wavefunction:

$$\rho_{ST}(\boldsymbol{r}) = \frac{\left\langle \Phi(\beta,\gamma) \,\middle|\, P^{T\dagger} \hat{\rho}_{ST}(\boldsymbol{r}) P^T \,\middle|\, \Phi(\beta,\gamma) \right\rangle}{\left\langle \Phi(\beta,\gamma) \,\middle|\, P^{T\dagger} P^T \,\middle|\, \Phi(\beta,\gamma) \right\rangle}, \tag{2.19}$$

where

$$\hat{\rho}_{ST}(\boldsymbol{r}) = \sum_{ij} \hat{P}_{ij}^S \hat{P}_{ij}^T \delta(\boldsymbol{r} - \hat{\boldsymbol{r}}_i)(\boldsymbol{r} - \hat{\boldsymbol{r}}_j). \tag{2.20}$$

Because the core nuclei have same numbers of $S=0, T=1$ and $S=1, T=0$ pairs in most cases, the difference $\rho_{NN}(\boldsymbol{r}) \equiv \rho_{10}(\boldsymbol{r}) - \rho_{01}(\boldsymbol{r})$ correspond to valence NN pair densities. In this definition, $S=0, T=1$ pairs are found in negative regions and $S=1, T=0$ pairs are found in positive regions.

Chapter 3

Validity of the $T\beta\gamma$-AMD+GCM

In order to check validity of the $T\beta\gamma$-AMD+GCM, I applied the method to ^{10}B, which is the lightest deformed $N = Z$ odd-odd nuclei. The issues needing confirmation are divided into three points; (i) the isospin projection is necessary or not, (ii) the approximation on isospin projection operator is appropriate or not, and (iii) the low-lying spectra in ^{10}B are reproduced or not.

3.1 Hamiltonian

The Hamiltonian used in this section has the form

$$H = K - K_{\mathrm{cm}} + V_{\mathrm{central}} + V_{\ell s} + V_{\mathrm{Coulomb}}, \tag{3.1}$$

where the K, K_{cm}, V_{central}, $V_{\ell s}$, and V_{Coulomb} are kinetic energy, kinetic energy of center of mass motion, central force, spin-orbit force, and Coulomb force, respectively. As the central force, I adopt the Volkov No.2 force [173]

$$V_{\mathrm{central}} = \sum_{i<j} \sum_{k=1,2} v_k \exp\left[-\left(\frac{\boldsymbol{r}_i - \boldsymbol{r}_j}{a_k}\right)^2\right] \left(W + BP_\sigma - HP_\tau - MP_\sigma P_\tau\right), \tag{3.2}$$

with the parameters of $v_1 = -60.65$ MeV, $v_2 = 61.14$ MeV, $a_1 = 1.80$ fm, and $a_2 = 1.01$ fm. $W = 0.40$ and $M = 0.60$ are determined α-α scattering phase shift. $B = 0.06$ and $H = 0.06$ are modified to reproduce relative energies between $T = 0$ and $T = 1$ spectra in [174]. These corrections correspond to changing $T = 0$, $S = 1$ interaction to $T = 1$, $S = 0$ interaction with the ratio $f = 1.27$. The spin-orbit interaction is based on the Gaussian three-range soft-core (G3RS) force [175, 176]

$$V_{\ell s} = \sum_{i<j} \sum_{k=1,2} u_k \exp\left[-\left(\frac{\boldsymbol{r}_i - \boldsymbol{r}_j}{b_k}\right)^2\right] \frac{1+P_\sigma}{2}\frac{1+P_\tau}{2} \boldsymbol{\ell}_{ij} \cdot \boldsymbol{s}_{ij}, \tag{3.3}$$

where

$$\boldsymbol{\ell}_{ij} = (\boldsymbol{r}_i - \boldsymbol{r}_j) \times \frac{\boldsymbol{p}_i - \boldsymbol{p}_j}{2} \tag{3.4}$$

and

$$\boldsymbol{s}_{ij} = \boldsymbol{s}_i + \boldsymbol{s}_j. \tag{3.5}$$

The parameters are $b_1 = 0.60$ fm, $b_2 = 0.447$ fm, and $u_1 = -u_2 = 1300$ MeV which were modified to fit the energy difference between $3/2^-$ and $1/2^-$ states in ^{9}Be [174].

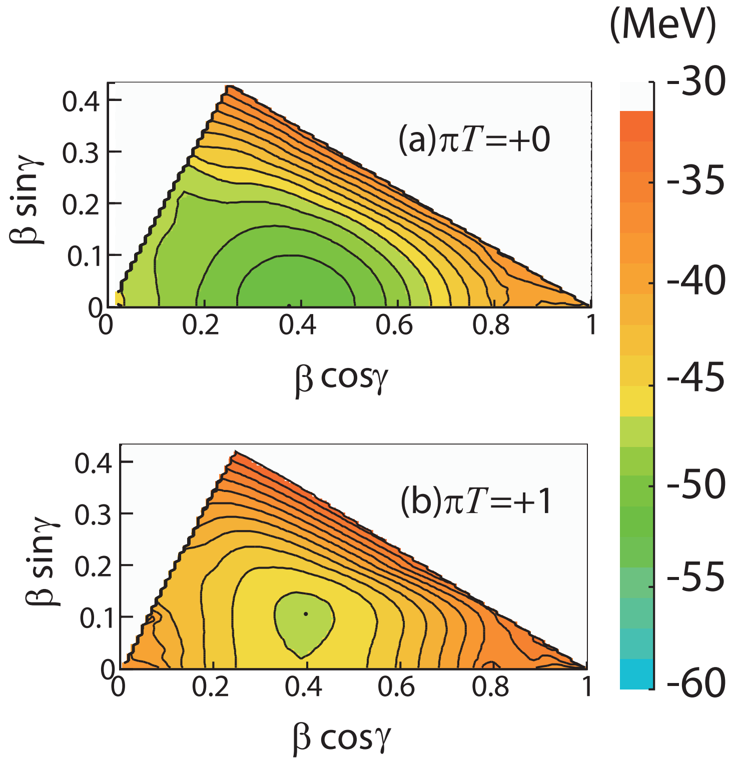

Figure 3.1: Energy surfaces on the $\beta\gamma$ plane obtained by the $T\beta\gamma$-AMD. The panel (a) and (b) refer to the $T = 0$ and $T = 1$ energy surfaces of ^{10}B . The energy minimum of each energy surface is shown by a dot.

3.2 Results

After performing the $T\beta\gamma$-AMD, I obtained the energy surfaces on the $\beta\gamma$ parameters for each isospin $T = 0$ and $T = 1$. The figure 3.1 shows the energy surfaces of the positive parity states in ^{10}B. The energy minimum is found at prolately deformed point $(\beta, \gamma) = (0.38, 0°)$ in the $\pi = +, T = 0$ surface and that is found at $(\beta, \gamma) = (0.41, 14.0°)$ in the $\pi = +, T = 1$ surface. It is expected that quantum fluctuations along deformation play crucial role in the low-lying states of ^{10}B because the states on the surfaces are smoothly changed along β and γ.

When I perform the energy variations before isospin projection, I cannot obtain such proper energy surfaces. In the figure 3.2 (a), the $\pi = +$ energy surface obtained without isospin projection is shown. The energy minimum is located near that in the $\pi = +, T = 0$ surface, but the surface is drastically changed between small and large β region. Even if I project the $\pi = +$ states to the isospin eigenstates, the smoothly connected surfaces cannot be obtained as shown in the figure 3.2 (b)(c). The major reason why the $\beta\gamma$-AMD cannot work in the $N = Z$ odd-odd system like ^{10}B is isospin competition. This is confirmed by checking the percentages of $T = 1$ states in the intrinsic wavefunctions obtained with the $\beta\gamma$-AMD shown in the figure 3.3. In the largely deformed states, the proton-neutron pair spatially develops isolated from the residual nuclei. As a result, the states without isospin projection contain the $T = 0$ and $T = 1$ pair with the same

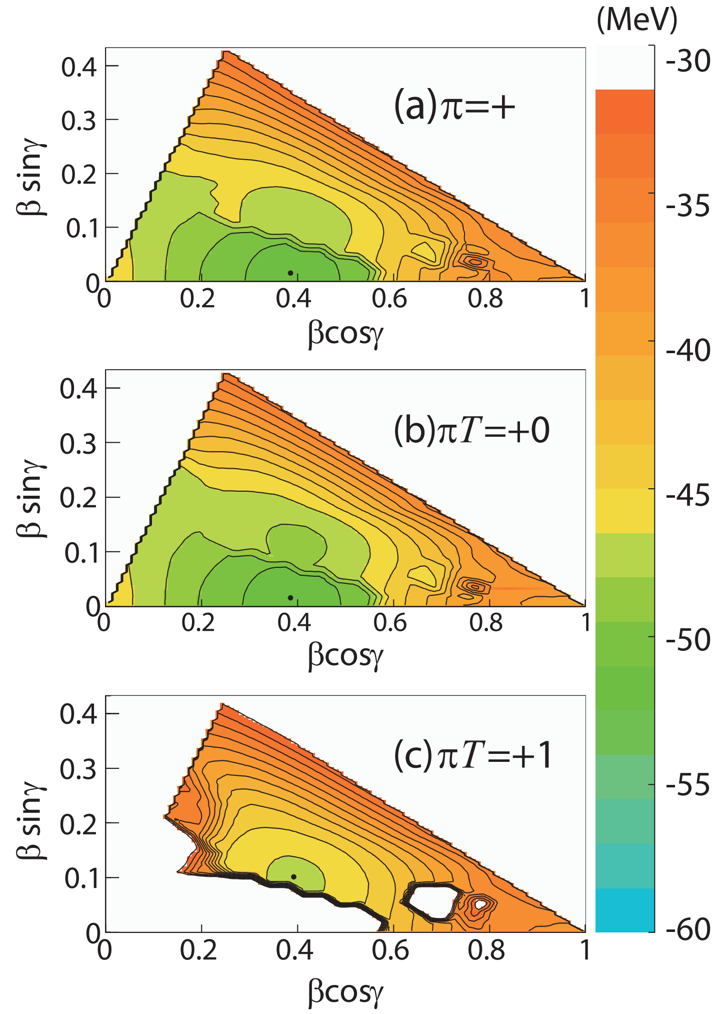

Figure 3.2: Energy surfaces of ^{10}B on the $\beta\gamma$ plane obtained with the $\beta\gamma$-AMD. (a) The $\pi = +$ energy surface without the isospin projection, and (b) $T = 0$ and (c) $T = 1$ projected $\pi = +$ energy surfaces are shown. The energy minimum of each energy surface is shown by a dot.

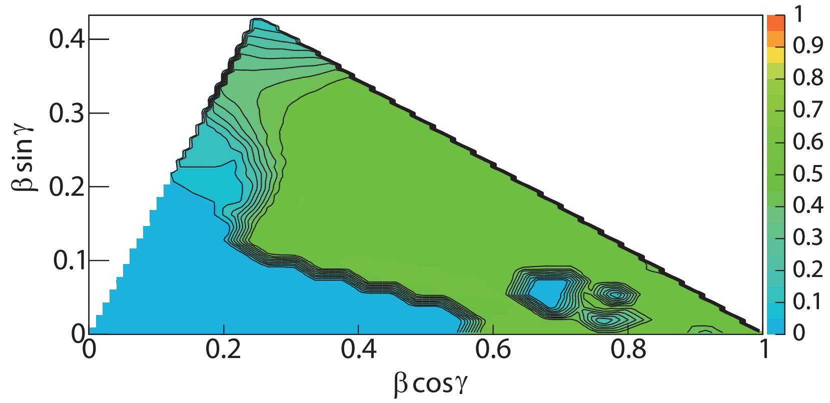

Figure 3.3: The ratios of the norms for the $\pi T = +1$ states to those for the $\pi = +$. These values are calculated using the $\beta\gamma$-AMD on the $\beta\gamma$ plane for ^{10}B.

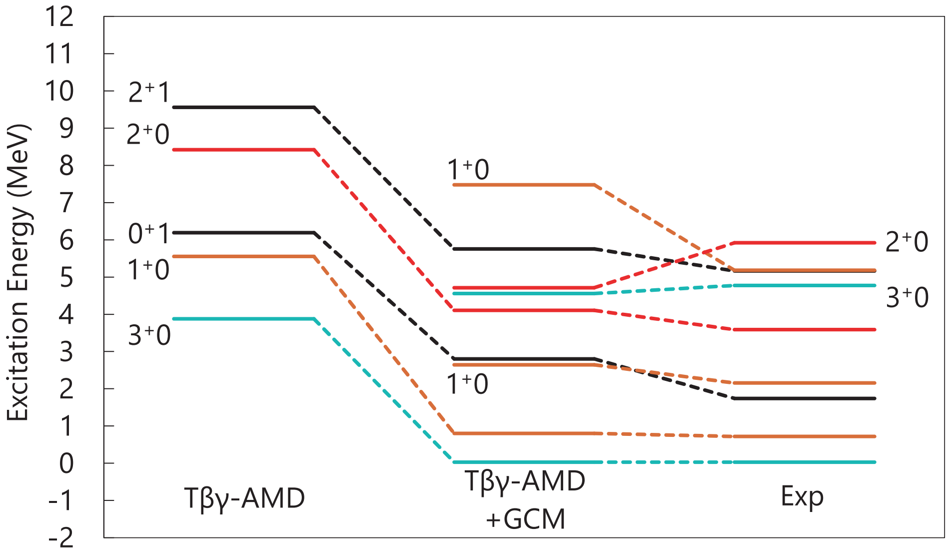

Figure 3.4: Spectra of ^{10}B with the $T\beta\gamma$-AMD+GCM. The experimental data are also shown (Ref. [177]). The minimum energies in the J^π-projected energy surfaces of the $T\beta\gamma$-AMD measured from the 3_1^+0 energy of the $T\beta\gamma$-AMD+GCM are also shown.

amplitudes preserving SU(4) symmetry. On the other hand, the $T = 0$ states dominate the small deformed states because of intrinsic spins of the proton-neutron pairs that allow additional binding energy of spin-orbit interactions.

The approximation in isospin projection operator (2.7) sufficiently works. I evaluated the expectation values T^2 of the states from the $T\beta\gamma$-AMD and obtained $\langle T^2 \rangle < 0.070$ for the $T = 0$ states and $2 < \langle T^2 \rangle < 2.015$ for the $T = 1$ states. This is reasonable to recognize the operator (2.7) as isospin projection in the AMD.

The energy spectra in the low-lying region are well reproduced (see Fig. 3.4). There are isovector states (0_1^+1, 2_1^+1) and isoscalar states ($1_{1,2,3}^+0$, $2_{1,2}^+0$, $3_{1,2}^+0$) below 6 MeV. The level orderings in each isospin are reproduced except for the 1_3^+0. The 0_1^+1 state is an isobaric analog state of ^{10}Be(0_1^+1). The ground state of 3_1^+0 is notable one for $N = Z$ odd-odd nuclei because this state is the $[jj]_{J=2j;T=0}$ state with $j = 3/2$ that is systematically found high-spin state in heavier nuclei (see Sec. 1.1.1.1). The $1_{1,2,3}^+0$ states can be candidates for the deuteron-type proton-neutron correlation which is considered as $[jj]_{J=1;T=0}$ in the heavier nuclei.

Chapter 4

Gamow-Teller transition strengths in the light $N = Z$ odd-odd nuclei

In this chapter, I show the calculated values of Gamow-Teller transition strengths by using $T\beta\gamma$-AMD+GCM in the light $N = Z$ odd-odd nuclei. Spectra, electro-magnetic moments, and electro-magnetic transition strengths are also shown in order to check reliability for each result.

4.1 Hamiltonian

I use the same Hamiltonian as that in the previous chapter (see Sec. 3.1) but the parameters are modified to study the p-shell and sd-shell nuclei systematically. I use $B = H = 0.125$ ($f = 1.67$) for ^{6}Li that reproduces S-wave NN scattering lengths both in the $T = 0$ and $T = 1$ channel and $B = H = 0.06$ ($f = 1.27$) for ^{10}B, ^{14}N, and ^{22}Na, which are same as the previous parameters.

4.2 p-shell nuclei

I have obtained the energy spectra for the p-shell odd-odd nuclei as shown in the figure 4.1. Those of ^{6}Li and ^{10}B are consistent with the experimental data but that of ^{14}N has many inconsistent results, that is, missing $0^+_2 1$, $1^+_3 0$, $3^+_{1,2} 0$, $5^+_1 0$, and $2^+_2 0$. These low-lying spectra in ^{14}N are also calculated with the NCSM using the interaction from the chiral effective theory but they are not sufficiently reach to reproducing experimental spectra (see Sec. 1.2.2). However, the obtained spectra except for $3^+_1 0$ apparently show agreement with experimental ones, thus there are rooms to discuss the details of these states.

I show the nuclear properties in Table 4.1. Because GT transitions are sensitive to the spin configurations, it should be examined whether $T\beta\gamma$-AMD+GCM can reproduce magnetic moments μ and $M1$ transition strengths. μ of ^{6}Li($1^+_1 0$), ^{10}B($3^+_1 0, 1^+_1 0$), and ^{14}N($1^+_1 0$) agree with the experimental data. $B(M1; 0^+_1 1 \to 1^+_1 0)$ of ^{6}Li is well reproduced but $B(M1; 0^+_1 1 \to 1^+_{1,2} 0)$ of ^{10}B do not quantitatively agree with the experimental data. However, $B(\mathrm{GT})$ is sufficiently reproduced to discuss relative strengths because $B(M1; 0^+_1 1 \to 1^+_1 0)$ is larger than $B(M1; 0^+_1 1 \to 1^+_2 0)$. I have also obtained qualitatively consistent results for ^{14}N that $B(M1; 0^+_1 1 \to 1^+_2 0)$ is larger than $B(M1; 0^+_1 1 \to 1^+_1 0)$ and

Table 4.1: Binding energies, μ and Q moments, and $M1$ and $E2$ transition strengths of ^{6}Li, ^{10}B, and ^{14}N. The calculated values obtained by $T\beta\gamma$-AMD+GCM are shown. For comparison, the values calculated by shell models are shown. Experimental data are taken from [177–179].

Observable	$T\beta\gamma$-AMD+GCM	SM	Exp
^{6}Li			
$\lvert E(1_1^+0)\rvert$ (MeV)	29.55	31.036 [180]	31.994
$\mu(1_1^+0)$ (μ_N)	0.87	0.840 [180]	0.82205
$Q(1_1^+0)$ (fm^2)	0.09	-0.025 [180]	-0.0818(17)
$B(E2; 3_1^+0 \to 1_1^+0)$	3.79	3.040 [180]	10.7(8)
$B(M1; 0_1^+1 \to 1_1^+0)$	13.73	15.374 [180]	15.4(3)
$B(E2; 2_1^+0 \to 1_1^+0)$	5.15	3.129 [180]	4.4(23)
$B(M1; 2_1^+1 \to 1_1^+0)$	0.01	0.113 [180]	0.15(3)
^{10}B			
$\lvert E(3_1^+0)\rvert$ (MeV)	60.35	60.567 [180]	64.751
$\mu(3_1^+0)$ (μ_N)	1.83	1.847 [180]	1.8006
$\mu(1_1^+0)$ (μ_N)	0.84	0.802 [180]	0.63(12)
$Q(3_1^+0)$ (fm^2)	8.45	5.682 [180]	8.47(6)
$B(E2; 1_1^+0 \to 3_1^+0)$	4.03	1.959 [180]	4.147(20)
$B(M1; 0_1^+1 \to 1_1^+0)$	14.98	14.3 [181]	7.5(34)
$B(M1; 1_2^+0 \to 0_1^+1)$	0.05	0.09 [182]	0.192(20)
$B(E2; 1_2^+0 \to 1_1^+0)$	9.23	3.384 [180]	15.6(17)
$B(E2; 1_2^+0 \to 3_1^+0)$	2.02	1.010 [180]	1.70(20)
$B(E2; 2_1^+0 \to 3_1^+0)$	0.34	1.0 [182]	1.2(4)
$B(E2; 3_2^+0 \to 1_1^+0)$	10.56	3.543 [180]	19.7(17)
$B(M1; 2_1^+1 \to 2_1^+0)$	1.84	3.1 [182]	2.52(68)
$B(M1; 2_1^+1 \to 1_2^+0)$	2.60	2.0 [182]	3.06(82)
$B(M1; 2_1^+1 \to 1_1^+0)$	0.31	0.2 [182]	0.32(9)
^{14}N			
$\lvert E(1_1^+0)\rvert$ (MeV)	108.60	108.41 [82]	104.66
$\mu(1_1^+0)$ (μ_N)	0.34	0.347 [82]	0.40376
$Q(1_1^+0)$ (fm^2)	0.53	1.19 [82]	1.93(8)
$B(M1; 0_1^+1 \to 1_1^+0)$	0.76	0.29 [82]	0.047(2)
$B(M1; 1_2^+0 \to 0_1^+1)$	3.72	–	1.8(11)
$B(E2; 1_2^+0 \to 1_1^+0)$	3.25	–	4.4(24)
$B(E2; 2_1^+0 \to 1_1^+0)$	2.95	–	3.6(8)
$B(M1; 2_1^+1 \to 2_1^+0)$	4.65	–	1.7(3)
$B(M1; 2_1^+1 \to 1_1^+0)$	0.00	–	0.59(4)

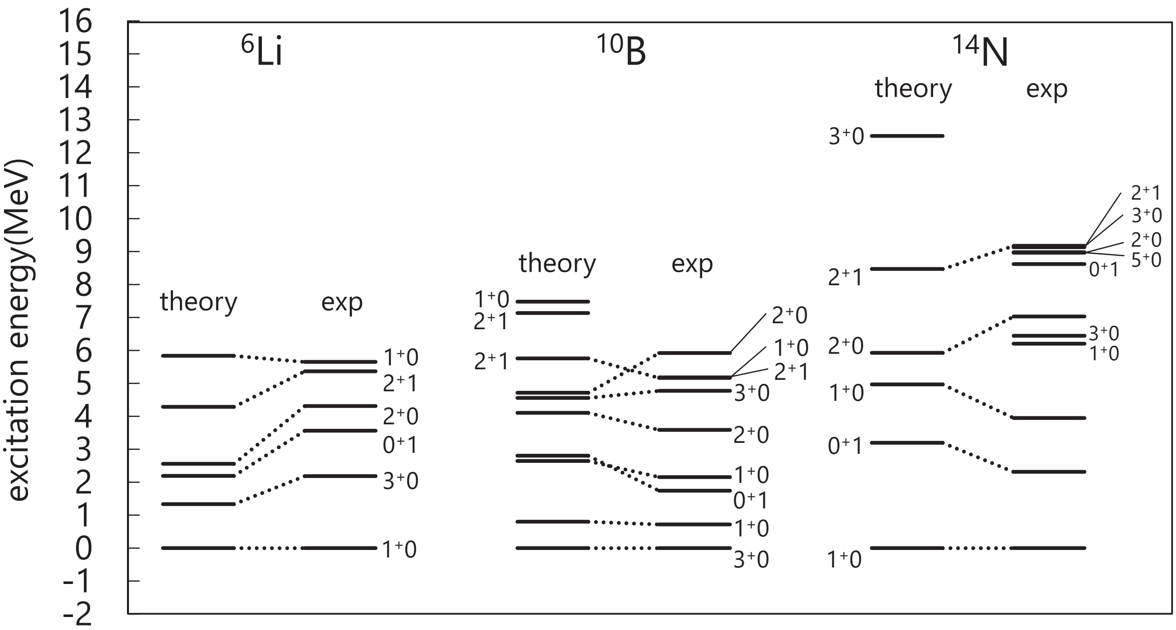

Figure 4.1: Spectra of ^{6}Li, ^{10}B, and ^{14}N calculated by $T\beta\gamma$-AMD+GCM and those of the experimental data [177–179].

$B(M1; 2_1^+1 \to 2_1^+0)$ is larger than $B(M1; 2_1^+1 \to 1_1^+0)$.

One of the advantages to use the $T\beta\gamma$-AMD to the p-shell nuclei is that the method offers the model spaces to describe deformation as cluster formation. This can be seen in the quadrupole moments Q and $B(E2)$ values. $Q(3_1^+0)$ is a close value to an experimental datum than that from the shell model. Moreover, it is succeeded in reproducing $B(E2; 1_1^+0 \to 3_1^+0)$, $B(E2; 1_2^+0 \to 1_1^+0)$, $B(E2; 1_2^+0 \to 3_1^+0)$, and $B(E2; 3_2^+0 \to 1_1^+0)$ though these values from the shell models are underestimated to the experimental data. This discrepancy is majorly from the clustering of ^{10}B into the $2\alpha + pn$ states and the shell model spaces is even insufficient to describe such strong correlation.

In the table 4.2, I show the GT strengths defined in Eq. (2.17). In the table, some final states exhaust the large fraction of the sum rule value $\sum_n B(\mathrm{GT}; 0_1^+1 \to 1_n^+0) = 3(N-Z) = 6$. This indicates that these final states approximately equal to the initial states rotated in the spin-isospin SU(4) space. These pairs of the $T=1$ states in $N=Z+2$ nuclei and the $T=0$ states in the $N=Z$ odd-odd nuclei are found as $[^6\mathrm{He}(0_1^+1), {}^6\mathrm{Li}(1_1^+0)]$, $[^{10}\mathrm{Be}(0_1^+1), {}^{10}\mathrm{B}(1_1^+0)]$, and $[^{14}\mathrm{C}(0_1^+1), {}^{14}\mathrm{N}(1_2^+0)]$ corresponding to the LeSGT in the $f_{7/2}$-shell nuclei.

The transition $B(\mathrm{GT}; {}^6\mathrm{He}(0_1^+1) \to {}^6\mathrm{Li}(1_1^+0))$ exhausts 88.5% of the sum rule though the strength to $^6\mathrm{Li}(1_2^+0)$ is weak enough. From the excited state $^6\mathrm{He}(2_1^+1)$, the strengths are fragmented into $^6\mathrm{Li}(1_2^+0, 2_1^+0, 3_1^+0)$. Concentration of the strengths is also found in $^{10}\mathrm{Be}(0_1^+1) \to {}^{10}\mathrm{B}(1_1^+0)$ exhausting 82.5% of the sum rule. Two excited sates $^{10}\mathrm{Be}(2_{1,2}^+1)$ have their counterparts. The GT strengths from $^{10}\mathrm{Be}(2_1^+1)$ are fragmented into $^{10}\mathrm{B}(1_2^+0, 2_{1,2}^+0, 3_2^+0)$ and those from $^{10}\mathrm{Be}(2_2^+1)$ are fragmented into $^{10}\mathrm{B}(1_3^+0, 2_{1,2}^+0, 3_1^+0)$. The strength from $^{14}\mathrm{C}(0_1^+1)$ is not concentrated into the ground state $^{14}\mathrm{N}(1_1^+0)$ but into the excited state $^{14}\mathrm{N}(1_2^+0)$. This strength is upto 72.0% of the sum rule value. However, the anomalously small $B(\mathrm{GT})$ value for $^{14}\mathrm{C}(0_1^+1) \to {}^{14}\mathrm{N}(1_1^+0)$ is not reproduced (see Sec. 1.2.2) though this

Table 4.2: Gamow-Teller transition strengths of ^{6}He $\to$ ^{6}Li, ^{10}Be $\to$ ^{10}B, and ^{14}C $\to$ ^{14}N. Calculated values of $B(\mathrm{GT})$ defined in Eq. (2.17) are shown. For comparison, the $B(\mathrm{GT})$ values calculated by shell models are shown. Experimental data are taken from [179, 183–186]. The values in the parenthesis are for the mirror transitions.

Initial→Final	$T\beta\gamma$-AMD+GCM	SM	Exp
^{6}He $\to$ ^{6}Li			
$0^+_1 1 \to 1^+_1 0$	5.31	5.213 [180]	4.809(8)
$0^+_1 1 \to 1^+_2 0$	0.00	–	–
$2^+_1 1 \to 1^+_1 0$	0.01	–	–
$2^+_1 1 \to 3^+_1 0$	0.97	–	–
$2^+_1 1 \to 2^+_1 0$	1.00	–	–
$2^+_1 1 \to 1^+_2 0$	1.10	–	–
^{10}Be $\to$ ^{10}B			
$0^+_1 1 \to 1^+_1 0$	4.95	(4.331) [180]	(3.5101(57))
$0^+_1 1 \to 1^+_2 0$	0.15	(0.497) [187]	(<0.813)
$0^+_1 1 \to 1^+_3 0$	0.00	–	–
$2^+_1 1 \to 3^+_1 0$	0.63	0.092 [180]	0.11(4)
$2^+_1 1 \to 1^+_1 0$	0.06	–	–
$2^+_1 1 \to 1^+_2 0$	0.81	–	–
$2^+_1 1 \to 2^+_1 0$	0.77	–	–
$2^+_1 1 \to 3^+_2 0$	1.71	–	–
$2^+_1 1 \to 1^+_3 0$	0.26	–	–
$2^+_1 1 \to 2^+_2 0$	0.86	–	–
$2^+_2 1 \to 3^+_1 0$	1.54	1.807 [180]	1.3(2)
$2^+_2 1 \to 1^+_1 0$	0.01	–	–
$2^+_2 1 \to 1^+_2 0$	0.23	–	–
$2^+_2 1 \to 2^+_1 0$	0.71	–	–
$2^+_2 1 \to 3^+_2 0$	0.26	–	–
$2^+_2 1 \to 1^+_3 0$	0.82	–	–
$2^+_2 1 \to 2^+_2 0$	0.79	–	–
^{14}C $\to$ ^{14}N			
$0^+_1 1 \to 1^+_1 0$	0.30	0.0175 [187]	$3.53(2) \times 10^{-6}$
		1.69×10^{-4} [82]	
$0^+_1 1 \to 1^+_2 0$	4.32	(4.445) [187]	2.76(11)
$2^+_1 1 \to 1^+_1 0$	1.13	–	0.27
$2^+_1 1 \to 2^+_1 0$	1.77	–	–
$2^+_1 1 \to 3^+_1 0$	2.35	–	–

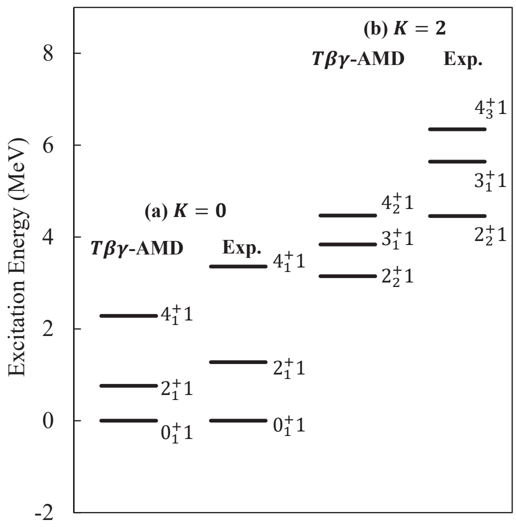

Figure 4.2: The spectra of ^{22}Ne in the $K = 0, 2$ bands below 8 MeV. For each band, calculated and experimental spectra [188] are shown in the left and right, respectively.

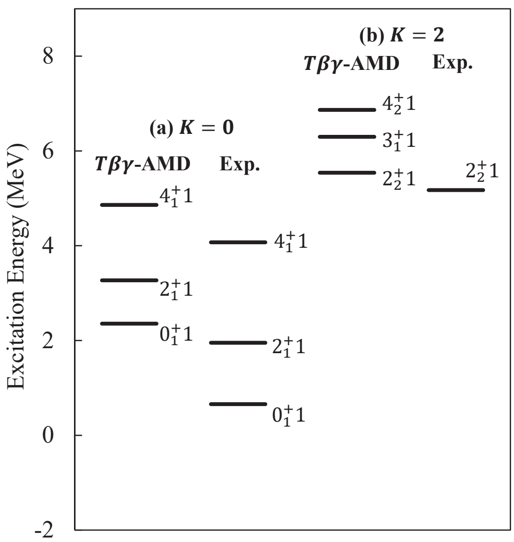

Figure 4.3: The spectra of ^{22}Na in the $T = 1$ $K = 0, 2$ bands below 8 MeV. For each band, calculated and experimental spectra [188] are shown in the left and right, respectively.

strength is rather smaller than that to ^{14}N(1_2^+0), but it is not quantitatively insufficient. The ground state ^{14}N(1_1^+0) corresponds to ^{14}C(2_1^+1) together with ^{14}N($2_1^+0, 3_1^+0$).

4.3 ^{22}Ne and ^{22}Na

4.3.1 Spectra and nuclear properties

Firstly, I show the energy spectra of ^{22}Ne and ^{22}Na in the low-lying states ($E < 8$ MeV). In the spectra of $T = 1$ states in ^{22}Na (Fig. 4.3), there are $K = 0$ and $K = 2$ bands in the low-lying states. This is analog feature of ^{22}Ne (Fig. 4.2) which contains only $T = 1$ states.

There are three bands with $K = 0, 1,$ and 3 in the $T = 0$ spectra (see Fig. 4.4). The ground state shows $K = 3$ nature and 3_1^+0, 4_1^+0, 5_1^+0 states are members of this band. The internal band $E2$ transitions $5_1^+0 \rightarrow 4_1^+0$, $4_1^+0 \rightarrow 3_1^+0$, and $5_1^+0 \rightarrow 3_1^+0$ are significantly strong as shown in Table 4.3 because of prolate deformation of the $K = 3$ band head. The wavefunction of the band head has the largest overlap of 89.7% with the $(\beta, \gamma) = (0.29, 0.19)$ state which contains dominant $K = 3$ component rather than the other K values.

The 1_1^+0 state is the $K = 0$ bandhead with rotational members of 1_1^+0, 3_2^+0, and 5_2^+0 which show the strong internal band $E2$ transitions $5_2^+0 \rightarrow 3_2^+0$ and $3_2^+0 \rightarrow 1_1^+0$ (see Table 4.3). $B(E2; 3_2^+0 \rightarrow 1_1^+0)$ is consistent with the experimental datum, but $B(E2; 5_2^+0 \rightarrow 3_2^+0)$ seems to correspond to the experimental $B(E2; 5_3^+0 \rightarrow 3_2^+0)$. The bandhead 1_1^+0 state has the largest overlap of 82.7% with the $(\beta, \gamma) = (0.31, 0.11)$ state which has dominant $K = 0$ component.

Table 4.3: The electric and magnetic moments and transition strengths in ^{22}Na. The calculated Q ($e\,\mathrm{fm}^2$) and μ (μ_N) moments, $B(E2)$ ($e^2\,\mathrm{fm}^4$), and $B(M1)$ (μ_N^2) are shown together with the experimental data from [188] and with the shell-model values from [189]. The binding energy (MeV) of the ground state ^{22}Na($3^+_1 0$) is also shown.

Observable	SM	$T\beta\gamma$-AMD +GCM	Exp
binding energy	–	173.041	174.1456
$Q(3^+_1 0)$	–	17.66	18.0(11)
$\mu(3^+_1 0)$	–	1.784	1.746(3)
$\mu(1^+_1 0)$	–	0.622	0.535(10)
$K=3$			
$B(E2; 5^+_1 0 \to 4^+_1 0)$	76.9	49.9	58(18)
$B(E2; 4^+_1 0 \to 3^+_1 0)$	87.9	56.8	91(3)
$B(E2; 5^+_1 0 \to 3^+_1 0)$	20.1	12.0	19.0(15)
$B(M1; 4^+_2 1 \to 5^+_1 0)$	–	2.29	–
$B(M1; 3^+_1 1 \to 4^+_1 0)$	–	3.35	–
$B(M1; 2^+_2 1 \to 3^+_1 0)$	–	3.97	–
$K=0$			
$B(E2; 3^+_2 0 \to 1^+_1 0)$	65.9	35.5	69(7)
$B(E2; 5^+_2 0 \to 3^+_2 0)$	51.3	41.2	51(22); $5^+_3 0 \to 3^+_2 0$
$B(M1; 0^+_1 1 \to 1^+_1 0)$	5.37	5.00	4.96(18)
$B(M1; 2^+_1 1 \to 3^+_2 0)$	–	3.28	–
$B(M1; 4^+_1 1 \to 3^+_2 0)$	2.33	0.27	> 5.37
$B(M1; 4^+_1 1 \to 5^+_2 0)$	3.06	3.02	2.2(9); $4^+_1 1 \to 5^+_3 0$
$K=1$			
$B(E2; 2^+_1 0 \to 1^+_2 0)$	–	43.9	–
$B(E2; 3^+_3 0 \to 2^+_1 0)$	–	10.2	–
$B(E2; 3^+_3 0 \to 1^+_2 0)$	–	13.9	–
$B(E2; 4^+_2 0 \to 3^+_3 0)$	–	14.0	–
$B(E2; 4^+_2 0 \to 2^+_1 0)$	65.9	24.4	–
$B(M1; 0^+_1 1 \to 1^+_2 0)$	4.46	4.12	4.3(13)
$B(M1; 2^+_1 1 \to 2^+_1 0)$	–	2.21	1.22(16)
$K=0,1$ inter-band			
$B(E2; 2^+_1 0 \to 1^+_1 0)$	–	4.1	0.10(7)
$B(E2; 3^+_2 0 \to 1^+_2 0)$	–	1.7	–
$B(E2; 1^+_1 0 \to 1^+_2 0)$	–	7.81	–
$B(E2; 2^+_1 0 \to 3^+_2 0)$	–	9.42	–

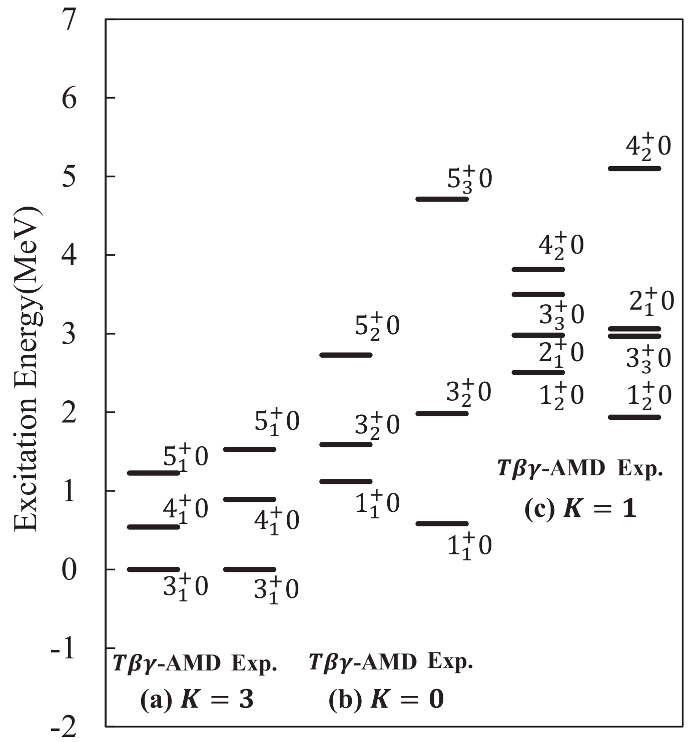

Figure 4.4: The spectra of ^{22}Na in the $T = 0$ $K = 0, 1, 3$ bands below 8 MeV. Calculated and experimental spectra [188] are shown in the left and right, respectively.

The 1_2^+0 and 2_1^+0 states make $K = 1$ band with strong $B(E2; 2_1^+0 \to 1_2^+0)$. The bandhead 1_2^+0 has the largest overlap of 76.6% with the $(\beta, \gamma) = (0.29, 0.19)$ state containing dominant $K = 1$ component. The deformation parameters for these three bandheads 3_1^+0, 1_1^+0, and 1_2^+0 are almost similar each other. This indicates that the low-lying spectra and band structures are dominated by spin configuration of valence proton-neutron pairs. Supporting this fact, the inter-band $E2$ transitions are significantly small as shown in Table 4.3.

$M1$ transition strengths and their reproductions must be carefully checked because these values directly correspond to the spin configurations related to GT transitions. (see Sec. 4.2). The $M1$ transition strengths are compared with the shell-model calculations and the experimental data (see Table 4.3). Many strong $M1$ transitions from the $T = 1, K = 0$ band to the $T = 0, K = 0, 1$ band are found and they are consistent with the shell model and the experiment except for the $B(M1; 4_1^+1 \to 3_2^+0)$.

The Gamow-Teller transition operator is defined in Eq. (2.17). This is a rotational operator in the spin-isospin spaces, but in principle, the spin operator $\boldsymbol{\sigma}$ can be coupled to orbital angular momenta because of spin-orbit interactions. As a result, if the core nuclei are strongly deformed system like ^{10}B and ^{22}Na, the rotation in the spin-isospin space can be partially broken into the transitions corresponding to the spin-flip operator $\sigma_\pm \propto \sigma_z \pm i\sigma_y$ causing $\Delta S_z = 1$ and the spin-conserving operator $\sigma_0 = \sigma_z$ causing $\Delta S_z = 0$.

The $B(\mathrm{GT}; {}^{22}\mathrm{Ne} \to {}^{22}\mathrm{Na})$ values are shown in Table 4.4. I obtained significantly strong strengths from the $K = 0, 2$ states to the $K = 0, 1, 3$ states though there are poor experimental data besides mirror transitions ^{22}Mg $\to$ ^{22}Na. The strengths from

Table 4.4: The GT transition strengths defined by Eq. ((2.17)). of ^{22}Ne $\to$ ^{22}Na. The experimental data are taken from [188].

Observable	$T\beta\gamma$-AMD+GCM	Exp
$K=2 \to K=3$		
$B(\mathrm{GT}; 4_2^+1 \to 5_1^+0)$	0.95	–
$B(\mathrm{GT}; 3_1^+1 \to 4_1^+0)$	1.27	–
$B(\mathrm{GT}; 2_2^+1 \to 3_1^+0)$	1.51	–
$K=0 \to K=0$		
$B(\mathrm{GT}; 0_1^+1 \to 1_1^+0)$	1.98	(0.949(28))
$B(\mathrm{GT}; 2_1^+1 \to 1_1^+0)$	0.30	–
$B(\mathrm{GT}; 2_1^+1 \to 3_2^+0)$	1.24	–
$B(\mathrm{GT}; 4_1^+1 \to 5_2^+0)$	1.12	–
$K=0 \to K=1$		
$B(\mathrm{GT}; 0_1^+1 \to 1_2^+0)$	1.55	(1.43(8))
$B(\mathrm{GT}; 2_1^+1 \to 1_2^+0)$	0.37	–
$B(\mathrm{GT}; 2_1^+1 \to 2_1^+0)$	0.82	–
$B(\mathrm{GT}; 4_1^+1 \to 3_2^+0)$	0.12	–
$K=0 \to K=3$		
$B(\mathrm{GT}; 2_1^+1 \to 3_1^+0)$	0.0015	0.00022

the $K=0$ ground bandhead ^{22}Ne(0_1^+1) are fragmented into the $K=0,1$ bandheads of ^{22}Na($1_{1,2}^+0$) reproducing the mirror transition strengths $B(\mathrm{GT}; {}^{22}\mathrm{Mg}(0_1^+1) \to {}^{22}\mathrm{Na}(1_{1,2}^+0))$. Also from the excited states of $K=0$ ground band, the strengths are fragmented into ^{22}Na($2_1^+0, 3_2^+0$). The strengths from the $K=0$ ground band of ^{22}Ne are mostly found in the $K=0,1$ bands of ^{22}Na, and thus SU(4) symmetry is preserved if $K=0,1$ bands are summed up. However, the GT strengths are fragmented into the half inside the $K=0,1$ bands. The essential point is that $S_z \approx 0$ nn pair in ^{22}Ne(0_1^+1) state becomes into $S_z \approx 0,1$ pn pair in ^{22}Na($1_{1,2}^+0$) by the operators σ_0 and $\sigma_\pm$, respectively. Therefore, SU(4) symmetry is partially broken into different K states as a result of spin-orbit interaction on the prolate deformation as shown in the succeeding sections.

From the $K=2$ band of ^{22}Ne, the strengths are concentrated into the $K=3$ band of ^{22}Na. The initial $K=2$ states contain $S_z=0$ nn pairs with $L_z=2$. The GT transition changes the $S_z=0$ nn pair into the $S_z=1$ pn pair. In this final state, spin-orbit interaction contributes additional binding energy when $S_z=1$ is aligned to $L_z=2$. Thus, the ground state in ^{22}Na has 3^+0.

4.3.2 Single-particle and Nilsson orbits

In order to see the details of $K=0,1,3$ bands in ^{22}Na, I have calculated the single-particle orbits of AMD wavefunction at $(\beta,\gamma)=(0.29,0.19)$ which has substantially large overlap with the $K=0,1,3$ bandheads. Single-particle energies, squared angular momenta, squared orbital angular momenta, and positive parity probabilities are obtained from the single-particle orbits (see Table 4.5). The Nilsson orbits $[Nn_z\Lambda\Omega]$ are used to describe the states of deformed states. N is a harmonic oscillator quantum and n_z is a z quantum of the harmonic oscillator. The z components of the angular momenta in the deformed system are defined as

$$\Omega = \sqrt{\left\langle \phi_i^{\text{s.p.}} \middle| \hat{j}_z^2 \middle| \phi_i^{\text{s.p.}} \right\rangle}, \tag{4.1}$$

$$\Lambda = \sqrt{\left\langle \phi_i^{\text{s.p.}} \middle| \hat{\ell}_z^2 \middle| \phi_i^{\text{s.p.}} \right\rangle}, \tag{4.2}$$

where the $|\phi_i^{\text{s.p.}}\rangle$ is an orthonormal base obtained by diagonalizing the Hamiltonian with the single-particle AMD base $|\phi_i\rangle$. The lower 20 orbits for 10 protons and 10 neutrons form the ^{20}Ne core and a proton and a neutron occupy the last two orbits. The ^{20}Ne core contain doubly-magic ^{16}O and the residual four nucleons in the *sd*-shell. These four nucleons are neither in the spherical $d_{5/2}$ orbits nor in the Nilsson $[Nn_z\Lambda\Omega] = [2201/2]$ orbits. This is due to the formation of α cluster at the surface of the ^{16}O.

The last valence proton and neutron are in the spin-orbit favored Nilsson orbit [2113/2] in the prolate deformation. These nucleons make the ground $K = 3$ bandhead with the $[211 + 3/2]^p[211 + 3/2]^n$ configuration. However, this orbit is not exactly equivalent to [2113/2] orbit but it contains the minor [2111/2] component. After the $J^\pi K$ projection, the $K = 0$ and $K = 1$ bandheads $1^+_{1,2}0$ are produced by $[211 + 3/2]^p[211 - 3/2]^n$ and $[211+3/2]^p[211-1/2]^n$, respectively. The intrinsic spin in the $[211+3/2]^p[211-3/2]^n$ is equal to $S_z = 0$, which is a spin anti-aligned state and that in the $[211+3/2]^p[211-1/2]^n$ is a spin-aligned state with $S_z = 1$.

Similarly, ^{20}Ne core is found in ^{22}Ne as well as in ^{22}Na and the two valence neutrons with $[211+3/2]^n[211-3/2]^n$ configuration, which make the $K = 0$ band, are found. This is consistent with another calculation using AMD [190].

The GT transitions $^{22}\text{Ne}(0^+_1 1) \to {}^{22}\text{Na}(1^+_{1,2}0)$ can be understood in the words of Nilsson orbit. Namely, the GT transitions occur in the valence nucleons as $nn \to pn$ because the α particle in the ^{20}Ne core is inert on the GT transition. In the transition $0^+_1 1 \to 1^+_1 0$, the spin-conserving transition with $\Delta S_z = 0$ is caused by $\sum_i \sigma_z^i \tau_\pm^i$ and the spin-flip transition with $\Delta S_z = 1$ is caused by $\sum_i \sigma_\pm^i \tau_\pm^i$ in the transition $0^+_1 1 \to 1^+_2 0$. In the Nilsson orbits, each transition corresponds to $[211 + 3/2]^n[211 - 3/2]^n \to [211 + 3/2]^p[211 - 3/2]^n$ and $[211+3/2]^n[211-3/2]^n \to [211+3/2]^p[211-1/2]^n$, respectively. This is SU(4) symmetry breaking between the $K = 0$ and $K = 1$ band in ^{22}Na.

Table 4.5: The single-particle properties of the major component of the ^{22}Na(3_1^+0) ground state at $(\beta,\gamma)=(0.29,0.19)$. The column labeled "parity" stands for the fraction of positive parity component in each single-particle state.

neutron						proton						
Energy	$\langle\hat{j}^2\rangle$	$\langle\hat{\ell}^2\rangle$	parity	Ω	Λ	Energy	$\langle\hat{j}^2\rangle$	$\langle\hat{\ell}^2\rangle$	parity	Ω	Λ	shell
−60.94	0.75	0.00	1.00	0.50	0.02	−55.98	0.75	0.00	1.00	0.50	0.02	$s_{1/2}$
−59.29	0.75	0.00	1.00	0.50	0.03	−54.38	0.75	0.00	1.00	0.50	0.02	
−38.17	3.25	2.03	0.00	0.51	0.21	−33.64	3.26	2.05	0.00	0.51	0.22	$p_{3/2}$
−36.60	3.29	2.03	0.00	0.52	0.23	−32.16	3.38	2.03	0.00	0.52	0.26	
−32.13	3.70	2.07	0.00	1.48	1.00	−27.66	3.65	2.09	0.00	1.46	1.01	
−31.12	3.72	2.08	0.00	1.47	1.00	−26.63	3.75	2.09	0.00	1.48	1.00	
−27.61	1.53	2.19	0.00	0.63	1.00	−23.66	1.39	2.03	0.00	0.63	0.98	$p_{1/2}$
−26.26	1.50	2.08	0.00	0.59	0.99	−21.80	1.48	2.09	0.00	0.61	1.00	
−18.37	5.42	4.07	0.97	0.56	0.31	−14.14	5.81	4.25	0.97	0.60	0.34	α in sd-shell
−17.25	6.12	4.46	0.98	0.60	0.39	−13.07	5.90	4.30	0.97	0.62	0.39	
−11.26	7.36	5.75	0.96	1.33	1.06	−7.29	7.32	5.77	0.98	1.38	1.05	$\approx$ [2113/2]

Chapter 5

SU(4) symmetry and its breaking in the Gamow-Teller transitions

In the previous chapter, I have obtained the strong GT transitions exhausting 50% of the Ikeda sum-rule; $\sum B(\mathrm{GT}) = 3(N-Z) = 6$ in $^{6}\mathrm{He}(0_1^+1) \to {}^{6}\mathrm{Li}(1_1^+0)$, $^{10}\mathrm{Be}(0_1^+1) \to {}^{10}\mathrm{B}(1_1^+0)$, and $^{14}\mathrm{C}(0_1^+1) \to {}^{14}\mathrm{N}(1_2^+0)$. This is a signature of SU(4) symmetry related to the $T=0, S=1$ proton-neutron pairs in the final states $^{6}\mathrm{Li}(1_1^+0)$, $^{10}\mathrm{B}(1_1^+0)$, and $^{14}\mathrm{N}(1_2^+0)$. The symmetry corresponds to the LS-coupling of the proton-neutron pairs and cluster formation in these light $N=Z$ odd-odd nuclei.

On the other hand, deformation causes fragmentation in the GT strengths of $^{22}\mathrm{Ne} \to {}^{22}\mathrm{Na}$. The GT strengths $^{22}\mathrm{Ne}(0_1^+1) \to {}^{22}\mathrm{Na}(1_{1,2}^+0)$ in the $T\beta\gamma$-AMD+GCM are consistent with those of the mirror nuclei $^{22}\mathrm{Mg}(0_1^+1) \to {}^{22}\mathrm{Na}(1_{1,2}^+0)$, which show significant fragmentation into two final states. This is related to spin-orbit interactions on quadrupole deformations, that is, SU(4) symmetry breaking.

5.1 Proton-neutron correlation as spatial development

Proton-neutron correlation in the p-shell nuclei might be realized as spatial development of the pn pair. To see this, I calculated the proton-neutron pair densities defined in Sec. 2.3 of the single $T\beta\gamma$-AMD wavefunctions which have the largest overlaps with the ground states $^{6}\mathrm{He}(0_1^+1)$, $^{10}\mathrm{Be}(0_1^+1)$, $^{14}\mathrm{C}(0_1^+1)$ and their GT final states $^{6}\mathrm{Li}(1_1^+0)$, $^{10}\mathrm{B}(1_1^+0)$, $^{14}\mathrm{N}(1_2^+0)$, respectively. In the figure 5.1, these densities are shown together with the one-body densities. $^{6}\mathrm{Li}(1_1^+0)$ has $\alpha + pn$ cluster structures as shown in Fig. 5.1(a-2). The pn pair has deuteron-like ($S=1, T=0$) nature and develops away from the α core. $^{6}\mathrm{He}(0_1^+1)$ has similar structure to $^{6}\mathrm{Li}(1_1^+0)$ (see Fig. 5.1(a-1)). There is a nn pair and the distance to the α core is close to that of the pn pair in $^{6}\mathrm{Li}(1_1^+0)$. Hence, the GT transition between these states are caused by the transition of $nn \to pn$ ($T=0$). In other words, the di-nucleon structure in $^{6}\mathrm{He}(0_1^+1)$ is also found in $^{6}\mathrm{Li}(1_1^+0)$ as a proton-neutron pair. This is one of realizations of SU(4) symmetry in the light nuclei, where two-nucleon correlations occur not as pairing but as di-nucleon formation.

In $^{14}\mathrm{N}(1_2^+0)$, the $T=0$ pn pair is located near the oblately deformed $^{12}\mathrm{C}$ core and there are no spatial developments (see Fig. 5.1(c-2)). Similarly, $^{14}\mathrm{C}(0_1^+1)$ contains the nn pair in the same p-orbit (see Fig. 5.1(c-1)). The GT transition occurs between these states but the picture of $nn \to pn$ ($T=0$) is ambiguous and rather it is a phenomenon

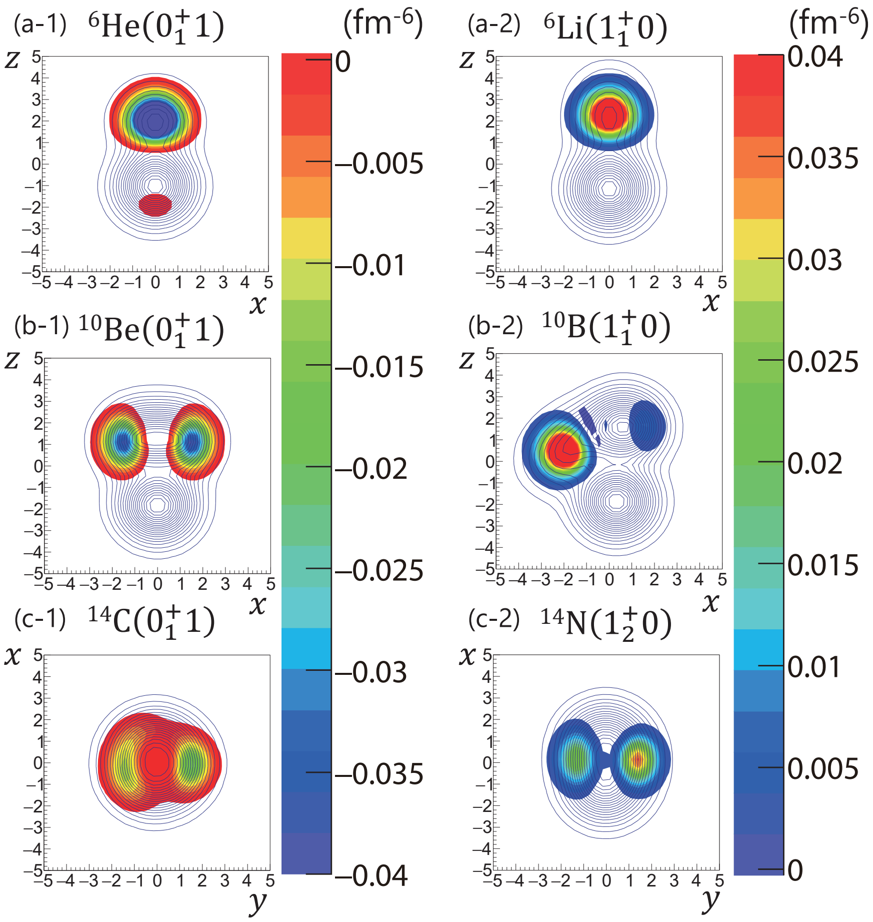

Figure 5.1: The colored contours correspond to two-nucleon pair densities $\rho_{NN}(\boldsymbol{r})$ of (a-1)^{6}He(0_1^+1), (b-1)^{10}Be(0_1^+1), (c-1)^{14}C(0_1^+1), (a-2)^{6}Li(1_1^+0), (b-2)^{10}B(1_1^+0), and (c-2)^{14}N(1_2^+0). The blue solid contours refer to the one-body density distribution $\rho(\boldsymbol{r})$.

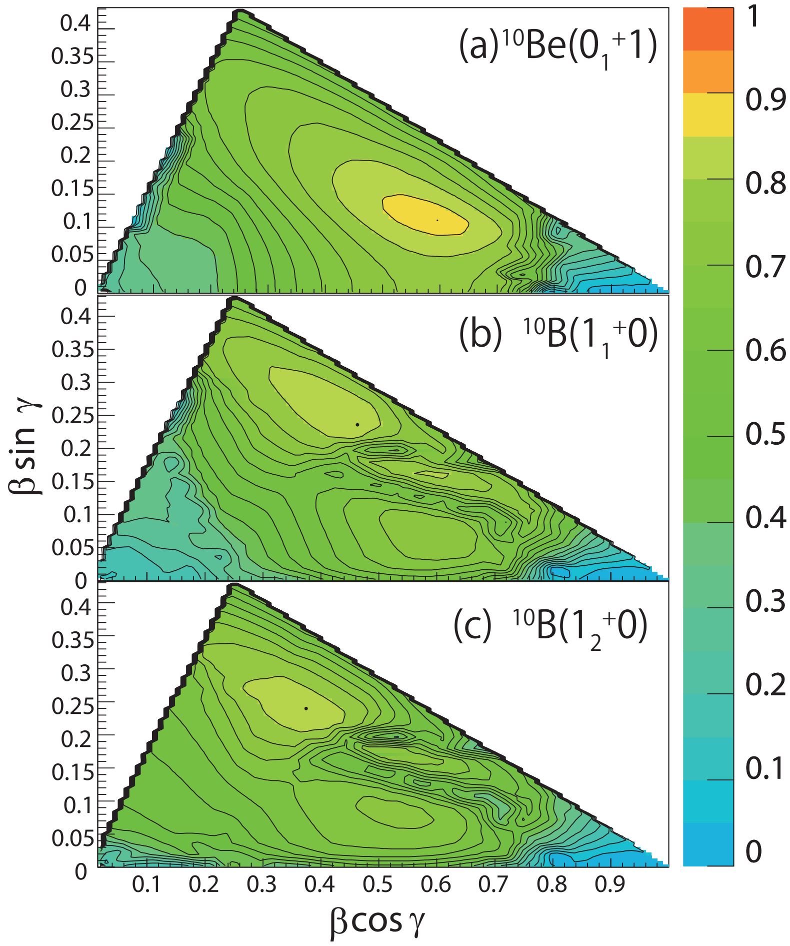

Figure 5.2: The overlap amplitudes $A(\beta,\gamma)$ of (a) ^{10}Be(0_1^+1), (b) ^{10}B(1_1^+0), and (c) ^{10}B(1_2^+0) defined in Eq. (5.1). The maximum point is shown by a dot.

in the two-hole states of the ^{16}O core.

^{10}Be(0_1^+1) and ^{10}B(1_1^+0) have 2α cores which are origins of deformation. The spatially developed pn pair is found in ^{10}B(1_1^+0) as well as ^{6}Li(1_1^+0) (see Fig. 5.1(b-2)). This is located at the point $(x,z)=(-2,0)$ (fm) whereas the nn pair in the ^{10}Be(0_1^+1) show p-shell nature (see Fig. 5.1(b-1)).

Apparently, the GT transition between these ^{10}Be(0_1^+1) and ^{10}B(1_1^+0) cannot occur. However, the nn pair in ^{10}Be(0_1^+1) can softly move away the 2α core. Therefore, the GT transition between these states become large. To see this, I define overlap amplitudes on the $\beta\gamma$ surfaces as

$$A(\beta_a,\gamma_a,J^\pi T) = \left|\sum_n \langle \beta_a,\gamma_a,n,J^\pi T;M\,|\,\Psi(J^\pi T;M)\rangle\right|^2 \tag{5.1}$$

$$= \sum_{nKbK'} f^{n*}_{aK}\mathcal{N}^{J^\pi T}_{aKbK'}g_{bK'}, \tag{5.2}$$

where the nth orthogonal bases at each (β,γ) point is defined as

$$|\beta_a,\gamma_a,n,J^\pi T;M\rangle = \sum_K f^n_{aK}P^J_{MK}P^TP^\pi\,|\Phi(\beta_a,\gamma_a)\rangle\,. \tag{5.3}$$

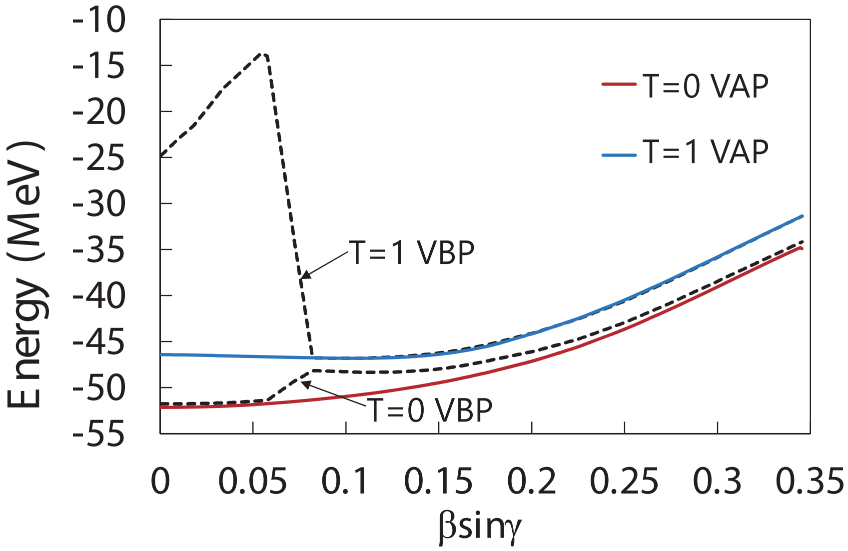

Figure 5.3: Restoration of SU(4) symmetry in the intrinsic states. The energy curves at $\beta\cos\gamma = 0.40$ of $T = 0$ and $T = 1$ states for ^{10}B are shown. Results with isospin projection before energy variations (solid lines, Fig. 3.1) and those without isospin projection before energy variations (dashed lines, Fig. 3.2) are shown.

The overlap amplitudes for $^{10}\mathrm{Be}(0^+_1 1)$ are shown in Fig. 5.2(a). There are soft regions along γ parameter from the maximum point towards $\gamma = 60°$. This indicates that the nn pair in $^{10}\mathrm{Be}(0^+_1 1)$ can move away from the 2α core. The di-neutron structures discussed in $^{10}\mathrm{Be}(0^+_1 1)$ correspond to this softly elongated overlap amplitudes (see Sec. 1.3.3).

The overlap amplitudes for $^{10}\mathrm{B}(1^+_{1,2}0)$ also have γ-elongated structures (see Fig. 5.2(b)(c)). The proton-neutron pairs in these states also move softly to the oblate $\gamma = 60°$ states. The β and γ parameters of these maximum points are similar to each other. This is consistent with that these states have the strong $B(E2; 1^+_2 0 \to 1^+_1 0)$ value, which corresponds to the similar deformation parameters. These states are not simple deformed states as discussed in the mean field approximations because I cannot find good K-quanta for these state and K-mixing occurs in these states. However, these 1^+0 states can be distinguished by spatial angular momenta L of the core rotations as shown in the next section.

As the proton-neutron pairs develops away from the core nuclei, SU(4) symmetry is somewhat restored. I show the one-dimensional energies surfaces of ^{10}B with $\beta\cos\gamma = 0.40$ in Fig. 5.3. In these surfaces, the parameter $\beta\sin\gamma$ corresponds to the distance between 2α core nuclei and the pn pair. In the small limit, the $T = 0$ and $T = 1$ spectra are split into the different states, but in the large limit, these different isospin states approach each other. This indicates restoration of SU(4) symmetry as spatial development of the proton-neutron pair.

These spatial developments are weakened as the mass number A increases (see Fig. 5.1). For the nn pairs in the $N = Z + 2$ nuclei, only in the $A = 6$ system spatially localized nn pair is found. On the other hand, for the pn pairs in the $N = Z$ odd-odd nuclei, $A = 6, 10$ system have $T = 0$ pn pair away from the core nuclei. This indicates that the $T = 0$ pn pairs in $N = Z$ odd-odd nuclei are seriously robuster than nn pairs in the ordinal even-even systems.

Table 5.1: Expectation values of the squared intrinsic spin and orbital angular momentum ($\langle \boldsymbol{S}^2 \rangle$ and $\langle \boldsymbol{L}^2 \rangle$) for ^{6}Li, ^{10}B, and ^{14}N obtained by $T\beta\gamma$-AMD+GCM and ^{6}He, ^{10}Be, and ^{14}C obtained by $\beta\gamma$-AMD+GCM. For harmonic oscillator quanta, values of the difference $\Delta\mathcal{N}_{\hbar\omega} = \langle \mathcal{N}_{\hbar\omega} \rangle - \mathcal{N}_{\hbar\omega,\mathrm{min}}$ from the minimum values for the $0\hbar\omega$ configurations are listed. $\mathcal{N}_{\hbar\omega,\mathrm{min}}$ for $A = 6, 10, 14$ nuclei are $\mathcal{N}_{\hbar\omega,\mathrm{min}} = 2, 6, 10$, respectively.

	$N = Z + 2$					$N = Z =$ odd							
nuclide	$J^\pi_n T$	$\langle \boldsymbol{S}^2 \rangle$	$\langle \boldsymbol{L}^2 \rangle$	$\Delta\mathcal{N}_{\hbar\omega}$	nuclide	$J^\pi_n T$	$\langle \boldsymbol{S}^2 \rangle$	$\langle \boldsymbol{L}^2 \rangle$	$\Delta\mathcal{N}_{\hbar\omega}$	$J^\pi_n T$	$\langle \boldsymbol{S}^2 \rangle$	$\langle \boldsymbol{L}^2 \rangle$	$\Delta\mathcal{N}_{\hbar\omega}$
^{6}He	$0^+_1 1$	0.12	0.12	1.45	^{6}Li	$0^+_1 1$	0.12	0.12	1.71	$1^+_1 0$	1.97	0.06	0.89
	$2^+_1 1$	0.19	5.65	1.63		$2^+_1 1$	0.20	5.64	1.91	$1^+_2 0$	1.90	5.75	1.20
										$2^+_1 0$	2.00	5.99	1.97
										$3^+_1 0$	2.01	6.01	0.70
^{10}Be	$0^+_1 1$	0.34	0.34	1.90	^{10}B	$0^+_1 1$	0.28	0.28	1.97	$1^+_1 0$	1.94	0.35	2.37
	$2^+_1 1$	0.30	6.00	1.94		$2^+_1 1$	0.27	6.04	1.90	$1^+_2 0$	1.92	5.43	1.77
										$2^+_1 0$	2.02	6.49	2.03
										$3^+_2 0$	1.97	7.53	2.21
	$2^+_2 1$	0.12	6.11	2.08		$2^+_2 1$	0.10	6.08	2.07	$1^+_3 0$	1.99	5.94	3.03
										$2^+_2 0$	2.02	6.61	2.44
										$3^+_1 0$	2.05	7.15	1.46
^{14}C	$0^+_1 1$	0.55	0.55	0.50	^{14}N	$0^+_1 1$	0.61	0.61	0.70	$1^+_2 0$	1.94	0.44	0.96
	$2^+_1 1$	0.19	5.79	0.74		$2^+_1 1$	0.21	5.83	0.88	$1^+_1 0$	1.89	5.56	0.45
										$2^+_1 0$	2.01	6.07	0.80
										$3^+_1 0$	2.02	6.22	1.32

5.2 LS-coupling proton-neutron pair and SU(4) symmetry

SU(4) symmetry between $N = Z + 2$ nuclei and $N = Z$ odd-odd nuclei corresponds to the LS-coupling pn pairs. To see this, I show the squared intrinsic spins and the orbital angular momenta in Table 5.1.

In the obtained states of $A = 6, 10, 14$, the spin expectation values $\langle S^2 \rangle$ are almost LS-coupling values $\langle S^2 \rangle = 2$ for the $T = 0$ states and $\langle S^2 \rangle = 0$ for the $T = 1$ states. As the mass number A increases, LS-coupling is broken into jj-coupling because of the spin-orbit potential. ^{6}He$(0^+_1 1)$ has almost pure $S = 0$ component with the 6% mixture of $S = 1$ component. In ^{14}C$(0^+_1 1)$, mixture of the $S = 1$ component is upto 27% which shows breaking into jj-coupling. On the other hand, $S = 1, T = 0$ pn pairs are not broken and show robuster nature than nn pairs as mixture of $S = 0$ components are less than 6%.

The orbital angular momenta have $\langle L^2 \rangle \approx 0$ or $\langle L^2 \rangle \approx 6$. In the $A = 6$ and $A = 14$ system, the orbital angular momenta dominantly come from the valence NN pairs with $L_{NN} = 0$ or $L_{NN} = 2$ because the cores of these nuclei are approximately spherical with $L_{\text{core}} = 0$. Thus, ^{6}He$(0^+_1 1)$, ^{6}Li$(1^+_1 0)$, ^{14}C$(0^+_1 1)$, and ^{14}N$(1^+_2 0)$ have the $L_{NN} = 0$ NN pairs and ^{6}He$(2^+_1 1)$, ^{6}Li$(1^+_2 0, 2^+_1 0, 3^+_1 0)$, ^{14}C$(2^+_1 1)$, and ^{14}N$(1^+_1 0, 2^+_1 0, 3^+_1 0)$ have the $L_{NN} = 2$ pairs.

GT transitions in $L_{NN} = 0$ and in $L_{\text{NN}} = 2$ are different as seen in the figure 5.4. The transitions in the $L_{NN} = 0$ states occur as $[L_{NN} = 0, S_{NN} = 0] \to [L_{NN} = 0, S_{NN} = 1]$ and the strengths are concentrated into the single states. On the other hand, the transitions in $L_{NN} = 2$ states show fragmentations because the transition corresponds to $[L_{NN} = 2, S_{NN} = 0] \to [L_{NN} = 2, S_{NN} = 1]$ and the final states are affected by spin-orbit interaction.

In the $A = 10$ systems, the orbital angular momentum from the core rotation $L_{\text{core}} = 2$ is produced because of deformation caused by the 2α clustering. As a result, $[L_{\text{core}} = 2, S_{NN} = 0] \to [L_{\text{core}} = 2, S_{NN} = 1]$ is found in addition to the transitions between the $L_{NN} = 0$ and $L_{NN} = 2$ states. ^{10}Be has two $L = 2$ states. One is $2^+_1 0$ $(K = 0)$ and the other is $2^+_2 0$ $(K = 2)$. In the former state, $L = 2$ quantum is originated from collective rotation $L_{\text{core}} = 2$ and the latter corresponds to $L_{NN} = 2$ as well as found in ^{6}He and ^{14}N. By comparing GT transitions from these initial states, the energy splitting in $[L_{\text{core}} = 2, S_{NN} = 0] \to [L_{\text{core}} = 2, S_{NN} = 1]$ is smaller than that in $[L_{NN} = 2, S_{NN} = 0] \to [L_{NN} = 2, S_{NN} = 1]$. In the final states of $L_{\text{core}} = 2$ transitions, spin-orbit interactions do not strongly affect the spectra because the rotation of the core does not directly couple to the intrinsic spin $S_{NN} = 1$.

SU(4) symmetry is realized as the LS-coupling NN pairs in the $L_{NN} = 0$ states. In fact, the $0^+_1 1$ states in the $N = Z + 2$ nuclei which are analogous to $0^+_1 1$ states in $N = Z$ odd-odd nuclei have large GT strengths to the 1^+0 states with $L_{NN} = 0$. However, the GT strengths decrease as the mass number A increases because the LS-coupling nn pair is broken into jj-coupling. In the $L_{NN} = 2$ states, the GT strengths are fragmented because the spin-orbit interaction between $L_{NN} = 2$ and $S_{NN} = 1$ is strong in the $N = Z$ odd-odd nuclei. In the $A = 10$ systems, we can find SU(4) symmetry not only in $[^{10}$Be$(0^+_1 1), {}^{10}$B$(1^+_1 0)]$ but also in the excited states: $[^{10}$Be$(2^+_1 1), {}^{10}$B$(1^+_2 0, 2^+_{1,2} 0, 3^+_2 0)]$. It is important that rotation of the 2α core does not affect SU(4) symmetry in the valence pn pairs.

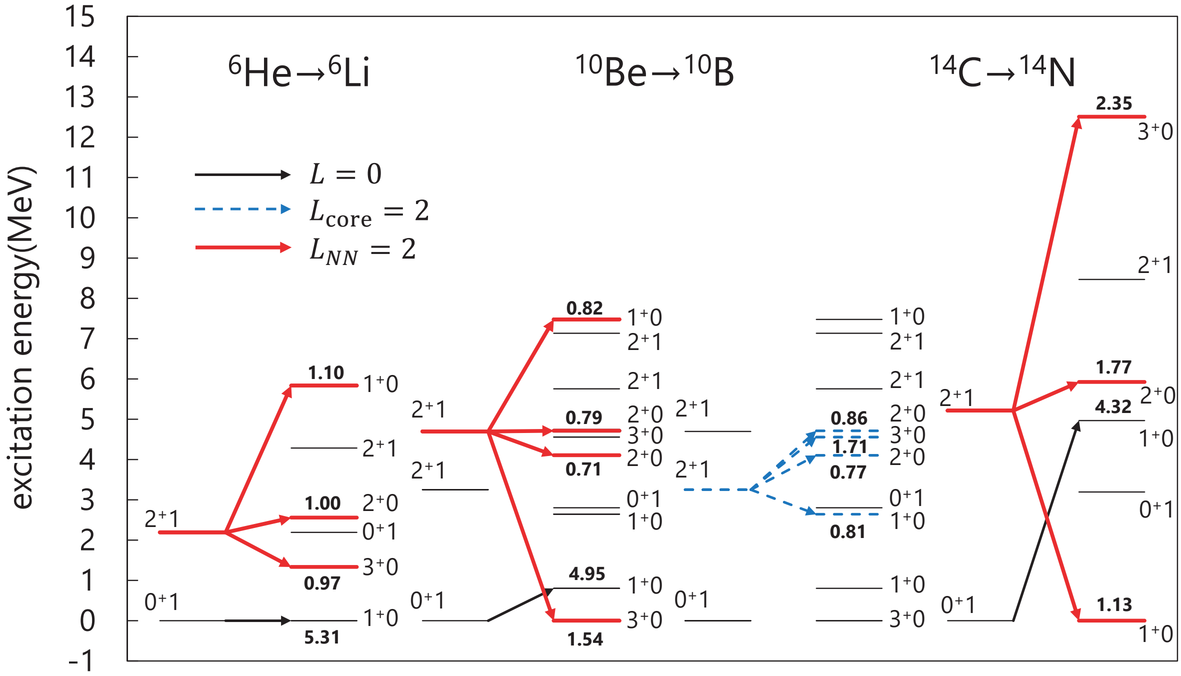

Figure 5.4: GT transitions ^{6}He $\to$ ^{6}Li, ^{10}Be $\to$ ^{10}B, and ^{14}C $\to$ ^{14}N calculated by $T\beta\gamma$-AMD+GCM. The number near each spectrum shows B(GT) value. The red solid arrows and blue dashed arrows refer to $L_{NN} = 2$ and $L_{\rm core} = 2$ states, respectively. The black arrows are $L = 0$ states.

The LS-coupling pn pairs do not mean that these states are LS-coupling states in the p-shell, but LS-coupling cluster states as shown in the two-body densities (see Sec. 5.1). These states contain higher shell components as a result of proton-neutron and 2α cluster formation. The expectation values of harmonic oscillator quanta

$$\hat{\mathcal{N}}_{\hbar\omega} = \sum_i \hat{a}_i^\dagger \hat{a}_i \tag{5.4}$$

and the differences from the minimum values $\mathcal{N}_{\hbar\omega,\rm min}$ for the $0\hbar\omega$ configurations

$$\Delta\mathcal{N}_{\hbar\omega} = \left\langle \hat{\mathcal{N}}_{\hbar\omega} \right\rangle - \mathcal{N}_{\hbar\omega,\rm min} \tag{5.5}$$

show how much the states have higher shell components. Here, $a_i^\dagger$ and a_i are the creation and annihilation operators of the harmonic oscillator with the width parameter ν. As shown in Table 5.1, all $T = 0$ states in $N = Z$ odd-odd nuclei have significant $\Delta\mathcal{N}_{\hbar\omega}$ values and ^{10}B has sufficiently large values to demonstrate importance of cluster formation. Therefore, the pn pairs are coupled into good LS states but they are made not only by the major shells but also by highly excited single particle orbits because of the quantum many-body correlations.

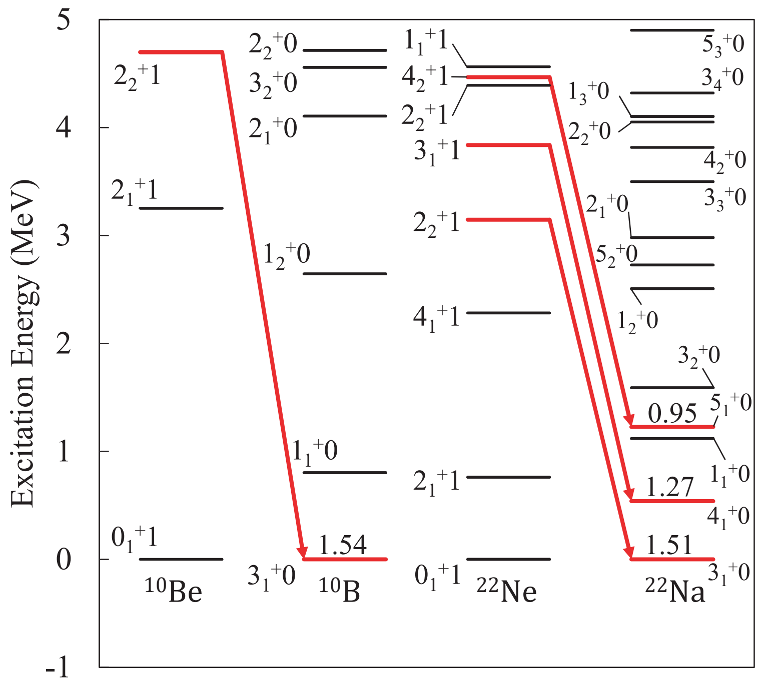

Figure 5.5: The GT transitions $K = 2 \to K = 3$ with large $B(\mathrm{GT})$ values are shown with red solid arrows. The number near each spectrum shows the $B(\mathrm{GT})$ value. The energy is measured from each ground state.

5.3 GT transitions in the deformed systems: ^{10}B and ^{22}Na

We have already seen the different deformed $N = Z$ odd-odd nuclei: ^{10}B and ^{22}Na. In the GT transition $^{10}\mathrm{Be} \to {}^{10}\mathrm{B}$, the strengths toward the ground $^{10}\mathrm{B}(3_1^+0)$ state come from the excited $^{10}\mathrm{Be}(2_2^+1)$ state. $^{10}\mathrm{Be}(2_2^+1) \to {}^{10}\mathrm{B}(3_1^+0)$ was determined as $[L_{NN} = 2, S_{NN} = 0] \to [L_{NN} = 2, S_{NN} = 1]$ in the previous chapter (see Sec. 5.2) but this is also considered as a $K = 2 \to K = 3$ transition since ^{10}Be and ^{10}B are deformed systems. Therefore, the GT transition strengths from the $K = 2$ side-bands of $N = Z + 2$ nuclei are universally large with the $K = 3$ ground states for both $A = 10$ and $A = 22$ systems (see Fig. 5.5).

On the other hand, the GT transitions from 0^+1 to 1^+0 states show different natures between the $A = 10$ and $A = 22$ systems. GT transition strengths from $^{10}\mathrm{Be}(0_1^+1)$ are concentrated into the lowest $^{10}\mathrm{B}(1_1^+0)$ state (see Fig. 5.6). This exhausts the most part of the sum-rule value $B(\mathrm{GT}) = 6$. From the excited state $^{10}\mathrm{Be}(2_1^+1)$, the GT transition strengths are fragmented into $^{10}\mathrm{B}(1_2^+0, 2_{1,2}^+0, 3_2^+0)$ but there is sufficiently small strength to the lowest 1_1^+0 state. This fragmentation does not indicate SU(4) symmetry breaking because these final states have similar excitation energies to the initial state and the LS-coupling proton-neutron pair is established in the final states with the core rotation: $[L_{\mathrm{core}} = 2, S_{NN} = 1]$ (see Sec. 5.2). In deed, the summation of the strengths $B(\mathrm{GT}; {}^{10}\mathrm{Be}(2_1^+1) \to {}^{10}\mathrm{B}(1_2^+0, 2_{1,2}^+0, 3_2^+0)) = 4.15$ exhausting the sum-rule value. This fact indicates that SU(4) symmetry is preserved in the transitions from $^{10}\mathrm{Be}(0_1^+1, 2_1^+1)$.

GT transition strengths from $^{22}\mathrm{Ne}(0_1^+1)$ are fragmented into the $^{22}\mathrm{Na}(1_{1,2}^+0)$ (see

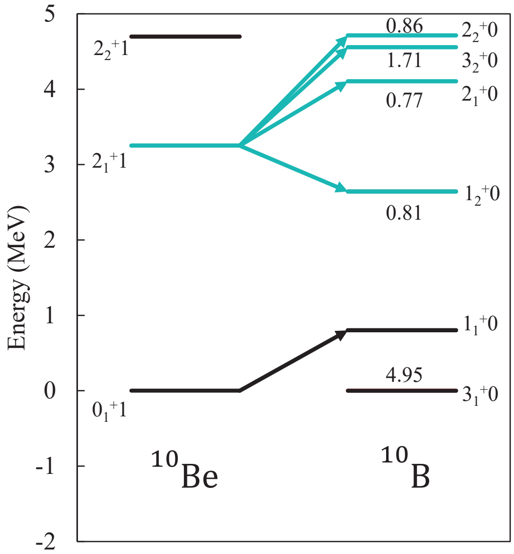

Figure 5.6: The spectra of initial and final states in $^{10}\mathrm{Be} \to {}^{10}\mathrm{B}(T = 0)$. The number near each spectrum shows the $B(\mathrm{GT})$ value. The energy is measured from each ground state. The states having large $B(\mathrm{GT})$ are connected by arrows.

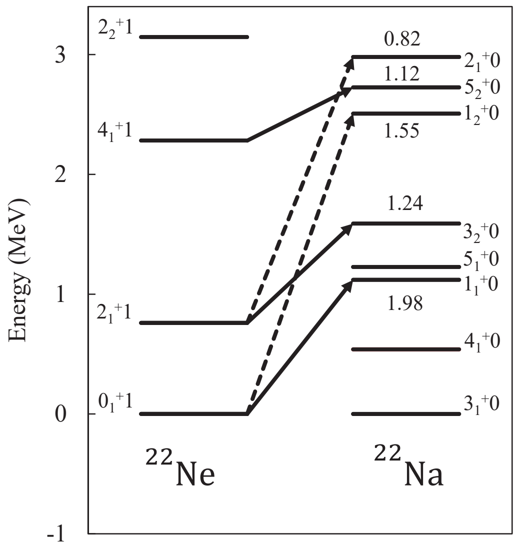

Figure 5.7: The spectra of initial and final states in $^{22}\mathrm{Ne} \to {}^{22}\mathrm{Na}$ $(T = 0)$. The number near each spectrum shows the $B(\mathrm{GT})$ value. The energy is measured from each ground state. The states having large $B(\mathrm{GT})$ are connected by arrows. The solid arrows correspond to $K = 0 \to K = 0$ transitions and the dashed arrows are $K = 0 \to K = 1$ ones.

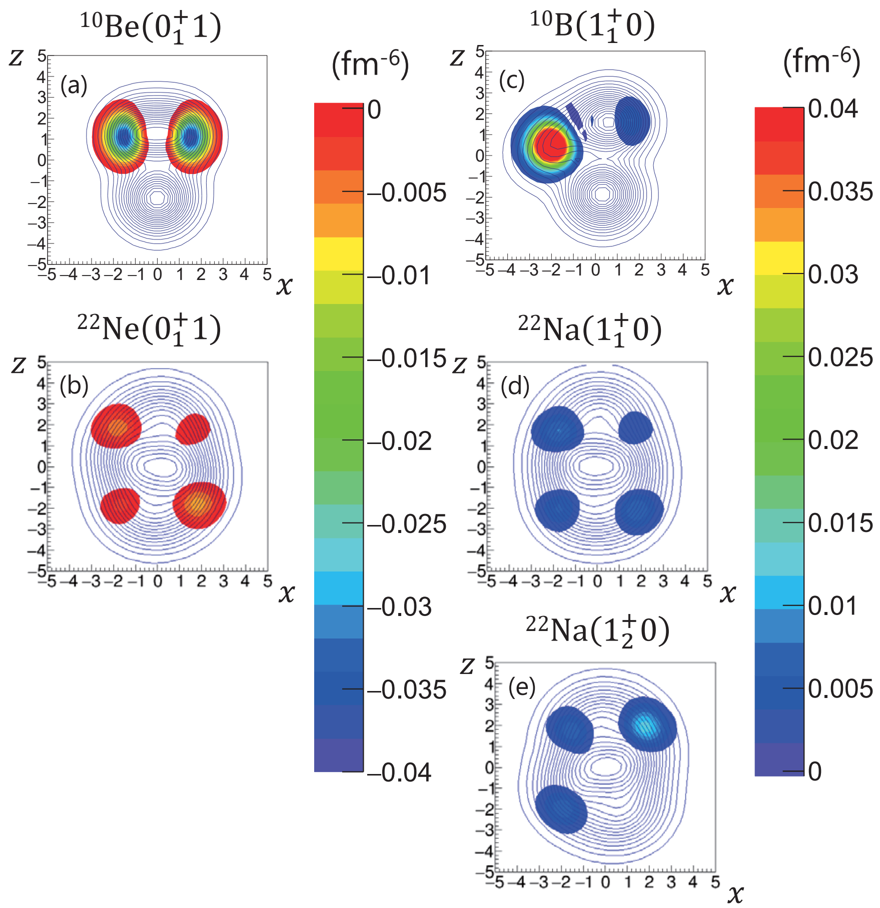

Figure 5.8: The two-nucleon pair density $\rho_{NN}(\boldsymbol{r})$ of (a) ^{10}Be($0^+_1 1$), (b) ^{22}Ne($0^+_1 1$), (c) ^{10}B($1^+_1 0$), (d) ^{22}Na($1^+_1 0$), and (e) ^{22}Na($1^+_2 0$). The one-body density distribution $\rho(\boldsymbol{r})$ is also shown by (blue) solid contour lines.

Fig. 5.7). The summation of GT strengths is $B(\text{GT}) = 3.53$ which exhausts large fraction of the sum-rule value. This indicates that SU(4) symmetry persists if both ^{22}Na($1^+_{1,2}0$) states are summed up. However, ^{22}Na($1^+_1 0$) and ^{22}Na($1^+_2 0$) have different $K = 0$ and $K = 1$ nature, respectively. Hence, SU(4) symmetry is broken by spin-orbit interaction on the deformation and the GT strengths are fragmented into these states. This type of fragmentation is also found in the transitions from ^{22}Ne($2^+_1 1$) which belongs to the $K = 0$ band. The strengths are fragmented into ^{22}Na($2^+_1 0, 3^+_2 0$) and $B(\text{GT}; {}^{22}\text{Ne}(2^+_1 1) \to {}^{22}\text{Na}(1^+_{1,2}0))$ are sufficiently small. This is different from GT transitions of ^{10}Be($2^+_1 1$) because the strength to the ^{10}B($1^+_2 0$) is sufficiently strong.

The densities also show different nature between $A = 10$ and $A = 22$ systems as a result of SU(4) symmetry and its breaking. I show one-body densities and proton-neutron pair densities of $A = 22$ system defined in Sec. 5.1 (see Fig. 5.8). All systems are prolately deformed but pn pair densities show differences. In ^{10}B($1^+_1 0$), the pn pair restores SU(4) symmetry as a result of spatial development away from the 2α core. On the other hand, in ^{22}Na($1^+_{1,2}0$), the proton-neutron pairs are broken into the Nilsson [2113/2] orbits. In these states, the spin directions of the pn pairs are fixed into the z axis, which is a direction of the prolate deformations.

The origin of SU(4) symmetry breaking in $^{22}\mathrm{Ne}(0^+_1 1) \to {}^{22}\mathrm{Na}(1^+_{1,2}0)$ is spin-orbit interaction on deformation. To see this in detail, I performed an analysis changing spin-orbit interaction from the weak limit to the strong limit. The range is adopted as $u_{\ell s} = 0$–2600 MeV. To convenience, I define a parameter λ as the ratio to the default spin-orbit interaction strength $u^0_{\ell s} = 1300$ MeV in Sec. 4.1:

$$u_{\ell s} = \lambda u^0_{\ell s}. \tag{5.6}$$

In order to see the continuous transition on λ, I changed it only on diagonalization in GCM but not on energy variations in the $T\beta\gamma$-AMD. In other words, I used the same bases on diagonalization in GCM for each λ as those obtained with $\lambda = 1.0$ in the $T\beta\gamma$-AMD.

In the figure 5.9, the $B(\mathrm{GT})$ spectra calculated with $\lambda = 0.0$, 0.5, 1.0, 1.5, 2.0 are shown for $^{10}\mathrm{Be} \to {}^{10}\mathrm{B}$ and $^{22}\mathrm{Ne} \to {}^{22}\mathrm{Na}$. In the $\lambda = 0.0$ limit, where are no spin-orbit interactions, SU(4) symmetry is exactly realized. The GT strengths are concentrated into the lowest $1^+_1 0$ state with a large percentage above 50% of the sum-rule both for $^{10}\mathrm{Be} \to {}^{10}\mathrm{B}$ and for $^{22}\mathrm{Ne} \to {}^{22}\mathrm{Na}$. As λ increases, the GT strengths from $^{22}\mathrm{Ne}(0^+_1 1)$ are fragmented into a few 1^+0 states. At the default strength $\lambda = 1.0$, the pn pair in $^{22}\mathrm{Na}$ is broken into $S_z = 0, 1$ states resulting $^{22}\mathrm{Na}(1^+_{1,2}0)$. Because the summation of these strengths are still over 50% of the sum-rule, SU(4) symmetry is broken only inside the pn pair but not in the $^{20}\mathrm{Ne}$ core. In the strong limit of spin-orbit interaction with $\lambda = 2.0$, the GT strengths are fragmented into many 1^+0 states. The peak position is pushed up into the higher energy and the strengths are widely distributed. jj-coupling limit is favored with strong spin-orbit interaction and thus deformation is suppressed into $\beta = 0.23$. In these states, six particles in the sd-shell participate in GT transitions and construct fragments in the 1^+0 final states.

SU(4) symmetry breaking is also found in $^{10}\mathrm{Be} \to {}^{10}\mathrm{B}$ as λ increases. However, this occurs at $\lambda = 1.5$ which is larger than $\lambda = 1.0$ where SU(4) symmetry breaking occurs in $^{22}\mathrm{Ne} \to {}^{22}\mathrm{Na}$. This refers to that SU(4) symmetry persists even with $\lambda = 1.0$ as a result of clustering of the NN pairs around the 2α core.

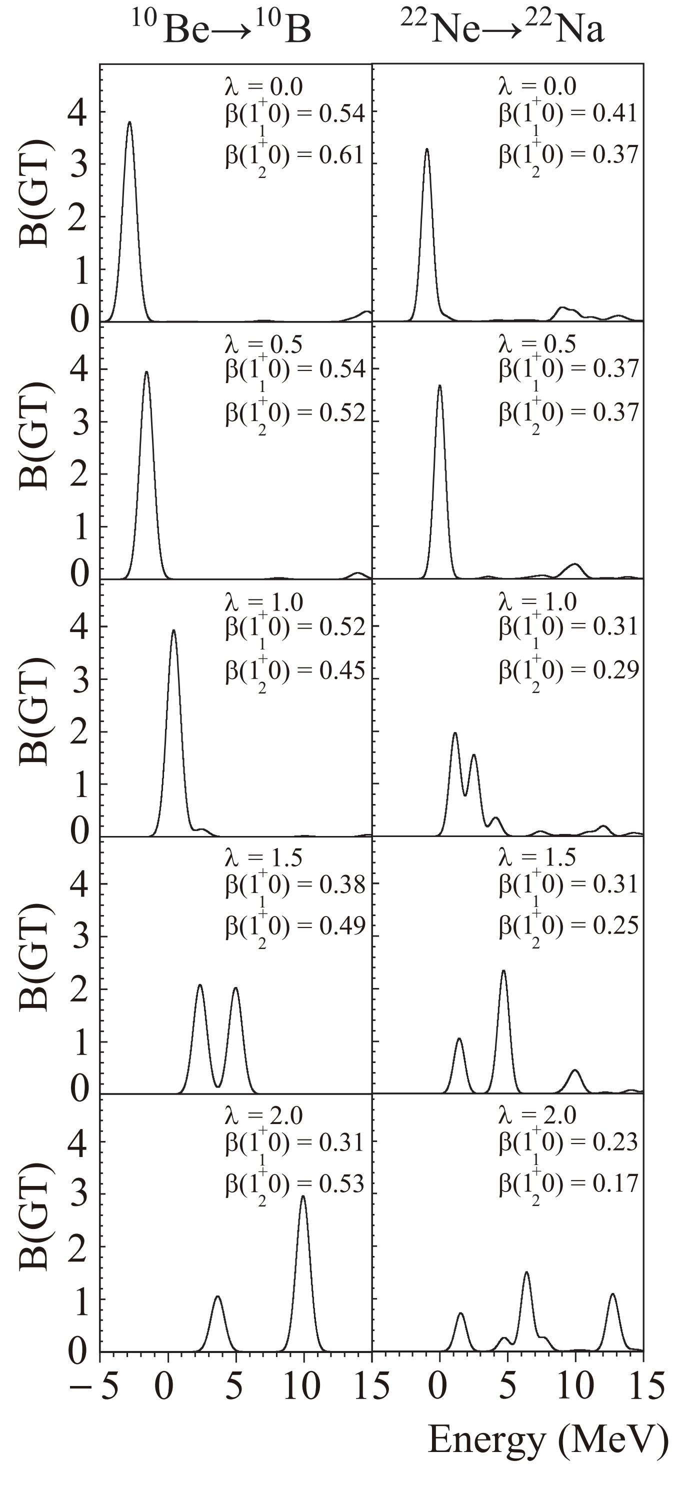

Figure 5.9: The B(GT) spectra obtained by the calculations with the modified spin-orbit strengths with $\lambda = 0.0, 0.5, 1.0, 1.5, 2.0$. The $\lambda = 1.0$ corresponds to the default strength. Each spectrum is smeared by Gaussian with $\sigma = 0.4$ in order to normalize the peak height to the B(GT) value for the case of an isolate peak. The left and right panels show $B(\mathrm{GT}; {}^{10}\mathrm{Be} \to {}^{10}\mathrm{B})$ and $B(\mathrm{GT}; {}^{22}\mathrm{Ne} \to {}^{22}\mathrm{Na})$, respectively. For each λ, the energies are measured from ${}^{10}\mathrm{B}(3_1^+0)$ and ${}^{22}\mathrm{Na}(3_1^+0)$, respectively.

Chapter 6

Conclusion

I have investigated SU(4) symmetry in the Gamow-Teller transitions and proton-neutron correlation focusing on the extremely light nuclei. This is a complementary work to the original idea of proton-neutron pairing and SU(4) symmetry in the heavier nuclei, in which the mean-field theories and shell models are well established.

Firstly, the problems on isospin competition between isoscalar and isovector states in the low-lying region are solved by isospin projection before energy variation in the antisymmetrized molecular dynamics (AMD) with the constraint on deformation. The method is named isospin-projected AMD ($T\beta\gamma$-AMD). The treatment of the projection operator is numerical and approximated, but it works in the light $N = Z$ odd-odd nuclei. By using this method, the proper intrinsic wavefunctions containing clusters and proton-neutron pairs are obtained for each deformation parameter and isospin eigenvalue.

A signature of SU(4) symmetry in the light $N = Z$ odd-odd nuclei has been found in the p-shell nuclei. I have investigated the Gamow-Teller transition strengths from the $J^\pi T = 0^+1$ states of $N = Z + 2$ nuclei and 1^+0 states of $N = Z$ odd-odd nuclei with the $T\beta\gamma$-AMD combined with generator coordinate method. I have obtained the strong Gamow-Teller transitions exhausting 50% of the sum-rule in ^{6}He$(0^+_1 1) \to {}^6$Li$(1^+_1 0)$, ^{10}Be$(0^+_1 1) \to {}^{10}$B$(1^+_1 0)$, and ^{14}C$(0^+_1 1) \to {}^{14}$N$(1^+_2 0)$, respectively. In these nuclei, SU(4) symmetry in the $A = 6$ and 10 system is realized as spatially developed NN pair formed in the intrinsic states. In other words, the GT transitions occur as the transition $nn \to pn$ between the initial and final states. The proton-neutron pair densities in these nuclei show the developed distances between the proton-neutron pairs and the core nuclei.

However, in the heavier nuclei ^{22}Na, spin-orbit interaction on quadrupole deformation breaks SU(4) symmetry. The proton-neutron pair is formed at the surface of the prolately deformed ^{20}Ne $= {}^{16}$O $+ \alpha$ core, but ^{22}Na$(1^+_{1,2}0)$ have different K-quanta with $K = 0$ and $K = 1$. Each state contains proton-neutron pair with anti-aligned spin ($S_z = 0$) and with aligned spin ($S_z = 1$), respectively. As a result, the strengths are fragmented into the half though the summation of the Gamow-Teller strengths ^{22}Ne$(0^+_1 1) \to {}^{22}$Na$(1^+_{1,2}0)$ is upto 50% of the sum-rule value. This is consistent with the Gamow-Teller strengths from the mirror nuclei ^{22}Mg$(0^+_1 1) \to {}^{22}$Na$(1^+_{1,2}0)$ which show fragmentation into two final states.

The idea of proton-neutron correlation has been extended into cluster formation of proton-neutron pairs. This type of proton-neutron pair has not been discussed in the context of proton-neutron correlation in the $N = Z$ nuclei because clustering is considered as a specific phenomenon in the extremely light nuclei. As shown in ^{22}Na$(1^+_{1,2}0)$, the idea is not valid in the heavier system because spin-orbit interactions break the ideal $T = 0, S = 1$ proton-neutron pairs. However, ^{10}B(1_1^+0) contains the proton-neutron pair which is spatially developed away from the 2α core. This is another possibility for proton-neutron correlation in the light $N = Z$ odd-odd nuclei.

The low-lying states of $N = Z$ odd-odd p-shell nuclei are constructed by LS-coupling $T = 0, S_{NN} = 1$ proton-neutron pairs. In these state, there are three groups of $T = 0, S_{NN} = 1$ proton-neutron states such as $L = 0$, $L_{NN} = 2$, and $L_{\text{core}} = 2$. The $L = 0$ and $L_{NN} = 2$ states are found in all p-shell nuclei. The Gamow-Teller transition strengths to the $L = 0$ states show SU(4) symmetric nature. On the other hand, the strengths to the $L_{NN} = 2$ states show SU(4) broken nature because the spin-orbit interaction between $L_{NN} = 2$ and $S_{NN} = 1$ causes energy splittings.

$L_{\text{core}} = 2$ states are found only in ^{10}B because they have deformed 2α cores. The Gamow-Teller transitions between $L_{\text{core}} = 2$ states also show SU(4) symmetry nature; $^{10}\text{Be}(2_1^+1) \to {}^{10}\text{B}(1_2^+0, 2_{1,2}^+0, 3_2^+0)$. Therefore, SU(4) symmetry is found in the excited states as well as in the ground states. It is important that rotation of the 2α core $L_{\text{core}} = 2$ is not directly coupled to $S_{NN} = 1$ of the proton-neutron pair with spin-orbit interaction.

SU(4) symmetry in the light nuclei is different from that in the heavier nuclei obtained with mean-field theories containing proton-neutron pairing. Clustering of two-nucleon pair can be another possibility for realizing SU(4) symmetry. These types of proton-neutron pairs show robuster nature for deformation than those in the mean-field theories as found in the rotational excited states of ^{10}B. The fragmentation of the Gamow-Teller strengths by spin-orbit interaction on deformation in ^{22}Na is consistent with other calculations in the heavier nuclei. This is a mechanism of SU(4) symmetry breaking discussed in $^{46}\text{Ti} \to {}^{46}\text{V}$ and $^{50}\text{Cr} \to {}^{50}\text{Mn}$ using shell models. This implies it is hopeless that we find ideal proton-neutron pairs in the heavier nuclei except for ^{42}Sc and the other LS-closed core + pn systems. Therefore, we have to develop further theoretical investigations of the light nuclei with the proper treatments on clustering phenomena of proton-neutron pairs.

Acknowledgment

I thank to Professor Yoshiko Kanada-En'yo for fruitful discussions and advises. I also thank to the members of Nuclear Theory Group for providing the comfortable environments for research and the members of Nuclear Many-Body Subgroup for profitable discussion. The works in this thesis were supported by Grants-in-Aid for Scientific Research from the Japan Society for the Promotion of Science (JSPS). Major parts of the computational calculations of this thesis were performed by the supercomputers at Yukawa Institute for Theoretical Physics (YITP).

Appendix A

Expectation values in the $T\beta\gamma$-AMD

In this chapter, I enumerate the analytical formalism of the expectation values of Hamiltonian and transition operators. For convenience, I define the bra parts of AMD wavefunctions in Eq. (2.1):

$$\langle\Psi| = \mathcal{A}\left[\langle \boldsymbol{W}_1| \langle \boldsymbol{\eta}_1| \langle m_1| \langle \boldsymbol{W}_2| \langle \boldsymbol{\eta}_2| \langle m_2| \cdots \langle \boldsymbol{W}_A| \langle \boldsymbol{\eta}_A| \langle m_A|\right] \tag{A.1}$$

A.1 Overlaps and many-body operators

The overlaps of single-particle orbits for spacial, spin, and isospin parts are defined as

$$\begin{aligned}\beta_{ij} &= \langle \boldsymbol{W}_i \,|\, \boldsymbol{Z}_j \rangle \\ &= \left(\frac{\pi}{2\nu}\right)^{\frac{3}{2}} \exp\left[-\frac{(\boldsymbol{W}_i^* - \boldsymbol{Z}_j)^2}{2}\right] \left(\frac{2\nu}{\pi}\right)^{\frac{3}{2}} \exp\left[+\frac{1}{2}\boldsymbol{W}_i^{*2}\right] \exp\left[+\frac{1}{2}\boldsymbol{Z}_j^2\right] \\ &= \exp\left(\boldsymbol{W}_i^* \cdot \boldsymbol{Z}_j\right), \end{aligned} \tag{A.2}$$

$$S_{ij} = \boldsymbol{\eta}_i^* \cdot \boldsymbol{\xi}_j, \tag{A.3}$$

$$T_{ij} = \delta_{m_i n_j}. \tag{A.4}$$

The overlap between two AMD wavefunctions are written in the form

$$\langle \Psi \,|\, \Phi \rangle = \det B, \tag{A.5}$$

where

$$B_{ij} = \beta_{ij} S_{ij} T_{ij}. \tag{A.6}$$

The differentials of overlap matrices for spatial and spin coordinates are

$$\frac{\partial B_{ij}}{\partial W_{k\mu}^*} = B_{ij} Z_{j\mu} \delta_{ik}, \tag{A.7}$$

$$\frac{\partial B_{ij}}{\partial \eta_{k\mu}^*} = \beta_{ij} \delta_{ik} \xi_{j\mu} \delta_{m_i n_j}. \tag{A.8}$$

The differentials of inverses of overlap matrices are

$$\frac{\partial B_{ij}^{-1}}{\partial W_{k\mu}^*} = B_{ik}^{-1} G_{jk;\mu}, \tag{A.9}$$

$$\frac{\partial B_{ij}^{-1}}{\partial \eta_{k\mu}^{*}} = B_{ik}^{-1} g_{jk;\mu}, \tag{A.10}$$

where

$$G_{jk;\mu} = -\sum_{\ell} Z_{\ell\mu} B_{k\ell} B_{\ell j}^{-1}, \tag{A.11}$$

$$g_{jk;\mu} = -\sum_{\ell} \xi_{\ell\mu} \beta_{k\ell} \delta_{m_k n_\ell} B_{\ell j}^{-1}. \tag{A.12}$$

The differentials of overlaps are

$$\frac{\partial \langle \Psi \,|\, \Phi \rangle}{\partial W_{k\mu}^{*}} = -G_{kk;\mu} \langle \Psi \,|\, \Phi \rangle, \tag{A.13}$$

$$\frac{\partial \langle \Psi \,|\, \Phi \rangle}{\partial \eta_{k\mu}^{*}} = -g_{kk;\mu} \langle \Psi \,|\, \Phi \rangle. \tag{A.14}$$

The expectation values of one-body operators are written as

$$\frac{\langle \Psi \,|\, O \,|\, \Phi \rangle}{\langle \Psi \,|\, \Phi \rangle} = \sum_{ij} \langle i \,|\, o \,|\, j \rangle B_{ji}^{-1}. \tag{A.15}$$

The expectation values of two-body operators are written as

$$\frac{\langle \Psi \,|\, O \,|\, \Phi \rangle}{\langle \Psi \,|\, \Phi \rangle} = \sum_{ijk\ell} \langle ij \,|\, o \,|\, k\ell \rangle \left(B_{ki}^{-1} B_{\ell j}^{-1} - B_{\ell i}^{-1} B_{kj}^{-1} \right). \tag{A.16}$$

A.2 Hamiltonians

The kinetic term is written as

$$\langle T \rangle = -\frac{\hbar^2 \nu}{2m} \sum_{ij} B_{ij} \left(W_i^{*} - Z_j \right)^2 B_{ji}^{-1} + \frac{3A\hbar^2 \nu}{2m}. \tag{A.17}$$

The kinetic term of center of mass motion is written as

$$\langle T_G \rangle = -\frac{\hbar^2 \nu A}{2M} \left(W_G^{*} - Z_G \right)^2 + \frac{3A\hbar^2 \nu}{2M}. \tag{A.18}$$

Volkov No.2 force is

$$\begin{aligned}&\langle V_{\mathrm{central}} \rangle \\ &= \frac{1}{2} \sum_{j\ell} \beta_{j\ell} \sum_{ik} \beta_{ik} X_{ijk\ell} \left(B_{ki}^{-1} B_{\ell j}^{-1} - B_{\ell i}^{-1} B_{kj}^{-1} \right) \sum_{n} v_n \left(1 - \lambda_n \right)^{\frac{3}{2}} \exp\left[-\frac{\lambda_n}{4} \boldsymbol{Z}_{ijk\ell}^2 \right].\end{aligned} \tag{A.19}$$

where, $\lambda_n, X_{ijk\ell}$, $\boldsymbol{Z}_{ijk\ell}$ is defined as

$$\lambda_n = \frac{1}{1 + a_n^2 \nu}, \tag{A.20}$$

$$X_{ijk\ell} = WS_{ik}S_{j\ell}\delta_{m_in_k}\delta_{m_jn_\ell} + BS_{i\ell}S_{jk}\delta_{m_in_k}\delta_{m_jn_\ell} - HS_{ik}S_{j\ell}\delta_{m_in_\ell}\delta_{m_jn_k} - MS_{i\ell}S_{jk}\delta_{m_in_\ell}\delta_{m_jn_k}, \tag{A.21}$$

$$Z_{ijk\ell;\mu} = W^*_{i\mu} - W^*_{j\mu} + Z_{k\mu} - Z_{\ell\mu}. \tag{A.22}$$

The spin-orbit part of G3RS forces is

$$\langle V_{\mathrm{LS}}\rangle = \frac{-i\hbar}{32}\sum_{j\ell}\beta_{j\ell}\sum_{ik}\beta_{ik}\left(B^{-1}_{ki}B^{-1}_{\ell j} - B^{-1}_{\ell i}B^{-1}_{kj}\right)\left(\delta_{m_in_k}\delta_{m_jn_\ell} - \delta_{m_in_\ell}\delta_{m_jn_k}\right)\times \times\sum_{\mu\nu\lambda}\epsilon_{\mu\nu\lambda}\left(\Sigma_{\mu ikj\ell} + \Sigma_{\mu j\ell ik} + \Sigma_{\mu jki\ell} + \Sigma_{\mu i\ell jk}\right)\left(W^*_{i\nu} - W^*_{j\nu}\right)\left(Z_{k\lambda} - Z_{\ell\lambda}\right)\times \times\sum_n v_n\left(1-\lambda_n\right)^{\frac{5}{2}}\exp\left[-\frac{\lambda_n}{4}\boldsymbol{Z}^2_{ijk\ell}\right]. \tag{A.23}$$

Here, the Σ is defined as

$$\Sigma_{\mu ikj\ell} = \langle\eta_i\,|\,\sigma_\mu\,|\,\xi_k\rangle\,S_{j\ell}. \tag{A.24}$$

Coulomb force approximated by 7-range Gaussians [191] are

$$V_{\mathrm{Coulomb}} = \sum_{i<j}\sum_{k=1}^{7} e^2\sqrt{\nu}C_k\exp\left[-\left(\frac{\boldsymbol{r}_i - \boldsymbol{r}_j}{\mu_k/\sqrt{\nu}}\right)^2\right]\frac{1+\tau_{i3}}{2}\frac{1+\tau_{j3}}{2} \tag{A.25}$$

with the parameters

k	μ_k	C_k
1	8.888194	0.437686
2	6.244998	−0.421877
3	4.358899	0.363035
4	3.000000	0.082946
5	2.000000	0.179389
6	1.224745	0.717984
7	0.500000	2.108250

(A.26)

The expectation value of this interaction is

$$\langle V_{\mathrm{Coulomb}}\rangle = \frac{1}{2}\sum_j\delta_{m_jp}\sum_i\delta_{m_ip}\sum_\ell B_{j\ell}\delta_{n_\ell p}\sum_k B_{ik}\delta_{n_kp}\left(B^{-1}_{ki}B^{-1}_{\ell j} - B^{-1}_{\ell i}B^{-1}_{kj}\right)\times \times\sum_n v_n\left(1-\lambda_n\right)^{\frac{3}{2}}\exp\left[-\frac{\lambda_1}{4}\boldsymbol{Z}^2_{ijk\ell}\right]^{2^{n-1}}. \tag{A.27}$$

Under the isospin-projection, however, Coulomb force is considered effective between neutrons as well as protons;

$$\langle V_{\mathrm{Coulomb}}\rangle = \frac{1}{4}\sum_{j\ell}B_{j\ell}\delta_{m_jn_\ell}\sum_{ik}B_{ik}\delta_{m_in_k}\delta_{m_im_j}\left(B^{-1}_{ki}B^{-1}_{\ell j} - B^{-1}_{\ell i}B^{-1}_{kj}\right)\times \times\sum_n v_n\left(1-\lambda_n\right)^{\frac{3}{2}}\exp\left[-\frac{\lambda_1}{4}\boldsymbol{Z}^2_{ijk\ell}\right]^{2^{n-1}}. \tag{A.28}$$

The differentials for spatial coordinates of one-body operators are

$$\frac{\partial \langle O \rangle}{\partial W^*_{P\mu}} = \sum_{ij} \delta_{iP} \frac{\partial \langle P \,|\, o \,|\, j \rangle}{\partial W^*_{P\mu}} + \langle i \,|\, o \,|\, j \rangle \frac{\partial B^{-1}_{ji}}{\partial W^*_{P\mu}}. \tag{A.29}$$

Those of two-body operators are

$$\frac{\partial \langle O \rangle}{\partial W^*_{P\mu}} = \sum_{ijk\ell} \left[\delta_{iP} \frac{\partial \langle ij \,|\, o \,|\, k\ell \rangle}{\partial W^*_{P\mu}} + \langle ij \,|\, o \,|\, k\ell \rangle \, G_{iP;\mu} \right] \left(B^{-1}_{kP} B^{-1}_{\ell j} - B^{-1}_{\ell P} B^{-1}_{kj} \right). \tag{A.30}$$

Replacing $\frac{\partial}{\partial W^*_{P\mu}}$ into $\frac{\partial}{\partial \eta^*_{P\mu}}$, we obtain the differentials for spin coordinates. The differentials of the kinetic term are

$$\begin{aligned} \frac{\partial \langle T \rangle}{\partial W^*_{P\mu}} = -\frac{\hbar^2 \nu}{2m} \sum_j B^{-1}_{jP} \sum_i \Big\{ \delta_{iP} \left[2 \left(W^*_{i\mu} - Z_{j\mu} \right) + Z_{j\mu} \left((\boldsymbol{W}^*_i - \boldsymbol{Z}_j)^2 - 3 \right) \right] + \\ \left[(\boldsymbol{W}^*_i - \boldsymbol{Z}_j)^2 - 3 \right] G_{iP;\mu} \Big\} B_{ij}, \end{aligned} \tag{A.31}$$

$$\frac{\partial \langle T \rangle}{\partial \eta^*_{P\mu}} = -\frac{\hbar^2 \nu}{2m} \sum_j B^{-1}_{jP} \sum_i \left\{ \beta_{ij} \delta_{m_i n_j} \left[(\boldsymbol{W}^*_i - \boldsymbol{Z}_j)^2 - 3 \right] \left(\xi_{j\mu} \delta_{iP} + g_{iP;\mu} S_{ij} \right) \right\}. \tag{A.32}$$

The differentials of the kinetic term of the center of mass motions are

$$\frac{\partial \langle T_G \rangle}{\partial W^*_{P\mu}} = -\frac{\hbar^2 \nu \sqrt{A}}{M} \left(W^*_{G\mu} - Z_{G\mu} \right), \tag{A.33}$$

$$\frac{\partial \langle T_G \rangle}{\partial \eta^*_{P\mu}} = 0, \tag{A.34}$$

where the coordinate of the center of mass $Z_{G\mu}$ is defines as

$$Z_{G\mu} = \frac{1}{\sqrt{A}} \sum_{i=1}^{A} Z_{i\mu}. \tag{A.35}$$

The differentials of Volkov No.2 force are

$$\begin{aligned} \frac{\partial \langle V_{\mathrm{central}} \rangle}{\partial W^*_{P\mu}} &= \sum_{j\ell} \beta_{j\ell} \sum_k \left(B^{-1}_{kP} B^{-1}_{\ell j} - B^{-1}_{\ell P} B^{-1}_{kj} \right) \sum_i \beta_{ik} X_{ijk\ell} \times \\ &\times \sum_n v_n \left(1 - \lambda_n\right)^{\frac{3}{2}} \exp\left[-\frac{\lambda_n}{4} Z^2_{ijk\ell} \right] \left[\delta_{iP} \left(Z_{k\mu} - \frac{\lambda_n}{2} Z_{ijk\ell;\mu} \right) + G_{iP;\mu} \right], \end{aligned} \tag{A.36}$$

$$\begin{aligned} \frac{\partial \langle V_{\mathrm{central}} \rangle}{\partial \eta^*_{P\mu}} &= \sum_{j\ell} \beta_{j\ell} \sum_k \left(B^{-1}_{kP} B^{-1}_{\ell j} - B^{-1}_{\ell P} B^{-1}_{kj} \right) \\ &\sum_i \beta_{ik} \left(\delta_{iP} X'_{ijk\ell;\mu} + g_{iP;\mu} X_{ijk\ell} \right) \sum_n v_n \left(1 - \lambda_n\right)^{\frac{3}{2}} \exp\left[-\frac{\lambda_n}{4} Z^2_{ijk\ell} \right]. \end{aligned} \tag{A.37}$$

Here, $X'_{ijk\ell;\mu}$ is defined as

$$\begin{aligned} X'_{ijk\ell;\mu} &= W\xi_{k\mu}S_{j\ell}\delta_{m_i n_k}\delta_{m_j n_\ell} + B\xi_{\ell\mu}S_{jk}\delta_{m_i n_k}\delta_{m_j n_\ell} \\ &\quad - H\xi_{k\mu}S_{j\ell}\delta_{m_i n_\ell}\delta_{m_j n_k} - M\xi_{\ell\mu}S_{jk}\delta_{m_i n_\ell}\delta_{m_j n_k}. \end{aligned} \tag{A.38}$$

The differentials of the spin-orbit part of G3RS force are

$$\begin{aligned} \frac{\partial \langle V_{\mathrm{LS}} \rangle}{\partial W^*_{P\tau}} = &\frac{-i\hbar}{16} \sum_{j\ell} \beta_{j\ell} \sum_k \left(B^{-1}_{kP} B^{-1}_{\ell j} - B^{-1}_{\ell P} B^{-1}_{kj} \right) \times \\ &\times \sum_i \beta_{ik} \left(\delta_{m_i n_k}\delta_{m_j n_\ell} + \delta_{m_i n_\ell}\delta_{m_j n_k} \right) \times \\ &\times \sum_n v_n \left(1-\lambda_n\right)^{\frac{5}{2}} \exp\left[-\frac{\lambda_n}{4} Z^2_{ijk\ell} \right] \times \\ &\times \sum_{\mu\nu\lambda} \epsilon_{\mu\nu\lambda} \left(\Sigma_{\mu ikj\ell} + \Sigma_{\mu j\ell ik} + \Sigma_{\mu jki\ell} + \Sigma_{\mu i\ell jk} \right) \times \\ &\times \left\{ \delta_{iP} \left[\left(Z_{k\tau} - \frac{\lambda_n}{2} Z_{ijk\ell;\tau} \right) \left(W^*_{i\nu} - W^*_{j\nu} \right) + \delta_{\tau\nu} \right] + \left(W^*_{i\nu} - W^*_{j\nu} \right) g_{iP;\tau} \right\} \times \\ &\times \left(Z_{k\lambda} - Z_{\ell\lambda} \right), \end{aligned} \tag{A.39}$$

$$\begin{aligned} \frac{\partial \langle V_{\mathrm{LS}} \rangle}{\partial \eta^*_{P\tau}} = &-\frac{i\hbar}{16} \sum_{j\ell} \beta_{j\ell} \sum_k \left(B^{-1}_{kP} B^{-1}_{\ell j} - B^{-1}_{\ell P} B^{-1}_{kj} \right) \times \\ &\times \sum_i \beta_{ik} \left(\delta_{m_i n_k}\delta_{m_j n_\ell} + \delta_{m_i n_\ell}\delta_{m_j n_k} \right) \times \\ &\times \sum_n v_n \left(1-\lambda_n\right)^{\frac{5}{2}} \exp\left[-\frac{\lambda_n}{4} Z^2_{ijk\ell} \right] \sum_{\mu\nu\lambda} \epsilon_{\mu\nu\lambda} \left(W^*_{i\nu} - W^*_{j\nu} \right) \left(Z_{k\lambda} - Z_{\ell\lambda} \right) \times \\ &\times \left\{ \delta_{iP} \left[\left(\sigma_\mu \xi_k\right)_\tau S_{j\ell} + \xi_{k\tau} \left\langle \sigma_\mu \right\rangle_{j\ell} + \xi_{\ell\tau} \left\langle \sigma_\mu \right\rangle_{jk} + \left(\sigma_\mu \xi_\ell\right)_\tau S_{jk} \right] + \right. \\ &\left. g_{iP;\tau} \left(\Sigma_{\mu ikj\ell} + \Sigma_{\mu j\ell ik} + \Sigma_{\mu jki\ell} + \Sigma_{\mu i\ell jk} \right) \right\}. \end{aligned} \tag{A.40}$$

Here, $\left\langle \sigma_\mu \right\rangle_{ij}$ is defined as

$$\left\langle \sigma_\mu \right\rangle_{ij} = \left\langle \eta_i \,|\, \sigma_\mu \,|\, \xi_j \right\rangle. \tag{A.41}$$

The differentials of Coulomb force are

$$\begin{aligned} \frac{\partial \langle V_{\mathrm{Coulomb}} \rangle}{\partial W^*_{P\mu}} = &\sum_j \delta_{m_j \mathrm{p}} \sum_i \delta_{m_i \mathrm{p}} \sum_\ell B_{j\ell} \delta_{n_\ell \mathrm{p}} \sum_k \delta_{n_k \mathrm{p}} B_{ik} \left(B^{-1}_{kP} B^{-1}_{\ell j} - B^{-1}_{\ell P} B^{-1}_{kj} \right) \times \\ &\times \sum_n v_n \left(1-\lambda_n\right)^{\frac{3}{2}} \exp\left[-\frac{\lambda_n}{4} Z^2_{ijk\ell} \right] \left[\delta_{iP} \left(Z_{k\mu} - \frac{\lambda_n}{2} Z_{ijk\ell;\mu} \right) + G_{iP;\mu} \right], \end{aligned} \tag{A.42}$$

$$
\begin{aligned}
\frac{\partial \left\langle V_{\text{Coulomb}} \right\rangle}{\partial \eta^*_{P\mu}} &= \sum_j \delta_{m_j \mathrm{p}} \sum_i \delta_{m_i \mathrm{p}} \sum_\ell B_{j\ell} \delta_{n_\ell \mathrm{p}} \times \\
&\times \sum_k \left(\delta_{iP} \xi_{k\mu} + g_{iP;\mu} S_{ik} \right) \left(B^{-1}_{kP} B^{-1}_{\ell j} - B^{-1}_{\ell P} B^{-1}_{kj} \right) \beta_{ik} \delta_{n_k \mathrm{p}} \times \\
&\times \sum_n v_n \left(1 - \lambda_n\right)^{\frac{3}{2}} \exp\left[-\frac{\lambda_n}{4} Z^2_{ijk\ell} \right]. \qquad \text{(A.43)}
\end{aligned}
$$

Under isospin projection, we have to consider the elements between neutrons

$$
\begin{aligned}
\frac{\partial \left\langle V_{\text{Coulomb}} \right\rangle}{\partial W^*_{P\mu}} &= \frac{1}{2} \sum_{j\ell} B_{j\ell} \delta_{m_j n_\ell} \sum_{ik} B_{ik} \delta_{m_i n_k} \delta_{m_i m_j} \left(B^{-1}_{kP} B^{-1}_{\ell j} - B^{-1}_{\ell P} B^{-1}_{kj} \right) \times \\
&\times \sum_n v_n \left(1 - \lambda_n\right)^{\frac{3}{2}} \exp\left[-\frac{\lambda_n}{4} Z^2_{ijk\ell} \right] \left[\delta_{iP} \left(Z_{k\mu} - \frac{\lambda_n}{2} Z_{ijk\ell;\mu} \right) + G_{iP;\mu} \right], \\
& \qquad \text{(A.44)}
\end{aligned}
$$

$$
\begin{aligned}
\frac{\partial \left\langle V_{\text{Coulomb}} \right\rangle}{\partial \eta^*_{P\mu}} &= \frac{1}{2} \sum_{j\ell} B_{j\ell} \delta_{m_j n_\ell} \sum_i \delta_{m_i m_j} \\
&\times \sum_k \left(\delta_{iP} \xi_{k\mu} + g_{iP;\mu} S_{ik} \right) \left(B^{-1}_{kP} B^{-1}_{\ell j} - B^{-1}_{\ell P} B^{-1}_{kj} \right) \beta_{ik} \delta_{m_i n_k} \times \\
&\times \sum_n v_n \left(1 - \lambda_n\right)^{\frac{3}{2}} \exp\left[-\frac{\lambda_n}{4} Z^2_{ijk\ell} \right]. \qquad \text{(A.45)}
\end{aligned}
$$

A.3 Constraints

The expectation values of coordinates should be subtracted by center-of-mass motion r_G as

$$
\left\langle r_\mu r_\nu \right\rangle = \frac{\left\langle \Phi \,\middle|\, \frac{1}{A} \sum_i \left(r^i_\mu - r_G \right) \left(r^i_\nu - r_G \right) P^T P^\pi \,\middle|\, \Phi \right\rangle}{\left\langle \Phi \,\middle|\, P^T P^\pi \,\middle|\, \Phi \right\rangle}. \qquad \text{(A.46)}
$$

The covariances are defined as

$$
\begin{aligned}
\frac{1}{A} \sum_i \left(r_{i\mu} - r_{G\mu} \right) \left(r_{i\nu} - r_{G\nu} \right) &= \frac{1}{A} \sum_i r_{i\mu} r_{i\nu} - A r_{G\mu} r_{G\nu} \\
&= \frac{A-1}{A^2} \sum_i r_{i\mu} r_{i\nu} - \frac{1}{A^2} \sum_{i \neq j} r_{i\mu} r_{j\nu}. \qquad \text{(A.47)}
\end{aligned}
$$

The expectation values of these operators are

$$
\begin{aligned}
&\left\langle \frac{1}{A} \sum_i \left(r_{i\mu} - r_{G\mu} \right) \left(r_{i\nu} - r_{G\nu} \right) \right\rangle \\
&= \frac{A-1}{4\nu A} \delta_{\mu\nu} + \frac{1}{4\nu A} \sum_{ij} B_{ij} \left(W^*_{i\mu} + Z_{j\mu} \right) \left(W^*_{i\nu} + Z_{j\nu} \right) B^{-1}_{ji} \\
&- \frac{1}{4\nu A} \left(W^*_{G\mu} + Z_{G\mu} \right) \left(W^*_{G\nu} + Z_{G\nu} \right). \qquad \text{(A.48)}
\end{aligned}
$$

The differentials are written as

$$
\begin{aligned}
&\frac{\partial}{\partial W^*_{P\tau}}\left\langle \frac{1}{A}\sum_i \left(r_{i\mu}-r_{G\mu}\right)\left(r_{i\nu}-r_{G\nu}\right)\right\rangle \\
=&\frac{1}{4\nu A}\sum_{ij} B_{ij}B^{-1}_{jP}\{\delta_{iP}\left[\delta_{\mu\tau}\left(W^*_{i\nu}+Z_{j\nu}\right)+\delta_{\nu\tau}\left(W^*_{i\mu}+Z_{j\mu}\right)+\right. \\
&\left. Z_{j\tau}\left(W^*_{i\nu}+Z_{j\nu}\right)\left(W^*_{i\mu}+Z_{j\mu}\right)\right]+ \\
&+G_{iP;\tau}\left(W^*_{i\nu}+Z_{j\nu}\right)\left(W^*_{i\mu}+Z_{j\mu}\right)\}-\frac{1}{4\nu A^{\frac{3}{2}}}\left[\delta_{\tau\mu}\left(W^*_{G\nu}+Z_{G\nu}\right)+\delta_{\nu\tau}\left(W^*_{G\mu}+Z_{G\mu}\right)\right],
\end{aligned}
\tag{A.49}
$$

$$
\begin{aligned}
&\frac{\partial}{\partial \eta^*_{P\tau}}\left\langle \frac{1}{A}\sum_i \left(r_{i\mu}-r_{G\mu}\right)\left(r_{i\nu}-r_{G\nu}\right)\right\rangle \\
=&\frac{1}{4\nu A}\sum_{ij}\beta_{ij}\delta_{m_i n_j}B^{-1}_{jP}\left(W^*_{i\nu}+Z_{j\nu}\right)\left(W^*_{i\mu}+Z_{j\mu}\right)\left(\xi_{j\tau}\delta_{Pi}+S_{ij}g_{iP;\tau}\right).
\end{aligned}
\tag{A.50}
$$

Therefore, the differentials of constraint potentials for β and γ parameters $\langle H_{\beta\gamma}\rangle$ are

$$
\begin{aligned}
\frac{\partial\left\langle H_{\beta\gamma}\right\rangle}{\partial t}=&\frac{2}{\langle x^2\rangle+\langle y^2\rangle+\langle z^2\rangle}\{(\beta\cos\gamma-X)\left[-\beta\cos\gamma\left(\partial_t\left\langle x^2\right\rangle+\partial_t\left\langle y^2\right\rangle+\partial_t\left\langle z^2\right\rangle\right)+\right. \\
&\left.\sqrt{\frac{\pi}{5}}\left(2\partial_t\left\langle z^2\right\rangle-\partial_t\left\langle x^2\right\rangle-\partial_t\left\langle y^2\right\rangle\right)\right]+ \\
&+(\beta\sin\gamma-Y)\left[-\beta\sin\gamma\left(\partial_t\left\langle x^2\right\rangle+\partial_t\left\langle y^2\right\rangle+\partial_t\left\langle z^2\right\rangle\right)\right. \\
&\left.+\sqrt{\frac{3\pi}{5}}\left(\partial_t\left\langle x^2\right\rangle-\partial_t\left\langle y^2\right\rangle\right)\right]\}.
\end{aligned}
\tag{A.51}
$$

A.4 Angular momenta and transition operators

$\boldsymbol{L}^2$ is defined as

$$
\boldsymbol{L}^2=\sum_i \boldsymbol{\ell}_i^2+\sum_{i\neq j}\boldsymbol{\ell}_i\cdot\boldsymbol{\ell}_j. \tag{A.52}
$$

The expectation value of the first term is

$$
\begin{aligned}
\frac{\langle i\,|\,\boldsymbol{\ell}^2\,|\,j\rangle}{B_{ij}}=&\left[\left(W^*_{i2}+Z_{j2}\right)^2+\left(W^*_{i3}+Z_{j3}\right)^2+2\right]W^*_{i1}Z_{j1} \\
&+\left[\left(W^*_{i3}+Z_{j3}\right)^2+\left(W^*_{i1}+Z_{j1}\right)^2+2\right]W^*_{i2}Z_{j2} \\
&+\left[\left(W^*_{i1}+Z_{j1}\right)^2+\left(W^*_{i2}+Z_{j2}\right)^2+2\right]W^*_{i3}Z_{j3} \\
&-\left(W^*_{i2}+Z_{j2}\right)\left(W^*_{i1}+Z_{j1}\right)W^*_{i1}Z_{j2} \\
&-\left(W^*_{i3}+Z_{j3}\right)\left(W^*_{i1}+Z_{j1}\right)W^*_{i1}Z_{j3} \\
&-\left(W^*_{i3}+Z_{j3}\right)\left(W^*_{i2}+Z_{j2}\right)W^*_{i2}Z_{j3} \\
&-\left(W^*_{i1}+Z_{j1}\right)\left(W^*_{i2}+Z_{j2}\right)W^*_{i2}Z_{j1} \\
&-\left(W^*_{i1}+Z_{j1}\right)\left(W^*_{i3}+Z_{j3}\right)W^*_{i3}Z_{j1} \\
&-\left(W^*_{i2}+Z_{j2}\right)\left(W^*_{i3}+Z_{j3}\right)W^*_{i3}Z_{j2}.
\end{aligned}
\tag{A.53}
$$

The expectation value of the second term is

$$
\begin{aligned}
\frac{\langle ij\,|\,\boldsymbol{\ell}_1\cdot\boldsymbol{\ell}_2\,|\,k\ell\rangle}{-B_{ik}B_{j\ell}} &= \left(W_{i1}^*+Z_{k1}\right)\left(W_{j1}^*+Z_{\ell1}\right)\left(Z_{k2}Z_{\ell2}+Z_{k3}Z_{\ell3}\right) \\
&+\left(W_{i2}^*+Z_{k2}\right)\left(W_{j2}^*+Z_{\ell2}\right)\left(Z_{k3}Z_{\ell3}+Z_{k1}Z_{\ell1}\right) \\
&+\left(W_{i3}^*+Z_{k3}\right)\left(W_{j3}^*+Z_{\ell3}\right)\left(Z_{k1}Z_{\ell1}+Z_{k2}Z_{\ell2}\right) \\
&-\left(W_{i2}^*+Z_{k2}\right)\left(W_{j1}^*+Z_{\ell1}\right)Z_{k1}Z_{\ell2} \\
&-\left(W_{i3}^*+Z_{k3}\right)\left(W_{j1}^*+Z_{\ell1}\right)Z_{k1}Z_{\ell3} \\
&-\left(W_{i1}^*+Z_{k1}\right)\left(W_{j2}^*+Z_{\ell2}\right)Z_{k2}Z_{\ell1} \\
&-\left(W_{i3}^*+Z_{k3}\right)\left(W_{j2}^*+Z_{\ell2}\right)Z_{k2}Z_{\ell3} \\
&-\left(W_{i1}^*+Z_{k1}\right)\left(W_{j3}^*+Z_{\ell3}\right)Z_{k3}Z_{\ell1} \\
&-\left(W_{i2}^*+Z_{k2}\right)\left(W_{j3}^*+Z_{\ell3}\right)Z_{k3}Z_{\ell2}.
\end{aligned}
\tag{A.54}
$$

$\boldsymbol{S}^2$ is defined as

$$
\boldsymbol{S}^2=\sum_i \boldsymbol{s}_i^2+\sum_{i\neq j}\boldsymbol{s}_i\cdot\boldsymbol{s}_j. \tag{A.55}
$$

The expectation value of the first term is

$$
\sum_{ij}\frac{3}{4}B_{ij}B_{ji}^{-1}=\frac{3}{4}A, \tag{A.56}
$$

because

$$
\left\langle i\,|\,\boldsymbol{s}^2\,|\,j\right\rangle=\frac{1}{2}\left(\frac{1}{2}+1\right)\left\langle i\,|\,j\right\rangle. \tag{A.57}
$$

The expectation value of the second term is

$$
\langle ij\,|\,\boldsymbol{s}_1\cdot\boldsymbol{s}_2\,|\,k\ell\rangle=\langle i\,|\,\boldsymbol{s}\,|\,k\rangle\cdot\langle j\,|\,\boldsymbol{s}\,|\,\ell\rangle. \tag{A.58}
$$

Here, single-particle expectation values $\langle i\,|\,\boldsymbol{s}\,|\,j\rangle$ are written as

$$
\langle i\,|\,\boldsymbol{s}\,|\,j\rangle=\frac{1}{2}\begin{pmatrix}\eta_{i2}^*\xi_{j1}+\eta_{i1}^*\xi_{j2}\\ i\eta_{i2}^*\xi_{j1}-i\eta_{i1}^*\xi_{j2}\\ \eta_{i1}^*\xi_{j1}-\eta_{i2}^*\xi_{j2}\end{pmatrix}\beta_{ij}\delta_{m_in_j}. \tag{A.59}
$$

In this thesis, E2 transitions are isoscalar transitions. The isospins are conserved between the initial states and the final states. Therefore, under isospin projection, as well as Coulomb force, we use the average of the proton transition parts and neutron transition parts;

$$
\begin{aligned}
\langle M(E2,2)\rangle = \frac{1}{2}\frac{1}{4}\sqrt{\frac{15}{2\pi}}&\left\{\sum_{ij}\frac{1}{4\nu}\right. \\
&\left[\left(W_{i1}^*+Z_{j1}\right)^2+2i\left(W_{i1}^*+Z_{j1}\right)\left(W_{i2}^*+Z_{j2}\right)-\left(W_{i2}^*+Z_{j2}\right)^2\right]B_{ij}B_{ji}^{-1} \\
&\left.-\frac{1}{4\nu}\left[\left(W_{G1}^*+Z_{G1}\right)^2+2i\left(W_{G1}^*+Z_{G1}\right)\left(W_{G2}^*+Z_{G2}\right)-\left(W_{G2}^*+Z_{G2}\right)^2\right]\right\},
\end{aligned}
\tag{A.60}
$$

$$
\begin{aligned}
\langle M(E2,1)\rangle = -\frac{1}{2}\frac{1}{2}\sqrt{\frac{15}{2\pi}}\,\{ \\
& \sum_{ij}\frac{1}{4\nu}\left[\left(W^*_{i1}+Z_{j1}\right)\left(W^*_{i3}+Z_{j3}\right)+i\left(W^*_{i2}+Z_{j2}\right)\left(W^*_{i3}+Z_{j3}\right)\right]B_{ij}B^{-1}_{ji} \\
& -\frac{1}{4\nu}\left[\left(W^*_{G1}+Z_{G1}\right)\left(W^*_{G3}+Z_{G3}\right)+i\left(W^*_{G2}+Z_{G2}\right)\left(W^*_{G3}+Z_{G3}\right)\right]\Bigg\}, \qquad \text{(A.61)}
\end{aligned}
$$

$$
\begin{aligned}
\langle M(E2,0)\rangle = \frac{1}{2}\frac{1}{4}\sqrt{\frac{5}{\pi}}\,\{ \\
& \sum_{ij}\frac{1}{4\nu}\left[2\left(W^*_{i3}+Z_{j3}\right)^2-\left(W^*_{i1}+Z_{j1}\right)^2-\left(W^*_{i2}+Z_{j2}\right)^2\right]B_{ij}B^{-1}_{ji} \\
& -\frac{1}{4\nu}\left[2\left(W^*_{G3}+Z_{G3}\right)^2-\left(W^*_{G1}+Z_{G1}\right)^2-\left(W^*_{G3}+Z_{G3}\right)^2\right]\Bigg\}, \qquad \text{(A.62)}
\end{aligned}
$$

$$
\begin{aligned}
\langle M(E2,-1)\rangle = \frac{1}{2}\frac{1}{2}\sqrt{\frac{15}{2\pi}}\,\{ \\
& \sum_{ij}\frac{1}{4\nu}\left[\left(W^*_{i1}+Z_{j1}\right)\left(W^*_{i3}+Z_{j3}\right)-i\left(W^*_{i2}+Z_{j2}\right)\left(W^*_{i3}+Z_{j3}\right)\right]B_{ij}B^{-1}_{ji} \\
& -\frac{1}{4\nu}\left[\left(W^*_{G1}+Z_{G1}\right)\left(W^*_{G3}+Z_{G3}\right)-i\left(W^*_{G2}+Z_{G2}\right)\left(W^*_{G3}+Z_{G3}\right)\right]\Bigg\}, \qquad \text{(A.63)}
\end{aligned}
$$

$$
\begin{aligned}
& \langle M(E2,-2)\rangle \\
& = \frac{1}{2}\frac{1}{4}\sqrt{\frac{15}{2\pi}}\left\{\sum_{ij}\frac{1}{4\nu}\right. \\
& \left[\left(W^*_{i1}+Z_{j1}\right)^2-2i\left(W^*_{i1}+Z_{j1}\right)\left(W^*_{i2}+Z_{j2}\right)-\left(W^*_{i2}+Z_{j2}\right)^2\right]B_{ij}B^{-1}_{ji} \\
& \left.-\frac{1}{4\nu}\left[\left(W^*_{G1}+Z_{G1}\right)^2-2i\left(W^*_{G1}+Z_{G1}\right)\left(W^*_{G2}+Z_{G2}\right)-\left(W^*_{G2}+Z_{G2}\right)^2\right]\right\}. \qquad \text{(A.64)}
\end{aligned}
$$

In this thesis, M1 transitions are isovector transitions. The isospins are changed with $\Delta T = 1$ between the initial states and the final states. Therefore, we use the difference of the proton transition parts and neutron transition parts;

$$\begin{aligned}\langle M(M1,1)\rangle = -\frac{1}{2}\frac{1}{2}\sqrt{\frac{3}{2\pi}}\{ \\ &\sum_{ij}\left[i(-1)^{n_j+1}\left(\left(W_{i3}^{*}Z_{j2}-W_{i2}^{*}Z_{j3}\right)+i\left(W_{i1}^{*}Z_{j3}-W_{i3}^{*}Z_{j1}\right)\right)S_{ij}\right. \\ &\left.+(-1)^{n_j+1}g_s^{\mathrm{IV}}\left(\left(\eta_{i2}^{*}\xi_{j1}+\eta_{i1}^{*}\xi_{j2}\right)+i\left(i\eta_{i2}^{*}\xi_{j1}-i\eta_{i1}^{*}\xi_{j2}\right)\right)\right]\beta_{ij}\delta_{m_in_j}B_{ji}^{-1} \\ &-\frac{i\sqrt{Z}}{\sqrt{A}}\left[-W_{Gp2}^{*}Z_{G3}+W_{Gp3}^{*}Z_{G2}+W_{G3}^{*}Z_{Gp2}-W_{G2}^{*}Z_{Gp3}\right] \\ &+\frac{\sqrt{Z}}{\sqrt{A}}\left[-W_{Gp3}^{*}Z_{G1}+W_{Gp1}^{*}Z_{G3}+W_{G1}^{*}Z_{Gp3}-W_{G3}^{*}Z_{Gp1}\right] \\ &+\frac{i\sqrt{N}}{\sqrt{A}}\left[-W_{Gn2}^{*}Z_{G3}+W_{Gn3}^{*}Z_{G2}+W_{G3}^{*}Z_{Gn2}-W_{G2}^{*}Z_{Gn3}\right] \\ &\left.-\frac{\sqrt{N}}{\sqrt{A}}\left[-W_{Gn3}^{*}Z_{G1}+W_{Gn1}^{*}Z_{G3}+W_{G1}^{*}Z_{Gn3}-W_{G3}^{*}Z_{Gn1}\right]\right\}, \end{aligned} \tag{A.65}$$

$$\begin{aligned}\langle M(M1,0)\rangle = \frac{1}{2}\frac{1}{2}\sqrt{\frac{3}{\pi}}\{ \\ &\sum_{ij}\left[i(-1)^{n_j+1}\left(W_{i2}^{*}Z_{j1}-W_{i1}^{*}Z_{j2}\right)S_{ij}+\right. \\ &\left.(-1)^{n_j+1}g_s^{\mathrm{IV}}\left(\eta_{i1}^{*}\xi_{j1}-\eta_{i2}^{*}\xi_{j2}\right)\right]\beta_{ij}\delta_{m_in_j}B_{ji}^{-1} \\ &-\frac{i\sqrt{Z}}{\sqrt{A}}\left[-W_{Gp1}^{*}Z_{G2}+W_{Gp2}^{*}Z_{G1}+W_{G2}^{*}Z_{Gp1}-W_{G1}^{*}Z_{Gp2}\right] \\ &\left.+\frac{i\sqrt{N}}{\sqrt{A}}\left[-W_{Gn1}^{*}Z_{G2}+W_{Gn2}^{*}Z_{G1}+W_{G2}^{*}Z_{Gn1}-W_{G1}^{*}Z_{Gn2}\right]\right\}, \end{aligned} \tag{A.66}$$

$$\begin{aligned}\langle M(M1,-1)\rangle = \frac{1}{2}\frac{1}{2}\sqrt{\frac{3}{2\pi}}\{ \\ &\sum_{ij}\left[i(-1)^{n_j+1}\left(\left(W_{i3}^{*}Z_{j2}-W_{i2}^{*}Z_{j3}\right)-i\left(W_{i1}^{*}Z_{j3}-W_{i3}^{*}Z_{j1}\right)\right)S_{ij}\right. \\ &\left.+(-1)^{n_j+1}g_s^{\mathrm{IV}}\left(\left(\eta_{i2}^{*}\xi_{j1}+\eta_{i1}^{*}\xi_{j2}\right)-i\left(i\eta_{i2}^{*}\xi_{j1}-i\eta_{i1}^{*}\xi_{j2}\right)\right)\right]\beta_{ij}\delta_{m_in_j}B_{ji}^{-1} \\ &-\frac{i\sqrt{Z}}{\sqrt{A}}\left[-W_{Gp2}^{*}Z_{G3}+W_{Gp3}^{*}Z_{G2}+W_{G3}^{*}Z_{Gp2}-W_{G2}^{*}Z_{Gp3}\right] \\ &-\frac{\sqrt{Z}}{\sqrt{A}}\left[-W_{Gp3}^{*}Z_{G1}+W_{Gp1}^{*}Z_{G3}+W_{G1}^{*}Z_{Gp3}-W_{G3}^{*}Z_{Gp1}\right] \\ &+\frac{i\sqrt{N}}{\sqrt{A}}\left[-W_{Gn2}^{*}Z_{G3}+W_{Gn3}^{*}Z_{G2}+W_{G3}^{*}Z_{Gn2}-W_{G2}^{*}Z_{Gn3}\right] \\ &\left.+\frac{\sqrt{N}}{\sqrt{A}}\left[-W_{Gn3}^{*}Z_{G1}+W_{Gn1}^{*}Z_{G3}+W_{G1}^{*}Z_{Gn3}-W_{G3}^{*}Z_{Gn1}\right]\right\}. \end{aligned} \tag{A.67}$$

Above them, I defined $W_{Gp\mu}, W_{Gn\mu}, Z_{Gp\mu}, Z_{Gn\mu}$ as

$$W_{Gp\mu} = \frac{1}{\sqrt{Z}} \sum_{m_i=p} W_{i\mu}, \tag{A.68}$$

$$W_{Gn\mu} = \frac{1}{\sqrt{N}} \sum_{m_i=n} W_{i\mu}, \tag{A.69}$$

$$Z_{Gp\mu} = \frac{1}{\sqrt{Z}} \sum_{n_i=p} Z_{i\mu}, \tag{A.70}$$

$$Z_{Gn\mu} = \frac{1}{\sqrt{N}} \sum_{n_i=n} Z_{i\mu}. \tag{A.71}$$

The expectation value of magnetic moment μ is written below. Because the isospins are conserved between the initial states and the final states, we use the average of the proton transition parts and neutron transition parts under isospin projection;

$$\begin{aligned} \langle\mu(1)\rangle = -\mu_N \frac{1}{2}\frac{1}{2}\sqrt{\frac{3}{2\pi}}\{ & \\ & \sum_{ij}\left[i\left(\left(W^*_{i3}Z_{j2} - W^*_{i2}Z_{j3}\right) + i\left(W^*_{i1}Z_{j3} - W^*_{i3}Z_{j1}\right)\right)S_{ij}\right. \\ & \left. + g_s^{\mathrm{IS}}\left(\left(\eta^*_{i2}\xi_{j1} + \eta^*_{i1}\xi_{j2}\right) + i\left(i\eta^*_{i2}\xi_{j1} - i\eta^*_{i1}\xi_{j2}\right)\right)\right]\beta_{ij}\delta_{m_in_j}B^{-1}_{ji} \\ & \left. -2i\frac{A-1}{A}\left[\left(-W^*_{G2}Z_{G3} + W^*_{G3}Z_{G2}\right) + i\left(-W^*_{G3}Z_{G1} + W^*_{G1}Z_{G3}\right)\right]\right\}, \end{aligned} \tag{A.72}$$

$$\begin{aligned} \langle\mu(0)\rangle = \mu_N \frac{1}{2}\frac{1}{2}\sqrt{\frac{3}{\pi}} & \left\{\sum_{ij}\left[i\left(W^*_{i2}Z_{j1} - W^*_{i1}Z_{j2}\right)S_{ij} + \right.\right. \\ & \left. g_s^{\mathrm{IS}}\left(\eta^*_{i1}\xi_{j1} - \eta^*_{i2}\xi_{j2}\right)\right]\beta_{ij}\delta_{m_in_j}B^{-1}_{ji} \\ & \left. -2i\frac{A-1}{A}\left(W^*_{G2}Z_{G1} - W^*_{G1}Z_{G2}\right)\right\}, \end{aligned} \tag{A.73}$$

$$\begin{aligned} \langle\mu(-1)\rangle = \mu_N \frac{1}{2}\frac{1}{2}\sqrt{\frac{3}{2\pi}}\{ & \\ & \sum_{ij}\left[i\left(\left(W^*_{i3}Z_{j2} - W^*_{i2}Z_{j3}\right) - i\left(W^*_{i1}Z_{j3} - W^*_{i3}Z_{j1}\right)\right)S_{ij}\right. \\ & \left. + g_s^{\mathrm{IS}}\left(\left(\eta^*_{i2}\xi_{j1} + \eta^*_{i1}\xi_{j2}\right) - i\left(i\eta^*_{i2}\xi_{j1} - i\eta^*_{i1}\xi_{j2}\right)\right)\right]\beta_{ij}\delta_{m_in_j}B^{-1}_{ji} \\ & \left. -2i\frac{A-1}{A}\left[\left(-W^*_{G2}Z_{G3} + W^*_{G3}Z_{G2}\right) - i\left(-W^*_{G3}Z_{G1} + W^*_{G1}Z_{G3}\right)\right]\right\}. \end{aligned} \tag{A.74}$$

The Gamow-Teller transition operator is defined in Eq. (1.1). The expectation value between the isospin eigenstates ($T = 0, 1$) is

$$\left\langle \Psi \,\middle|\, P^T \sum_i \sigma^i_\mu \tau^i_\pm \,\middle|\, \Phi \right\rangle. \tag{A.75}$$

To obtain this value, we have to calculate the spin-isospin overlaps between the $N = Z+2$ nuclei and the $N = Z$ odd-odd nuclei as follows.

$$
\begin{aligned}
&\frac{1}{2}\sum_i \det\left[\begin{pmatrix} \beta_{11} & \cdots & \beta_{1i} & \cdots & \beta_{1A} \\ \beta_{21} & \cdots & \beta_{2i} & \cdots & \beta_{2A} \\ \vdots & & \vdots & & \vdots \\ \beta_{A1} & \cdots & \beta_{Ai} & \cdots & \beta_{AA} \end{pmatrix}\right. \\
&\otimes \begin{pmatrix} S_{11} & \cdots & \langle \boldsymbol{\eta}_1 \,|\, \sigma_\mu \,|\, \boldsymbol{\xi}_i \rangle & \cdots & S_{1A} \\ S_{21} & \cdots & \langle \boldsymbol{\eta}_2 \,|\, \sigma_\mu \,|\, \boldsymbol{\xi}_i \rangle & \cdots & S_{2A} \\ \vdots & & \vdots & & \vdots \\ S_{A1} & \cdots & \langle \boldsymbol{\eta}_A \,|\, \sigma_\mu \,|\, \boldsymbol{\xi}_i \rangle & \cdots & S_{AA} \end{pmatrix} \\
&\otimes \left.\begin{pmatrix} T_{11} & \cdots & \langle m_1 \,|\, \tau_\pm \,|\, n_i \rangle & \cdots & T_{1A} \\ T_{21} & \cdots & \langle m_2 \,|\, \tau_\pm \,|\, n_i \rangle & \cdots & T_{2A} \\ \vdots & & \vdots & & \vdots \\ T_{A1} & \cdots & \langle m_A \,|\, \tau_\pm \,|\, n_i \rangle & \cdots & T_{AA} \end{pmatrix}\right] \\
&+(-1)^{T+1} \det\left[\begin{pmatrix} \beta_{11} & \cdots & \beta_{1i} & \cdots & \beta_{1A} \\ \beta_{21} & \cdots & \beta_{2i} & \cdots & \beta_{2A} \\ \vdots & & \vdots & & \vdots \\ \beta_{A1} & \cdots & \beta_{Ai} & \cdots & \beta_{AA} \end{pmatrix}\right. \\
&\otimes \begin{pmatrix} S_{11} & \cdots & \langle \boldsymbol{\eta}_1 \,|\, \sigma_\mu \,|\, \boldsymbol{\xi}_i \rangle & \cdots & S_{1A} \\ S_{21} & \cdots & \langle \boldsymbol{\eta}_2 \,|\, \sigma_\mu \,|\, \boldsymbol{\xi}_i \rangle & \cdots & S_{2A} \\ \vdots & & \vdots & & \vdots \\ S_{A1} & \cdots & \langle \boldsymbol{\eta}_A \,|\, \sigma_\mu \,|\, \boldsymbol{\xi}_i \rangle & \cdots & S_{AA} \end{pmatrix} \\
&\otimes \left.\begin{pmatrix} \left\langle m_1 \middle| \tau_{pn}^\dagger \middle| n_1 \right\rangle & \cdots & \left\langle m_1 \middle| \tau_{pn}^\dagger \tau_\pm \middle| n_i \right\rangle & \cdots & \left\langle m_1 \middle| \tau_{pn}^\dagger \middle| n_A \right\rangle \\ \left\langle m_2 \middle| \tau_{pn}^\dagger \middle| n_1 \right\rangle & \cdots & \left\langle m_2 \middle| \tau_{pn}^\dagger \tau_\pm \middle| n_i \right\rangle & \cdots & \left\langle m_2 \middle| \tau_{pn}^\dagger \middle| n_A \right\rangle \\ \vdots & & \vdots & & \vdots \\ \left\langle m_A \middle| \tau_{pn}^\dagger \middle| n_1 \right\rangle & \cdots & \left\langle m_A \middle| \tau_{pn}^\dagger \tau_\pm \middle| n_i \right\rangle & \cdots & \left\langle m_A \middle| \tau_{pn}^\dagger \middle| n_A \right\rangle \end{pmatrix}\right]. \qquad \text{(A.76)}
\end{aligned}
$$

Bibliography

[1] H. Morita, Y. Kanada-En'yo, *Prog. Theor. Exp. Phys.*, 2016:103D02, 2016.

[2] H. Morita, Y. Kanada-En'yo, *Phys. Rev. C*, 96:044318, 2017.

[3] H. Morita, Y. Kanada-En'yo, *Phys. Rev. C*, 98:034307, 2018.

[4] S. Frauendorf, A. O. Macchiavelli, *Prog. Part. Nucl. Phys.*, 78:24–90, 2014.

[5] A. Macchiavelli *et al.*, *Phys. Rev. C*, 61:041303, 2000a.

[6] A. Macchiavelli *et al.*, *Phys. Lett. B*, 480:1–6, 2000b.

[7] W. Satula, J. Dobaczewski, W. Nazarewicz, *Phys. Rev. Lett.*, 81:3599–3602, 1998.

[8] J. Dobaczewski *et al.*, *Phys. Rev. C*, 63:024308, 2001.

[9] E. Wigner, *Phys. Rev.*, 51:106, 1937.

[10] W. Satula *et al.*, *Phys. Lett. B*, 407:103–109, 1997.

[11] I. Bentley, S. Frauendorf, *Phys. Rev. C*, 88:014322, 2013.

[12] H. Yadav, H. Toki, A. Faessler, *Phys. Lett. B*, 81:119–123, 1979.

[13] H. Toki, H. Yadav, A. Faessler, *Phys. Lett. B*, 71:1–4, 1977.

[14] B. Cederwall *et al.*, *Nucl. Phys. A*, 542:454–478, 1992.

[15] A. Petrovici, K. Schmid, A. Faessler, *Nucl. Phys. A*, 571:77–92, 1994.

[16] D. Rudolph *et al.*, *Phys. Rev. Lett.*, 80:3018–3021, 1998.

[17] H. Wolter, A. Faessler, P. Sauer, *Phys. Lett. B*, B 31:516, 1970.

[18] H. Wolter, A. Faessler, P. Sauer, *Nucl. Phys. A*, A167:108, 1971.

[19] T. Sandhu, M. Rustgi, A. Goodman, *Phys. Rev. C*, 12:1340–1345, 1975.

[20] W. Satula, R. Wyss, *Phys. Lett. B*, 393:1–6, 1997.

[21] A. Goodman, *Phys. Rev. C*, 58:R3051–R3054, 1998.

[22] A. Goodman, *Phys. Rev. C*, 60:014311, 1999.

[23] K. Kaneko, M. Hasegawa, J. Zhang, *Phys. Rev. C*, 59:740–745, 1999.

[24] M. Hasegawa, K. Kaneko, *Phys. Rev. C*, 59:1449–1455, 1999.

[25] A. Petrovici, K. Schmid, A. Faessler, *Nucl. Phys. A*, 647:197–216, 1999.

[26] D. Jenkins *et al.*, *Phys. Rev. C*, 65:064307, 2002.

[27] J. Terasaki, R. Wyss, P. Heenen, *Phys. Lett. B*, 437:1–6, 1998.

[28] W. Satula, R. Wyss, *Phys. Rev. Lett.*, 86:4488–4491, 2001.

[29] S. Frauendorf, J. Sheikh, *Phys. Rev. C*, 59:1400–1404, 1999.

[30] A. Goodman, *Phys. Rev. C*, 63:044325, 2001.

[31] Y. Sun, J. Sheikh, *Phys. Rev. C*, 64:031302, 2001.

[32] W. A. Friedman, G. F. Bertsch, *Phys. Rev. C*, 76:057301, 2007.

[33] C. Qi *et al.*, *Phys. Rev. C*, 84:021301, 2011.

[34] B. Cederwall *et al.*, *Nature*, 469:68–71, 2011.

[35] P. A. Soderstrom *et al.*, *Phys. Rev. C*, 86:054320, 2012.

[36] H. Sagawa, Y. Tanimura, K. Hagino, *Phys. Rev. C*, 87:034310, 2013.

[37] Y. Tanimura, H. Sagawa, K. Hagino, *Prog. Theor. Exp. Phys.*, page 053D02, 2014.

[38] Y. Tanimura, H. Sagawa, *Phys. Rev. C*, 93:064319, 2016.

[39] D. Gambacurta, D. Lacroix, *Phys. Rev. C*, 91:014308, 2015.

[40] E. Ha, M.-K. Cheoun, F. Simkovic, *Phys. Rev. C*, 92:044315, 2015.

[41] E. Ha, M.-K. Cheoun, H. Sagawa, *Phys. Rev. C*, 97:024320, 2018.

[42] J. Fujita, Y. Futami, K. Ikeda, *Prog. Theor. Phys.*, 38:107, 1967.

[43] R. Doering *et al.*, *Phys. Rev. Lett.*, 35:1691–1693, 1975.

[44] H. Sagawa, N. Vangiai, *Phys. Lett. B*, 113:119–123, 1982.

[45] G. Bertsch, I. Hamamoto, *Phys. Rev. C*, 26:1323–1326, 1982.

[46] O. Scholten, G. Bertsch, H. Toki, *Phys. Rev. C*, 27:2975–2976, 1983.

[47] T. Suzuki, H. Sagawa, *Eur. Phys. J. A*, 9:49–53, 2000.

[48] C. L. Bai *et al.*, *Phys. Lett. B*, 675:28–31, 2009a.

[49] C. L. Bai *et al.*, *Phys. Rev. C*, 79:041301, 2009b.

[50] I. Hamamoto, H. Sagawa, *Phys. Rev. C*, 48:R960–R963, 1993.

[51] H. Z. Liang *et al.*, *Phys. Rev. C*, 98:014311, 2018.

[52] C. L. Bai *et al.*, *Phys. Lett. B*, 719:116–120, 2013.

[53] C. L. Bai *et al.*, *Phys. Rev. C*, 90:054335, 2014.

[54] J. A. Briz *et al.*, *Phys. Rev. C*, 92:054326, 2015.

[55] E. Nacher *et al.*, *Phys. Rev. Lett.*, 92:232501, 2004.

[56] A. B. Perez-Cerdan *et al.*, *Phys. Rev. C*, 88:014324, 2013.

[57] P. Sarriguren, A. Algora, J. Pereira, *Phys. Rev. C*, 89:034311, 2014.

[58] P. Sarriguren, *Phys. Rev. C*, 91:044304, 2015.

[59] P. Sarriguren *et al.*, *Nucl. Phys. A*, 635:55–85, 1998.

[60] E. Poirier *et al.*, *Phys. Rev. C*, 69:034307, 2004.

[61] K. Kaneko, Y. Sun, T. Mizusaki, *Phys. Rev. C*, 97:054326, 2018.

[62] E. Ha, M.-K. Cheoun, *Phys. Rev. C*, 88:017603, 2013.

[63] E. Ha, M.-K. Cheoun, *Phys. Rev. C*, 94:054320, 2016.

[64] E. Ha, M.-K. Cheoun, *Eur. Phys. J. A*, 53:26, 2017.

[65] Y. Fujita *et al.*, *Phys. Rev. C*, 91:064316, 2015.

[66] T. Adachi *et al.*, *Phys. Rev. C*, 73:024311, 2006.

[67] Y. Fujita *et al.*, *Phys. Rev. Lett.*, 95:212501, 2005.

[68] T. Adachi *et al.*, *Phys. Rev. C*, 85:024308, 2012.

[69] K. Hara *et al.*, *Phys. Rev. C*, 68:064612, 2003.

[70] Y. Fujita *et al.*, *Phys. Lett. B*, 365:29–34, 1996.

[71] H. Fujita *et al.*, *Phys. Rev. C*, 75:034310, 2007a.

[72] Y. Fujita *et al.*, *Phys. Rev. C*, 67:064312, 2003.

[73] Y. Fujita *et al.*, *Phys. Rev. Lett.*, 112:112502, 2014.

[74] K. Win *et al.*, *Phys. Rev. C*, 96:064309, 2017.

[75] Y. Fujita *et al.*, *Phys. Rev. C*, 75:057305, 2007b.

[76] M. Konieczka, M. Kortelainen, W. Satula, *Phys. Rev. C*, 97:034310, 2018.

[77] M. Honma *et al.*, *J. Phys. Conf. Ser.*, 20:7, 2005.

[78] B. Jancovici, I. Talmi, *Phys. Rev.*, 95:289, 1954.

[79] A. Negret *et al.*, *Phys. Rev. Lett.*, 97:062502, 2006a.

[80] S. Aroua *et al.*, *Nucl. Phys. A*, 720:71–83, 2003.

[81] Y. Kanada-En'yo, T. Suhara, *Phys. Rev. C*, 89:044313, 2014.

[82] P. Maris *et al.*, *Phys. Rev. Lett.*, 106:202502, 2011.

[83] K. Ikeda, T. Marumori, K. Takada, *Prog. Theor. Phys.*, 27:1077–1078, 1962.

[84] J. Eichler, A. Faessler, *Nucl. Phys. A*, A157:166, 1970.

[85] H. Horiuchi, *Prog. Theor. Phys.*, 51:1266–1268, 1974.

[86] Y. Suzuki, K. Ikeda, *Prog. Theor. Phys.*, 51:1621–1623, 1974.

[87] H. Bando, *Nucl. Phys. A*, 261:269–281, 1976.

[88] Y. Suzuki, *Prog. Theor. Phys.*, 55:1751–1768, 1976a.

[89] Y. Suzuki, *Prog. Theor. Phys.*, 56:111–123, 1976b.

[90] H. Kazama, K. Kato, H. Tanaka, *Prog. Theor. Phys.*, 71:215–218, 1984.

[91] H. Kazama, K. Kato, H. Tanaka, *Prog. Theor. Phys.*, 75:571–582, 1986.

[92] K. Ikeda, N. Takigawa, H. Horiuchi, *Prog. Theor. Phys. Suppl.*, E68:464, 1968.

[93] H. Horiuchi, K. Ikeda, *Prog. Theor. Phys.*, 40:277, 1968.

[94] A. Tohsaki *et al.*, *Phys. Rev. Lett.*, 87:192501, 2001.

[95] Y. Funaki *et al.*, *Phys. Rev. C*, 67:051306, 2003.

[96] T. Yamada, P. Schuck, *Phys. Rev. C*, 69:024309, 2004.

[97] H. Matsumura, Y. Suzuki, *Nucl. Phys. A*, 739:238–258, 2004.

[98] Y. Funaki *et al.*, *Phys. Rev. Lett.*, 101:082502, 2008.

[99] Y. Funaki *et al.*, *Phys. Rev. C*, 80:064326, 2009.

[100] T. Ichikawa *et al.*, *Phys. Rev. C*, 83:061301, 2011a.

[101] B. Zhou *et al.*, *Phys. Rev. C*, 86:014301, 2012.

[102] B. Zhou *et al.*, *Phys. Rev. Lett.*, 110:UNSP 262501, 2013.

[103] W. Horiuchi, Y. Suzuki, *Phys. Rev. C*, 89:011304, 2014.

[104] Y. Funaki, *Phys. Rev. C*, 92:021302, 2015.

[105] B. Zhou *et al.*, *Phys. Rev. C*, 94:044319, 2016.

[106] K. Kato, H. Kazama, H. Tanaka, *Prog. Theor. Phys.*, 76:75–92, 1986.

[107] N. Itagaki, W. von Oertzen, S. Okabe, *Phys. Rev. C*, 74:067304, 2006.

[108] T. Suhara, Y. Kanada-En'yo, *Phys. Rev. C*, 84:024328, 2011.

[109] N. Furutachi, M. Kimura, *Phys. Rev. C*, 83:021303, 2011.

[110] T. Ichikawa *et al.*, *Phys. Rev. Lett.*, 107:112501, 2011b.

[111] T. Suhara *et al.*, *Phys. Rev. Lett.*, 112:062501, 2014.

[112] Y. Kanada-En'yo, *Phys. Rev. C*, 92:064326, 2015.

[113] T. Baba, M. Kimura, *Phys. Rev. C*, 94:044303, 2016.

[114] T. Baba, M. Kimura, *Phys. Rev. C*, 95:064318, 2017.

[115] H. Yamaguchi *et al.*, *Phys. Lett. B*, 766:11–16, 2017.

[116] T. Baba, M. Kimura, *Phys. Rev. C*, 97:054315, 2018.

[117] T. Suhara, Y. Kanada-En'yo, *Phys. Rev. C*, 82:044301, 2010a.

[118] T. Baba, Y. Chiba, M. Kimura, *Phys. Rev. C*, 90:064319, 2014.

[119] H. Horiuchi, *Prog. Theor. Phys.*, 53:447–460, 1975.

[120] Y. Fujiwara, *Prog. Theor. Phys.*, 62:122–137, 1979a.

[121] Y. Fujiwara, *Prog. Theor. Phys.*, 62:138–152, 1979b.

[122] A. Kruppa, K. Kato, *Prog. Theor. Phys.*, 84:1145–1159, 1990.

[123] A. Ono *et al.*, *Prog. Theor. Phys.*, 87:1185–1206, 1992a.

[124] Y. Kanada-En'yo, H. Horiuchi, A. Ono, *Phys. Rev. C*, 52:628–646, 1995.

[125] Y. Kanada-En'yo, H. Horiuchi, *Phys. Rev. C*, 52:647–662, 1995a.

[126] Y. Kanada-En'yo, *Prog. Theor. Phys.*, 117:655–680, 2007a.

[127] Y. Kanada-En'yo, H. Horiuchi, *Prog. Theor. Phys.*, 93:115–136, 1995b.

[128] A. Dote, H. Horiuchi, Y. Kanada-En'yo, *Phys. Rev. C*, 56:1844–1854, 1997.

[129] Y. Taniguchi, M. Kimura, H. Horiuchi, *Prog. Theor. Phys.*, 112:475–487, 2004.

[130] Y. Yamamoto, T. Togashi, K. Kato, *Prog. Theor. Phys.*, 124:315–330, 2010.

[131] Y. Kanada-En'yo, *Phys. Rev. C*, 75:024302, 2007b.

[132] Y. Kanada-En'yo, *Phys. Rev. C*, 81:034321, 2010.

[133] Y. Kanada-En'yo, T. Suhara, *Phys. Rev. C*, 85:024303, 2012.

[134] P. Navratil, J. Vary, B. Barrett, *Phys. Rev. Lett.*, 84:5728–5731, 2000a.

[135] P. Navratil, J. Vary, B. Barrett, *Phys. Rev. C*, 62:054311, 2000b.

[136] R. Roth *et al.*, *Phys. Rev. Lett.*, 107:072501, 2011.

[137] P. Maris *et al.*, *Phys. Rev. C*, 90:014314, 2014.

[138] C. W. Johnson, *Phys. Rev. C*, 91:034313, 2015.

[139] P. Maris, J. P. Vary, A. M. Shirokov, *Phys. Rev. C*, 79:014308, 2009.

[140] Y. Taniguchi, Y. K. En'yo, M. Kimura, *Phys. Rev. C*, 80:044316, 2009.

[141] T. Ichikawa, Y. Kanada-En'yo, P. Moeller, *Phys. Rev. C*, 83:054319, 2011c.

[142] Y. Kanada-En'yo, Y. Hidaka, *Phys. Rev. C*, 84:014313, 2011.

[143] M. Kimura, *Phys. Rev. C*, 69:044319, 2004.

[144] T. Suhara, Y. Kanada-En'yo, *Prog. Theor. Phys.*, 123:303–325, 2010b.

[145] M. Kimura, N. Furutachi, *Phys. Rev. C*, 83:044304, 2011.

[146] K. Kaneko *et al.*, *Phys. Rev. C*, 83:014320, 2011.

[147] I. Tanihata *et al.*, *Phys. Lett. B*, 287:307–311, 1992a.

[148] T. Myo *et al.*, *Phys. Rev. C*, 76:024305, 2007.

[149] N. Furutachi *et al.*, *Prog. Theor. Phys.*, 122:865–880, 2009.

[150] S. Watanabe *et al.*, *Phys. Rev. C*, 89:044610, 2014.

[151] I. Tanihata *et al.*, *Phys. Lett. B*, 289:261–266, 1992b.

[152] T. Suzuki *et al.*, *Phys. Rev. Lett.*, 75:3241–3244, 1995.

[153] Y. Tosaka, Y. Suzuki, *Nucl. Phys. A*, 512:46–60, 1990.

[154] Y. Tosaka, Y. Suzuki, K. Ikeda, *Prog. Theor. Phys.*, 83:1140–1147, 1990.

[155] J. Meng, P. Ring, *Phys. Rev. Lett.*, 77:3963–3966, 1996.

[156] J. Meng *et al.*, *Prog. Part. Nucl. Phys.*, 57:470 – 563, 2006.

[157] K. Hagino, H. Sagawa, *Phys. Rev. C*, 72:044321, 2005.

[158] K. Hagino *et al.*, *Phys. Rev. Lett.*, 99:022506, 2007.

[159] Y. Kanada-En'yo, *Phys. Rev. C*, 76:044323, 2007c.

[160] N. Itagaki *et al.*, *Phys. Rev. C*, 78:017306, 2008.

[161] F. Kobayashi, Y. Kanada-En'yo, *Phys. Rev. C*, 88:034321, 2013.

[162] Y. Kanada-En'yo, H. Feldmeier, T. Suhara, *Phys. Rev. C*, 84:054301, 2011.

[163] F. Kobayashi, Y. Kanada-En'yo, *Prog. Theor. Phys.*, 126:457–482, 2011.

[164] F. Kobayashi, Y. Kanada-En'yo, *Phys. Rev. C*, 93:024310, 2016.

[165] W. Satula *et al.*, *Phys. Rev. Lett.*, 103:012502, 2009.

[166] W. Satula *et al.*, *Phys. Rev. C*, 81:054310, 2010.

[167] W. Satula *et al.*, *Phys. Rev. Lett.*, 106:132502, 2011.

[168] W. Satula *et al.*, *Phys. Rev. C*, 86:054316, 2012.

[169] W. Satula *et al.*, *Phys. Rev. C*, 94:024306, 2016.

[170] Y. Kanada-En'yo, *Phys. Rev. Lett.*, 81:5291, 1998.

[171] D. L. Hill, J. A. Wheeler, *Phys. Rev.*, 89:1102, 1953.

[172] K. Ikeda, *Prog. Theor. Phys.*, 31:434, 1964.

[173] A. B. Volkov, *Nucl. Phys.*, 74:33, 1965.

[174] Y. Kanada-En'yo, H. Morita, F. Kobayashi, *Phys. Rev. C*, 91:054323, 2015.

[175] N. Yamaguchi *et al.*, *Prog. Theor. Phys.*, 62:1018, 1979.

[176] R. Tamagaki, *Prog. Theor. Phys.*, 39:91, 1968.

[177] D. R. Tilley *et al.*, *Nucl. Phys. A*, 745:155, 2004.

[178] D. R. Tilley *et al.*, *Nucl. Phys. A*, 708:3, 2002.

[179] F. Ajzenberg-Selove, *Nucl. Phys. A*, 523:1, 1991.

[180] P. Navratil, W. Ormand, *Phys. Rev. C*, 68:034305, 2003.

[181] F. C. Barker, *Aust. J. Phys.*, 34:7, 1981.

[182] D. Kurath, *Nucl. Phys. A*, 317:175, 1979.

[183] F. Ajzenberg-Selove, *Nucl. Phys. A*, 490:1, 1988.

[184] I. Daito *et al.*, *Phys. Lett. B*, 418:27, 1998.

[185] A. Negret *et al.*, *Phys. Rev. Lett.*, 97:062502, 2006b.

[186] J. Rapaport *et al.*, *Phys. Rev. C* , 39:1929, 1989.

[187] W.-T. Chou, E. K. Warburton, B. A. Brown, *Phys. Rev. C* , 47:163, 1993.

[188] M. S. Basunia, *Nuclear Data Sheets*, 127:69, 2015.

[189] J. D. MacArthur *et al.*, *Can. J. Phys.*, 54:1134, 1976.

[190] M. Kimura, *Phys. Rev. C*, 75:034312, 2007.

[191] A. Ono *et al.*, *Prog. Theor. Phys.*, 87:1185, 1992b.